LUND UNIVERSITY

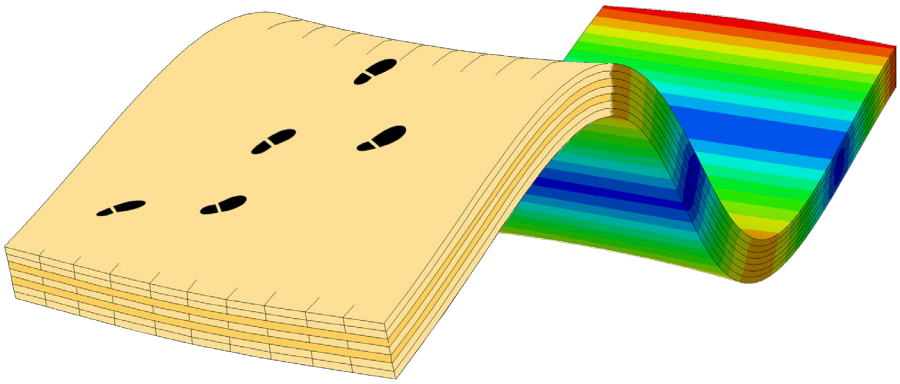

UTILISATION OF HARDWOOD IN CROSS-LAMINATED TIMBER

A numerical study on vibrations in floors

JOHANNES JONASSON and OLLE KARLSSON

Structural Mechanics

Master's Dissertation

DEPARTMENT OF CONSTRUCTION SCIENCES
DIVISION OF STRUCTURAL MECHANICS

ISRN LUTVDG/TVSM--22/5258--SE (1-133) | ISSN 0281-6679
MASTER'S DISSERTATION

UTILISATION OF HARDWOOD IN CROSS-LAMINATED TIMBER

A numerical study on vibrations in floors

JOHANNES JONASSON and OLLE KARLSSON

Supervisor: **PETER PERSSON**, Associate Professor, Division of Structural Mechanics, LTH.
Assistant Supervisor: **BENJAMIN BONDSMAN**, MSc, Division of Structural Mechanics, LTH.
Examiner: Dr **HENRIK DANIELSSON**, Division of Structural Mechanics, LTH.

Printed by V-husets tryckeri LTH, Lund, Sweden, June 2022 *(Pl)*.

For information, address:
Division of Structural Mechanics,
Faculty of Engineering LTH, Lund University, Box 118, SE-221 00 Lund, Sweden.
Homepage: www.byggmek.lth.se

Abstract

Cross-laminated timber (CLT) is an engineered wood product consisting of several layers of laminations bonded together with adhesives. In contrast to heavier construction materials, timber and other lightweight building materials are more prone to serviceability issues due to vibrations. In Sweden, the raw material used for CLT is mainly pine and spruce, which are softwoods. However, different wood species are available, such as birch and beech, which are the most common hardwood species in Sweden and Europe, respectively. In addition, previous research indicates potential advantages with utilisation of hardwood in CLT with regard to vibroacoustic performance. Thus, the present work aims to further examine if benefits with regard to vibrations in CLT floor panels can be obtained by utilising hardwood.

Initially, three different numerical models were created to determine a suitable modelling approach for CLT. A high-fidelity model where each lamination was modelled individually, a layered model where each layer was modelled individually, and a two-dimensional composite model were created. In addition, experimental testing was carried out on a real CLT panel to obtain data which the numerical models could be compared to. The layered model matched the experimental results the best and was thus considered for further validation.

The material parameters of the layered model were calibrated with Newton optimisation, where the most influential parameters of the model were altered. Several different calibrations were performed, where the most accurate calibration with regard to the normalised relative frequency difference (NRFD) yielded an average NRFD of less than one percent considering the first nine modes. Consequently, this modelling approach was considered valid.

A case study was conducted to determine the effect utilisation of different wood species has on the dynamic behaviour of CLT floor panels. Three differently sized panels with different lay-ups were tested, where all three panels fulfil the current design criteria to ensure practical relevance. The dynamic behaviour was evaluated by the means of modal properties, frequency response functions and acceleration response from footfall loading.

The analysis on the modal properties showed that changing material from spruce to birch and beech had little effect on the modal order for all tested panels. The material change did however affect the natural frequencies of the tested floor panels to various degrees, and the fundamental frequency was generally lowered.

The effect on the frequency response functions showed that the natural frequencies were altered, and that the fundamental frequency was generally lowered when utilising birch and beech instead of spruce. In addition, the magnitude of the accelerations was observed to be lowered when utilising birch and beech, where the larger panels were affected slightly more by material change than the smaller panels.

The acceleration response from footfalls was analysed by simulating five consecutive steps walking straight across the length of the CLT panels. For each panel and for each wood species, ten different walking frequencies were tested.

The walking frequency was shown to have a large impact on the acceleration response of the panels. By examining the frequency content of the acceleration response with a fast Fourier transformation, it was observed that the response was amplified if a harmonic of the walking frequency matched the fundamental frequency of the panel. In addition, up to the ninth harmonic of the walking frequency amplify the acceleration response to a large extent. Consequently, design methods considering only a single walking frequency might not yield the largest acceleration response.

Utilising hardwood yielded a significant reduction in acceleration response due to footfalls. The RMS values of the acceleration responses was reduced by up to 70% when using birch and beech instead of spruce. In addition, the reduction was more significant for the larger panels.

Acknowledgements

This dissertation marks the end to a long academic journey which once upon a time began in Helsingborg. A few people have been largely influential on the final outcome of this dissertation due to their support and assistance during the entire work, and to these we would like to express our sincerest gratitude.

We would like to thank our main supervisor, Peter Persson, and our examiner, Henrik Danielsson, who throughout the entire semester have never been hesitant in discussing ideas and helping whenever needed. Their great expertise has been of enormous help. We would also like to extend our thanks to Benjamin Bondsman for assisting us with the experimental testing and Ola Flodén for assisting us with the model calibration.

Lastly, our friends and family who have been part of this six-year long journey deserve our sincerest gratitude.

Lund, 2022.

Contents

1 Introduction

This chapter provides an introduction to the dissertation, explaining the background of the work together with the aim and objectives. In addition, the methodology is presented followed by the limitations.

1.1 Background

Wood is a natural, sustainable, and fully renewable material with many uses. It has been used for building throughout the ages, most commonly for small structures, such as one-family dwellings. In recent times, it has also been used for construction of taller multi-storey buildings as knowledge and experience of wood as a construction material has increased and new wood-based products have been developed.

Cross-laminated timber (CLT) is an engineered wood product with continuously increased usage in the construction industry. CLT is constructed of several layers of laminations that are bonded together with adhesives, see Figure 1.1. The raw material used for CLT is mainly pine and spruce, which are softwoods. In contrast to heavier construction materials such as concrete, timber and other lightweight building materials are more prone to serviceability issues due to vibrations. In general, vibrations can be experienced as disturbing, especially if they are not self-induced and occupants may experience discomfort and feel unsafe if the dynamic response of a floor is too large.

Vibrations can originate from external or internal sources and can be transmitted from one part of the structure to another. Some examples of external sources are wind, industrial activities, and transportation systems. Internal sources may be from ventilation or pumping equipment but can also be from daily activities of the occupants, such as walking, jumping, dancing, and these are usually the most problematic. Even if vibrations are transmitted throughout the whole building, floor vibrations are usually of special interest as occupants are in constant contact with the floor [1].

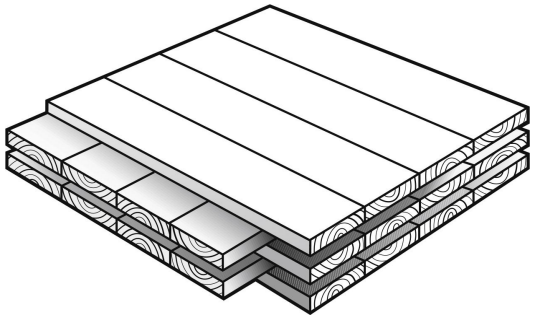

Figure 1.1: Illustration of the structure of CLT, showing individual laminations.

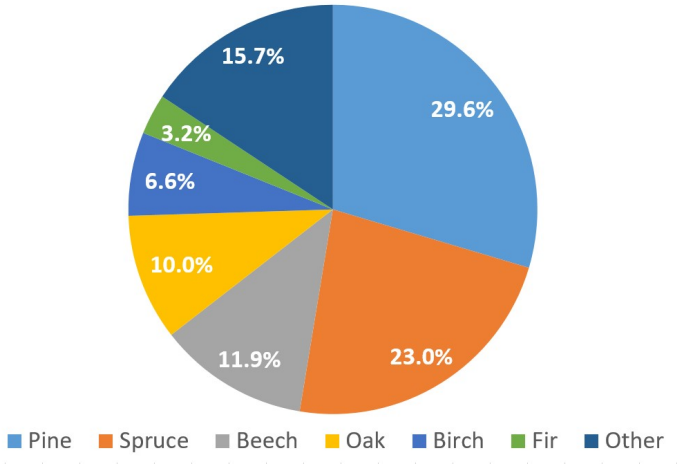

Figure 1.2: European growing stock 2020 according to the FOREST EUROPE Liaison Unit Bratislava [4].

Wood species can be categorised into two primary types: softwoods and hardwoods. Softwood originates from coniferous trees, which usually remains evergreen, i.e. they retain green leaves throughout the year. Most hardwood originates from deciduous trees which lose their leaves annually. The trees from which hardwood is obtained tend to be slower growing, meaning the wood is usually denser and thus heavier. Hardwood typically also have higher strength and stiffness than softwood [2], however a large variation between species, in-species and even within a single tree exists. Previous research indicates potential advantages with utilization of hardwoods in CLT with regard to its low-frequency vibroacoustic response [3].

Six genera of tree species represent 83.8% of the growing stock in Europe [4]. The softwoods pine (29.6%) and spruce (23.0%) account for the largest share, followed by the hardwoods beech (11.9%), oak (10.0%), birch (6.6%) and the softwood fir (3.2%), see Figure 1.2. Additionally, birch is the most common growing hardwood species in Sweden [5].

1.2 Aim and objectives

The aim of the dissertation is to study potential improved dynamic performance in CLT with a more diverse and informed material selection, and thus potentially establish further incentive for utilising other wood species than spruce in CLT. To fulfil this aim, the following research questions have been formulated:

- What is a viable modelling approach for modelling the dynamic behaviour of real CLT-panel?
- How does the method of modelling footfall affect the dynamic behaviour of a CLT floor panel? Is the behaviour altered with different walking speeds?
- Can vibrations in CLT floors be reduced by utilising hardwood?

1.3 Methodology

The methodology approach applied to fulfil the presented aim and objectives consisted of four parts: literature review, experimental analysis, numerical modelling, and numerical analyses.

The literature review included a wide scope of topics. Four topics were of particular interest: cross-laminated timber, vibrations in CLT floors, stiffness properties of various wood species, and finite element footfall modelling. Sufficient knowledge about cross-laminated timber as a construction material was collected in conjunction with previous research regarding vibrations in CLT-floors. The collection of information of mechanical parameters were also of high importance for the analyses. A lot of the information gathered in the literature review is occurring throughout the entire report, however the majority is concentrated to Chapters 2–5.

An experimental analysis was conducted so that the numerical models could be validated. Experimental modal analysis was carried out on a real CLT-panel and the modal behaviour was compared with the modal behaviour of the finite element models of the panel. In addition, the material parameters of the model were calibrated with Newton optimisation to determine if the numerical model could mimic realistic modal behaviour, and thus validate the modelling approach. Numerical modelling, the experimental approach and model validation is contained in Chapters 6–8.

After validating the modelling approach, various numerical analyses were conducted in a case study which studied the change in dynamic behaviour as a result of utilising different wood species in a small, medium and a large panel. The results from the case study are presented in Chapter 9.

A discussion is held in Chapter 10, followed by a summary of the main conclusions in Chapter 11.

1.4 Limitations

- The work will be limited to studying the dynamic behaviour of CLT floor panels.
- Only linear elastic material behaviour is considered.
- The European wood species spruce, birch and beech will be examined with regard to vibrations.

2 Wood as construction material

This chapter presents the fundamental material structure of wood, variations in wood, and basic modelling assumptions such as linear elasticity and orthotropy.

2.1 Material structure

Wood is a highly anisotropic material with different mechanical properties along each of its axes. Three axes are used to describe the principal directions of wood, see Figure 2.1. The longitudinal axis L is parallel with the axis of the trunk and is also known as the fibre- or grain direction. The radial axis R is perpendicular to the grain and normal to the annual growth rings. The tangential axis T is perpendicular to the grain and tangent to the annual growth rings.

The stiffness and strength of timber are the highest when it is loaded parallel with the longitudinal axis, and considerably lower when loaded perpendicular to the longitudinal axis. The reason for this behaviour descends from that the structure of trees has evolved for millions of years to provide a most efficient system to support the crown of the tree [6].

In general, four orders of structural variation in wood can be recognised: macroscopic, microscopic, ultrastructural and molecular [6]. A sound understanding of these structural levels is beneficial for understanding the mechanical behaviour of wood. However, the dissertation will not delve very deep in explaining these concepts, and as such, the reader is referred to literature for a more complete treatment regarding the structural levels. Instead, a general overview of the micro- and macrostructure will be presented. The following subsections regarding micro- and macrostructure are based

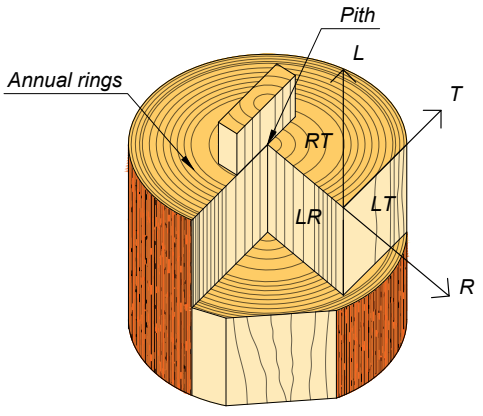

Figure 2.1: Principal directions of wood (Figure used with permission from [7]).

on literature covering pine and spruce, which both are coniferous tree species. The structure of wood from deciduous and coniferous trees are similar, but differences do exist. However, these are not significant for this dissertation, and thus not presented.

2.1.1 Macrostructure

Macrostructure refers to that which can be observed by the human eye [8]. The macrostructure consists of several distinct zones across the cross section of a tree trunk, see Figure 2.2. The outermost layer is the bark which can be separated into outer bark and inner bark. The outer bark is mainly made of dead cells and serves as a protective function from the outside environment such as birds, insects, fungi and other organisms. The inner bark consists of living cells which transport nutrients from the crown of the tree to the living cells in the branches, stem and root of the tree [9].

The cambium is the layer of growth found under the bark along the side of the entire length of the stem. Of the cells formed in the cambium during the growing season some will remain as cambial cells while others closer to the outside of the zone will develop into bark, or if on the inside, into wood [8].

Sapwood is the region that contains cells where nutrients are stored and sap (containing water and minerals) are transported along the trunk and into the branches and twigs, where photosynthesis occurs. During photosynthesis, nutrient salts, and solar energy are converted into nutrients that are transported to all living cells of the tree [8].

The inner core is composed entirely out of dead cells and is called heartwood. Heartwood usually has higher strength and density than sapwood and is usually not formed until the tree is around 30 years old for pine and spruce. The pith is in the center of the trunk and is the oldest part of the tree [8].

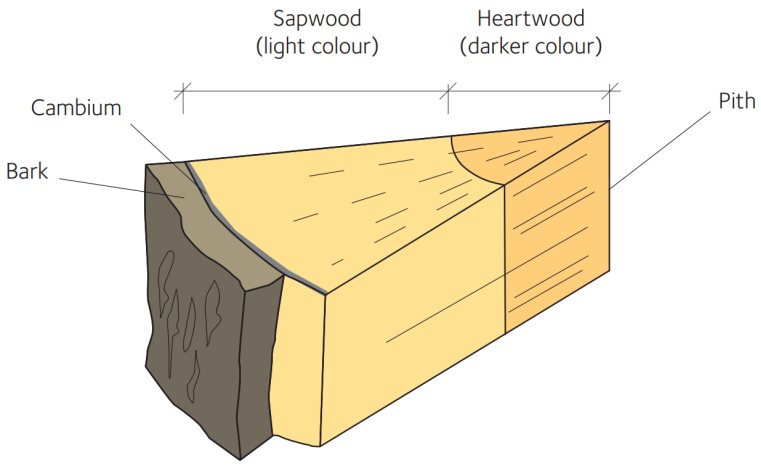

Figure 2.2: Structural features of softwood on a macro level [9].

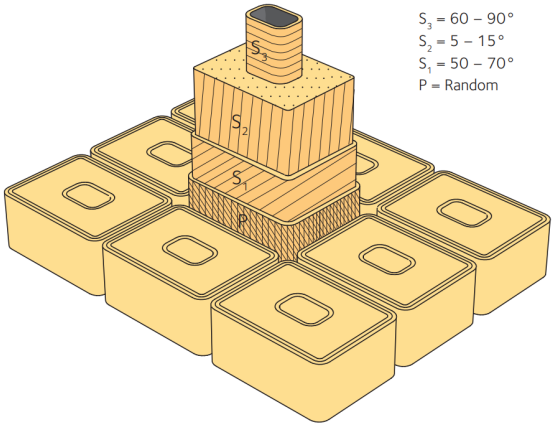

Figure 2.3: The structure of a softwood cell [9].

2.1.2 Microstructure

Microstructure refers to that which can be seen under a microscope. Long cells oriented in the longitudinal direction of the trunk, with some small deviation, make up the main building blocks of wood, see Figure 2.3. These cells are a type of fibre with a length of around 2–6 mm. The cells are hollow which partly explains why wood is stronger and stiffer in the longitudinal direction compared to the transversal- and radial directions [8].

2.2 Variations in wood

As the material properties have been largely determined by nature, large variations must be expected. The wood properties differ between different species of wood, between different trees of the same species and even within the same tree. They also depend on the plant site and the growth conditions for the tree. Furthermore, there is a major impact of imperfections such as knots and fibre disturbances [8].

2.2.1 Clearwood and timber

Clearwood refers to wood specimens that consist of only straight fibres and without anomalies. Timber on the other hand, refers to large wood specimen, usually boards, that include natural characteristics such as knots, spiral grain, juvenile wood and reaction wood. Clearwood is only dependent on the properties of the wood fibres, whereas abnormalities in timber can have a large effect on the properties of the timber.

When testing the mechanical properties of wood, a large variation in testing methods and testing specimens may be employed. Different research performs testing on different specimen, e.g. clearwood, timber, or complete CLT-panels. This is important to consider, as comparing structural timber graded based on strength and abnormalities, against clear wood of other materials can result in an unfair comparison which does not necessarily reflect reality well.

2.2.2 Strength grading

Knowledge of the material properties of timber is a requirement to use it in load-bearing structures. Timber for structural purposes is graded based on its bending strength according to most standards [10]. The mean modulus of elasticity in bending, and the density, are controlled so that they both correspond to the strength grade. An estimation is done for the other parameters based on these values. There are currently two types of grading: visual strength grading and machine strength grading. For more information on this subject, the reader is referred to [9].

2.2.3 Moisture content

Most properties of wood are affected by its moisture content as wood is a hygroscopic material. It undergoes both volumetric changes and changes of the mechanical properties depending on the atmospheric humidity. Both the strength of the wood and its stiffness generally decrease as the moisture content increases [8]. 12% moisture content is used in most standards of testing wood strength. This corresponds to EN 1995-1-1 Service class 1 which states that the average moisture content in most softwoods do not exceed 12%. Service class 1 applies for most indoor usage, highly relevant for this dissertation [11].

2.3 Linear elasticity and orthotropy

A material which follows the same stress-strain curve independent of loading and unloading is called path independent: a one-to-one relation between stresses and strains exist [12]. For linear elastic behaviour, the stress-strain curve is linear. This can further be generalized to a three-dimensional case, where three principal directions exist. For such a case of linear elasticity, the generalised Hooke's law can be written as

$$\boldsymbol{\sigma} = \mathbf{D}\boldsymbol{\varepsilon} \tag{2.1}$$

where $\boldsymbol{\sigma}$ is the stress vector, $\boldsymbol{\varepsilon}$ is the strain vector and $\mathbf{D}$ is the constitutive matrix:

$$\boldsymbol{\sigma} = \begin{bmatrix} \sigma_{xx} \\ \sigma_{yy} \\ \sigma_{zz} \\ \sigma_{xy} \\ \sigma_{xz} \\ \sigma_{yz} \end{bmatrix} \quad \mathbf{D} = \begin{bmatrix} D_{11} & D_{12} & ... & D_{16} \\ D_{21} & D_{22} & ... & D_{26} \\ \vdots & \vdots & \ddots & \vdots \\ D_{61} & D_{62} & ... & D_{66} \end{bmatrix} \quad \boldsymbol{\varepsilon} = \begin{bmatrix} \varepsilon_{xx} \\ \varepsilon_{yy} \\ \varepsilon_{zz} \\ \gamma_{xy} \\ \gamma_{xz} \\ \gamma_{yz} \end{bmatrix}$$

The constitutive matrix $\mathbf{D}$ can be inverted, yielding the strain-stress relation, with the compliance matrix $\mathbf{C} = \mathbf{D}^{-1}$.

$$\boldsymbol{\varepsilon} = \mathbf{C}\boldsymbol{\sigma} \tag{2.2}$$

In general, the constitutive matrix also changes depending on the chosen coordinate system. An elastic symmetry plane is said to exist if there are two mirrored coordinate systems leaving the constitutive matrix unaffected. If three symmetry planes exist and the coordinate axes are colinear with them, the constitutive matrix can be reduced to 12 independent material parameters, in contrast to 36 independent. The material is then called orthotropic, a representation often used for modelling wood. The equivalent holds for the compliance matrix, which after this reduction assumes the following form:

$$\mathbf{C} = \begin{bmatrix} \frac{1}{E_1} & -\frac{v_{21}}{E_2} & -\frac{v_{31}}{E_3} & 0 & 0 & 0 \\ -\frac{v_{12}}{E_1} & \frac{1}{E_2} & -\frac{v_{32}}{E_3} & 0 & 0 & 0 \\ -\frac{v_{13}}{E_1} & -\frac{v_{23}}{E_2} & \frac{1}{E_3} & 0 & 0 & 0 \\ 0 & 0 & 0 & \frac{1}{G_{12}} & 0 & 0 \\ 0 & 0 & 0 & 0 & \frac{1}{G_{13}} & 0 \\ 0 & 0 & 0 & 0 & 0 & \frac{1}{G_{23}} \end{bmatrix} \tag{2.3}$$

If the principal directs of wood are assumed to be colinear with the chosen coordinate system (which in general is the case for wood), the indices 1, 2 and 3 can be replaced with the principal directions L, T and R.

3 Cross-laminated timber

This chapter presents an introduction to CLT, how it is manufactured, and an explanation of the phenomenon rolling shear.

3.1 General

Cross-laminated timber (CLT) consists of an odd number of layers (albeit at least three layers) where each layer is constructed with multiple wood laminations. In general, each layer is orientated 90 degrees relative to the adjacent layers, see Figure 3.1. However, for longer spans it might be beneficial to have the two outermost layers orientated in the same direction, to increase the load-carrying capacity and stiffness in that direction.

The orthogonal orientation of the layers homogenizes the material, diminishing influences from woods inherent anisotropic characteristics. In addition, CLT in contrast to glued laminated timber, acquires significant load-bearing properties in two directions instead of a single direction. Generally, the orientation of laminations in the outer-most layers is in the main load-bearing direction.

CLT has seen an exponential growth in use and production the last couple of decades. It is usually utilized as load-bearing elements in structures such as apartment buildings, schools, industrial facilities, houses, and bridges. A panel can be made as large as 4.8 m wide, 30 m long and with a thickness of 60-500 mm. It should be noted that these sizes are on the extreme end of the spectrum and lengths of up to 12 m are much more common with a 2–3 m width. Generally, CLT is constructed with softwoods such as pine and spruce [13].

The individual laminations of a CLT panel are usually produced with a height of 20–60 mm and a width of 40–300 mm. The length of an individual lamination is naturally limited due to the dimensional properties of sawn timber. Sawn timber usually are

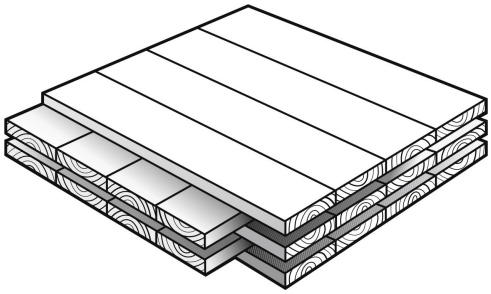

Figure 3.1: Typical structure of a 5 layer CLT panel. The orthogonal orientation between adjacent layers can be seen.

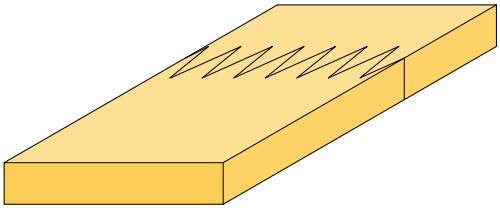

Figure 3.2: Finger joints used for laminations in CLT-panels.

four to five meters long, which is insufficient when creating long laminations needed for larger CLT panels. This problem is usually solved by merging two timber boards together with so called finger joints. At the end the boards, "fingers" are machined. These "fingers" are symmetrical and tapered and can be used to bond two boards together with adhesives, see Figure 3.2. This method is utilized in a wide range of engineered wood products [14].

3.2 Manufacturing

The manufacturing process of CLT is rather similar independent of region or country. In Figure 3.3, the full life cycle of a CLT-panel from a tree to recycling is shown. After a tree has been sawn into timber, the timber is strength graded. Next, longer laminations are created by joining timber boards together with finger joints followed by planing. The planing is usually needed for proper bonding with the adhesive used for gluing layers together.

Laminations are mostly glued on their top- and bottom surfaces, however sometimes they may also be edge-glued. By edge-gluing laminations, stresses can be transferred not only vertically between layers, but also horizontally between individual laminations. It also eliminates the possibility of gaps occurring in the CLT-panel, due to the horizontal pressing that is needed while the glue hardens. Generally, laminations are not edge-glued due to the increased manufacturing costs [15].

After applying the glue, the layers are pressed together using either vacuum or hydraulic pressure. When the glue has hardened, the panel is ready for post-processing and finishing, e.g. with CNC (Computer Numerical Control) machinery. It is then packaged and sent away for storage or to a construction site for assembly into a building.

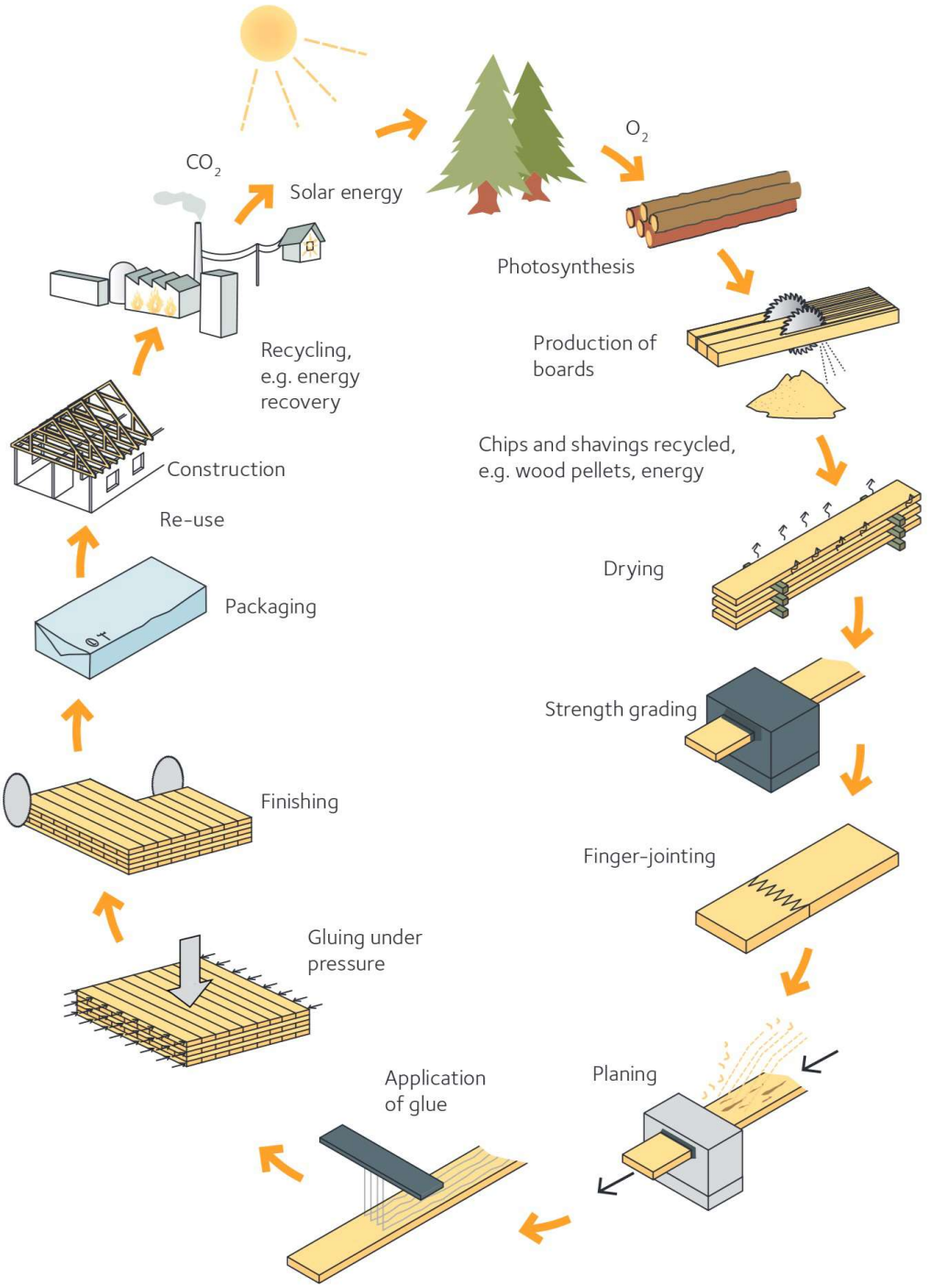

Figure 3.3: The life cycle of a CLT panel, from tree to recycling [13].

3.3 Rolling shear

A phenomenon that is considered to have a large impact on the behaviour of cross-laminated timber is rolling shear. For a CLT panel subjected to out-of-plane loading, the transverse laminations experience shear stresses that acts perpendicular to the fibre direction, which in turn causes the fibres to roll over each other, see Figure 3.4. It is important to bear in mind, that the rolling shear modulus is significantly lower than that of the shear modulus in the fibre direction.

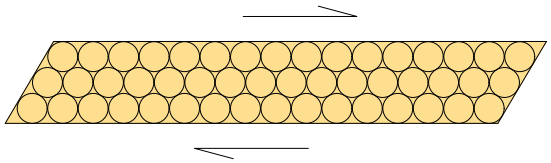

Figure 3.4: Rolling shear phenomenon in CLT.

4 Structural dynamics

This chapter introduces the basic governing theory regarding structural dynamics necessary for the dissertation. The equation of motion, damping, modal analysis, mode super-position, frequency response functions and dynamic evaluation metrics are introduced.

4.1 Equation of motion

For a multi-degree-of-freedom (MDOF) linear-elastic dynamic system in free vibration, the generalised equation of motion in matrix form is:

$$\mathbf{M}\ddot{\mathbf{u}}(t) + \mathbf{C}\dot{\mathbf{u}}(t) + \mathbf{K}\mathbf{u}(t) = \mathbf{p}(t) \tag{4.1}$$

where $\mathbf{M}$, $\mathbf{C}$ and $\mathbf{K}$ are the mass matrix, the damping matrix, and the stiffness matrix, respectively. $\mathbf{p}(t)$ is the external force vector and $\mathbf{u}$ is the displacement vector, and dot and double dot denotes first and second derivatives with respect to time, i.e. velocity and acceleration. The damping is proportional to the velocity, which is called viscous damping.

4.2 Damping

Damping is the dissipation of energy in a dynamic system, causing the vibration amplitudes to diminish over time [16]. Ideally, the damping matrix would be assembled methodically in the same manner as the mass and stiffness matrix. However, damping parameters are not as well-defined as stiffness and mass properties and a damping matrix is therefor difficult to assemble with such an approach. Thus, it is usually defined at a system level [17].

Damping can be applied with various approaches, one which is modal damping. Modal damping means that each mode is damped individually. Thus, if a certain level of critical damping is known for a certain mode, it can be applied for that mode explicitly.

Another approach for modelling damping is Rayleigh damping. For such a case, the damping matrix $\mathbf{C}$ is determined proportionally in relation to the mass and stiffness matrices according to

$$\mathbf{C} = a_0\mathbf{K} + a_1\mathbf{M} \tag{4.2}$$

where a_0 and a_1 are the Rayleigh damping parameters.

4.3 Modal analysis

The impact of damping regarding the natural frequencies of a MDOF system in free vibration is governed by

$$\omega_{nD} = \omega_n \sqrt{1 - \zeta_n^2} \tag{4.3}$$

where ω_n is the natural frequency and ζ_n is the damping ratio. The impact on the natural frequencies for damping ratios $\zeta_n < 20\%$ is rather small. This range is applicable to most structures, and thus also the CLT-panels considered in this dissertation.

By neglecting damping from Equation 4.1 and only considering free vibration the following expression is formed:

$$\mathbf{M}\ddot{\mathbf{u}}(t) + \mathbf{K}\mathbf{u}(t) = \mathbf{0} \tag{4.4}$$

The displacements $\mathbf{u}$ can be described as a function of the deflected mode shape, $\boldsymbol{\phi}_n$ and the time variation of the modal coordinates $q_n(t)$:

$$\mathbf{u}(t) = \sum_{n=1}^{N} \boldsymbol{\phi}_n q_n(t) = \boldsymbol{\Phi}\mathbf{q}(t) \tag{4.5}$$

where the modal coordinates are described by

$$q_n(t) = \boldsymbol{\phi}_n (A_n \cos \omega_n t + B_n \sin \omega_n t) \tag{4.6}$$

Substitution of Equation 4.5 into Equation 4.4 yields the eigenvalue problem for dynamic systems in free vibration:

$$[\mathbf{K} - \omega_n^2 \mathbf{M}]\boldsymbol{\phi}_n = \mathbf{0} \tag{4.7}$$

from which the eigenvalues and eigenvectors can be extracted. This equation system possess a trivial solution in $\boldsymbol{\phi_n} = \mathbf{0}$, however this implies no motion and is thus of no interest. A non-trivial solution can be acquired from the characteristic equation

$$\det[\mathbf{K} - \omega_n^2 \mathbf{M}] = 0 \tag{4.8}$$

The natural frequencies for all modes can be calculated with Equation 4.8 and substituted into Equation 4.7 to solve for the eigenvectors (mode shapes). A diagonal

matrix for eigenfrequencies and one matrix for the eigenvectors can then be assembled according to:

$$\mathbf{\Phi} = [\phi_{jn}] = \begin{bmatrix} \phi_{11} & \phi_{12} & \dots & \phi_{1N} \\ \phi_{21} & \phi_{22} & \dots & \phi_{2N} \\ \vdots & \vdots & \ddots & \vdots \\ \phi_{N1} & \phi_{N2} & \dots & \phi_{NN} \end{bmatrix}; \quad \mathbf{\Omega}^2 = \begin{bmatrix} \omega_1^2 & & & \\ & \omega_2^2 & & \\ & & \ddots & \\ & & & \omega_3^2 \end{bmatrix} \tag{4.9}$$

After eigenfrequencies and eigenvectors have been extracted from Equation 4.8 and collected in the modal matrix and diagonalized natural frequency matrix in Equation 4.9, mode super-position can be utilized to solve the system. The following coordinate transformation is introduced:

$$\mathbf{u}(t) = \mathbf{\Phi}\boldsymbol{\eta}(t) = \sum_{r=1}^{N} \boldsymbol{\phi}_r \boldsymbol{\eta}_r \tag{4.10}$$

Substituting Equation 4.10 into Equation 4.1 and pre-multiplying with the transpose of the modal matrix results in the diagonalized equation of motions expressed in the principal coordinates $\boldsymbol{\eta}(t)$:

$$\boldsymbol{M}\ddot{\boldsymbol{\eta}} + \boldsymbol{C}\dot{\boldsymbol{\eta}} + \boldsymbol{K}\boldsymbol{\eta} = \boldsymbol{f}(t) \tag{4.11}$$

where

$$\begin{aligned} \boldsymbol{M} &= \mathbf{\Phi}^{\boldsymbol{T}}\mathbf{M}\mathbf{\Phi} \\ \boldsymbol{C} &= \mathbf{\Phi}^{\boldsymbol{T}}\mathbf{C}\mathbf{\Phi} \\ \boldsymbol{K} &= \mathbf{\Phi}^{\boldsymbol{T}}\mathbf{K}\mathbf{\Phi} \\ \boldsymbol{f}(t) &= \mathbf{\Phi}^{\boldsymbol{T}}\mathbf{p}(t) \end{aligned}$$

Equation 4.11 is coupled by non-zero off-diagonal terms in the modal damping matrix, $\boldsymbol{C}$. To counter this, modal damping can be introduced according to

$$\boldsymbol{C} = \Phi^T\mathbf{C}\Phi = diag(C_r) = diag(2\zeta_r\omega_r M_r) \tag{4.12}$$

where the modal damping factor ζ_r usually is assumed for each mode, depending on the type of structure. It can also be determined experimentally.

Introducing modal damping creates a set of uncoupled modal equations of motion in the modal space according to:

$$M_r\ddot{\eta}_r + 2M_r\omega_r\zeta_r\dot{\eta}_r + \omega_r^2 M_r\eta_r = f_r(t) \tag{4.13}$$

where $r = 1, 2, 3, ..., N$.

4.4 Modal truncation

Consider a dynamic system, for which the dynamic response is determined by number of modes, J:

$$\mathbf{u} = \sum_{n=1}^{J} \boldsymbol{\phi}_n \mathbf{q}_n \tag{4.14}$$

By truncating the number of included modes, and instead including a number of modes $N < J$, the computational power needed for calculating the response can be significantly lessened. It is however important to note that this truncation introduces an error, which needs to be small enough, so it does not alter the systems response excessively.

4.5 Frequency response functions

Experimental modal analysis (EMA) is used to determine a certain set of dynamic parameters for a system: often natural frequencies, damping ratios and mode shapes. In EMA, the structure is modelled as linearly elastic and viscously damped, i.e. it follows the form of Equation 4.1, however, the amplitude is instead expressed as a complex amplitude:

$$\mathbf{M}\ddot{\mathbf{u}}(t) + \mathbf{C}\dot{\mathbf{u}}(t) + \mathbf{K}\mathbf{u}(t) = \mathbf{p}e^{i\omega t} \tag{4.15}$$

The steady-state solution can be found as

$$\mathbf{u}(t) = \mathbf{U}e^{i\omega t} = \sum_{r=1}^{N} \frac{\boldsymbol{\phi}_r \boldsymbol{\phi}_r^T \mathbf{p}}{K_r} \frac{1}{[1 - (\omega/\omega_r)^2] + i[2\zeta_r(\omega/\omega_r)]} e^{i\omega t} \tag{4.16}$$

where $\boldsymbol{\phi}_r$ are the mode shapes of the undamped system, ω and ω_r is the forcing frequency and the natural frequency. If the system is excited harmonically only in a certain coordinate, e.g. coordinate a, the steady-state displacement response in another coordinate, e.g. coordinate b is called the frequency-response function (FRF), for the response at b due to excitation at a. The FRF for coordinate a excited in coordinate b, can be expressed as:

$$H_{ab}(f) = H_{u_a/p_b}(f) = \sum_{r=1}^{N} \frac{\boldsymbol{\phi}_r \boldsymbol{\phi}_r^T}{K_r} \frac{1}{[1 - (\omega/\omega_r)^2] + i[2\zeta_r(\omega/\omega_r)]} \tag{4.17}$$

The following can be concluded from the FRF matrix:

- The FRF matrix is symmetric: $H_{ab}(f) = H_{ba}(f)$.
- Peaks occur in the FRFs near the natural frequencies.
- The FRF is defined in the frequency domain and is normalised in relation to the load with the unit $[(\mathrm{m/s^2})/\mathrm{N}]$.

From the FRFs, it is possible to then determine the mode shapes, the natural frequencies and the modal damping ratios. The process of determining these dynamic properties via the means of EMA will be discussed further in Chapter 7.

4.6 Evaluation metrics

This section introduces different evaluation metrics which can be used for evaluating the dynamic response of structures.

4.6.1 Root mean square

The root mean square is the mean value of a set of data points, regardless of the sign of the data points, i.e. the mean magnitude is calculated. In Equation 4.18, n is the number of data points and x_i is the value of i:th data point.

$$\mathrm{RMS} = \sqrt{\frac{1}{n}\sum_{i=1}^{n} x_i^2} \tag{4.18}$$

4.6.2 Modal assurance criterion

Modal resemblance between different models (or the same model) can be evaluated with the Modal Assurance Criterion (MAC) according to

$$\mathrm{MAC} = \frac{|\boldsymbol{\phi}_i^T \boldsymbol{\phi}_j|^2}{(\boldsymbol{\phi}_i^T \boldsymbol{\phi}_i)(\boldsymbol{\phi}_j^T \boldsymbol{\phi}_j)} \tag{4.19}$$

where $\boldsymbol{\phi}_i$ is the i-th mode shape and $\boldsymbol{\phi}_j$ is the j-th mode shape. Two mode shapes with no resemblance produces a MAC-value of 0, whereas two identical modes produce a MAC-value of 1. Consequently, perfect mode resemblance causes the MAC-matrix to approach unity, i.e. all the diagonal elements are equal to 1, and all the other elements are zero. If a model is compared to itself with a MAC, it is referred to as an AutoMAC, whereas if two different models are compared to each other, it is compared to as a CrossMAC.

4.6.3 Normalised relative frequency difference

The difference in natural frequencies between models/measurements can be evaluated with the Normalized Relative Frequency Difference (NRFD) according to

$$\text{NRFD} = \frac{(f_{ni,A}) - (f_{ni,B})}{(f_{ni,B})} \tag{4.20}$$

where $f_{ni,A}$ denotes the natural frequency of the i:th eigenmode of model A and $f_{ni,B}$ denotes the natural frequency of the i:th eigenmode of reference model B.

5 Material properties

This chapter presents a literature review regarding material properties of different wood species. The testing methods, testing specimens and resulting parameters will be covered for each source if possible. The literature review is followed by a compilation of the collected mechanical parameters.

The wood species of interest for the case study in Chapter 9 are spruce, birch and beech. However, the material properties of pine, ash, and oak have also been studied and are presented in this chapter.

It is worth noting that determining material properties for wood is something that requires extensive research, and due to time constraints, the extent of the literature review is therefore limited.

5.1 Literature review

In [2], the mechanical properties of various wood species were studied with a literature review. In total 20 different papers were reviewed, all identifiable by their unique paper ID provided in the paper. The same ID:s are included in this chapter to provide the reader with means of finding the origin of the presented values. A preferred approach to extracting the values from the literature review could have been to examine the original sources. However, this was not possible as several of the papers were written in a language not spoken by the authors of this dissertation.

The authors of [2] highlight that many papers in the literature review employed different testing methods when determining the mechanical parameters of wood. In addition, the authors pointed out that most hardwood generally have a higher density and longitudinal elastic modulus than most softwood. A high correlation between these two parameters was also indicated, as the results showed that wood with high density generally had a high elastic modulus.

In [18], tests of the rolling shear modulus of various European wood species are reported. The studied specimens included Norway spruce, poplar, European birch, European beech, European ash, and pine. The testing method used was based on EN 408, normally used for determining longitudinal shear properties, see Figure 5.1. The tested laminations in the reference series had an aspect ratio (lamination width in relation to lamination height) of 4 and the sawing distance from the pith was 60 mm. Different series of specimens were tested, where for example the sawing pattern and aspect ratio varied. In total, 342 tests were conducted to examine the rolling shear modulus of the above-mentioned species. As prescribed in EN 408, all specimens were conditioned in 20 degrees Celsius and 65% relative humidity. Testing of Norway spruce resulted in a mean value of the rolling shear modulus of circa 100 MPa. All hardwood

species indicated higher values of the rolling shear modulus. The authors proposed a set of values for the rolling shear modulus for the six tested timber species based on the results from their own testing, combined with results from previous research.

In [19], a compilation of mechanical properties of spruce collected from nine different sources are presented. The compilation includes mechanical properties of Engelmann-, Black-, Red-, White-, Silver-, Sitka- and Norway spruce, from which an average set of mechanical parameters for spruce was calculated. The author highlights a strong linear correlation between the longitudinal elastic modulus and the density. Correlation between the tangential elastic modulus and the density was also found, however it was not quite as pronounced. The correlation between the other parameters and the density was low.

In [20], tests of the rolling shear modulus of beech are reported. In total 52 tests were conducted with the two-plate method described in EN 789, see Figure 5.1. The test specimen had a length of 100 mm in the longitudinal direction, a width of 133 mm in the tangential direction and a height of 33 mm in the radial direction. Most of the specimen were without knots and defects, however some included the pith. The specimens were sawn in four different annual ring orientation patterns: quarter-sawn, semi-quarter-sawn, flat-sawn and patterns including the pith.

The rolling shear tests reported in [20] indicated significantly higher values for the rolling shear modulus for beech compared to that of spruce and fir. The mean rolling shear modulus was determined to 370 MPa, whereas the highest value was as high as 419 MPa. The highest modulus was acquired from the semi-quarter-sawn boards and lowest from the quarter-sawn boards.

In [21], a study investigating potential benefits of using birch for CLT was conducted in response to birch growing in large and cut-able quantities close to the Russian sawmill HasslacherLes. The aim of the project was to establish a complete profile of the mechanical properties of birch to allow for design according to EN 1995-1-1.

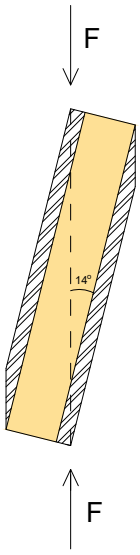

Figure 5.1: Test setup according to EN 408 and EN 789.

The tests in [21] were carried out on both individual timber boards and on CLT made of birch. The birch used for testing was cut and kiln-dried to a moisture content of 12%. 4412 boards were stress graded using the dynamic modulus of elasticity with the device GoldenEye 706 from MiCROTEC. Before this, visual grading according to DIN 4073–5 had been performed. The mean longitudinal elastic modulus was determined to almost 16 000 MPa and the mean density to 594 kg/m^3, with coefficient of variations of 12% and 7%, respectively. The bending strength and longitudinal elastic modulus of 20 CLT specimens with five layers were tested with a four-point bending test according to EN 16351:2013. The same bending test was performed on 20 CLT specimens with shorter span to determine the rolling shear properties. In addition, 20 test specimens had their compressive strength and elastic modulus perpendicular to the grain tested according to ÖNORM EN 408:2010. The parameters which were not tested were determined based on formal relationships.

In [22], stiffness parameters of various wood species available in Scandinavia are presented. There is however no information on how these values were obtained.

5.2 Compilation of mechanical parameters

Table 5.1 shows the stiffness parameters for different strength classes of structural timber according to SS-EN 338 [10]. Due to the absence of the rolling shear modulus G_{RT} in SS-EN 338, it was instead calculated as the ratio between the longitudinal shear modulus and the rolling shear modulus as found as the average in [19].

Tables 5.2 and 5.3 show the compiled mechanical parameters for various hardwoods and softwoods, respectively. Previous research indicates that Poisson's ratio impact the modal behaviour very little [3, 23, 24]. This was further examined in Chapter 8 with a sensitivity analysis which showed that Poisson's ratio had a negligible effect on the modal behaviour. Poisson's ratio was thus not included in the collection of mechanical parameters. To account for uncertainties in availability of material properties, low and high values of birch and beech are also presented, for later use in the case study in Chapter 9.

Table 5.1: Material parameters of structural timber strength classes according to SS-EN 338, with the exception of G_{RT}. Moduli in MPa and mass density in kg/m^3.

Class	E_{L}	E_{R}	E_{T}	G_{LT}	G_{LR}	G_{RT}	ρ
C14	7 000	230	230	440	440	31	350
C18	9 000	300	300	560	560	40	380
C24	11 000	370	370	690	690	49	420
C30	12 000	400	400	750	750	53	460
C40	14 000	470	470	880	880	63	480
C50	16 000	530	530	1000	1000	71	520

Table 5.2: Compilation of mechanical parameters for various hardwoods. Moduli in MPa and mass density in kg/m^3. *) The radial E-modulus of 1 100 MPa is used for the analysis in Chapter 9 instead of 650 MPa as the lower value for birch. This as 650 MPa was determined for design purposes which uses the lowest value of E_R and E_T for both.

Birch	E_L	E_R	E_T	G_{LT}	G_{LR}	G_{RT}	ρ
[18]	-	-	-	-	-	180	612
[2] ID: 6	14 500–16 500	1 110	620	-	-	-	510–830
[2] ID: 19	15 250	1 260	640	-	-	-	-
[2] ID: 17	-	-	-	-	-	-	607–675
[21]	15 000	650	650	850	850	175	620
[22]	13 000–15 000	-	-	-	-	-	580–620
Low	13 000	1 110*(650)	620	850	850	175	510
High	16 500	1 260	650	850	850	180	830

Beech	E_L	E_R	E_T	G_{LT}	G_{LR}	G_{RT}	ρ
[18]	-	-	-	-	-	350	720
[2] ID: 6	10 000–18 000	1 310	680	-	-	-	540–910
[2] ID: 19	13 060	-	-	-	-	-	-
[25]	10 560	1 510	730	1 240	940	380	-
[22]	10 000–16 000	-	460	-	-	-	640–680
Low	10 000	1 310	460	1 240	940	350	540
High	18 000	1 510	730	1 240	940	380	910

Ash	E_L	E_R	E_T	G_{LT}	G_{LR}	G_{RT}	ρ
[18]	-	-	-	-	-	401	798
[2] ID: 2	15 800	1 500	800	-	-	-	-
[22]	8 300–13 400	-	-	-	-	-	530–780

Oak	E_L	E_R	E_T	G_{LT}	G_{LR}	G_{RT}	ρ
[22]	10 000–13 000	-	-	-	-	-	650–720
[26] (comp.)	13 988	848	617	1 596	1 188	460	620–670
[26] (ten.)	9 508	1 348	810	1 600	1 190	460	620–670

Table 5.3: Compilation of mechanical parameters for various softwoods. [a)] 4% Moisture content (MC) [b)] 7% MC [c)] 12% MC [e)] 12% MC [f)] 8.1% MC [g)] 12.4% MC [h)] 10% MC [i)] 11.10% MC.

Spruce	E_{L}	E_{R}	E_{T}	G_{LT}	G_{LR}	G_{RT}	ρ
[2] ID: 1	10 300	690	410	-	-	-	-
[2] ID: 2	10 000	800	450	-	-	-	439–519
[2] ID: 3	-	-	-	-	-	-	450–529
[2] ID: 7	11 900	817	420	-	-	-	-
[2] ID: 10	12 800	625	397	-	-	-	-
[2] ID: 13	6 084–11 178	214–404	149–493	-	-	-	-
[2] ID: 17	10 700	710	430	-	-	-	-
[19]	10 991	716	435	682	693	49	390
[22]	8 300–13 000	-	440	-	-	-	370–400
-	-	-	-	-	-	-	-
-	-	-	-	-	-	-	-

Pine	E_{L}	E_{R}	E_{T}	G_{LT}	G_{LR}	G_{RT}	ρ
[2] ID: 4[a)]	16 500	970	-	-	-	-	590
[2] ID: 4[b)]	15 600	1 030	-	-	-	-	590
[2] ID: 4[c)]	15 500	970	-	-	-	-	590
[2] ID: 8	11 866–13 634	5 266–5 842	-	-	-	-	365
[2] ID: 19	11 520	1 000	650	-	-	-	-
[2] ID: 20[e)]	14 300	700	545	-	-	-	505
[2] ID: 20[f)]	15 621	804	682	-	-	-	520–530
[2] ID: 20[g)]	14 998	763	532	-	-	-	530–540
[2] ID: 20[h)]	16 300	1 100	570	-	-	-	550
[2] ID: 20[i)]	10 283	1994	994	-	-	-	505
[22]	10 000–12 000	-	460	-	-	-	450–500
-	-	-	-	-	-	-	-

6 Numerical modelling

This chapter covers the basics of the finite element method and introduces the software used in the dissertation, together with its scripting functionality. The different modelling approaches used in the dissertation are then introduced, together with their respective presumptions, advantages and disadvantages. Lastly, a convergence study on the mesh density is presented.

6.1 Finite element method

The CLT-panels were modelled using the finite element method (FEM), which is a numerical approach used to solve general differential equations in an approximate manner.

The finite element method is used for solving partial differential equations which describe a physical problem assumed to hold over a certain region which can be one-, two- or three-dimensional. To solve the problem, the entire region is split into smaller parts called finite elements. An approximation which describes how a variable change over each element can then be made. This approximation determines the behaviour of the element and is usually a linear or quadratic polynomial. Variables are determined in certain nodal points, often located at the boundary of each element, and then interpolated between these points with the approximations. After the behaviour of all elements has been determined, the elements can then be patched together, employing some specific rules, to model the entire region. With this region an approximate solution for the behaviour of the entire body can be attained. The collection of all elements is called a finite element mesh.

In other words, the finite element method typically involves dividing the considered region into a collection of subdomains, where each subdomain is represented by a set of element equations. The elements equations are then assembled into a global system of equations to determine the behaviour of the entire region.

A real physical problem has an infinite number of unknowns in-between the known nodal points, i.e. it is continuous. In the FE method, this continuous problem is instead discretized into a finite number of nodal points. The more degrees of freedom one introduces by refining the model, the more accurate the approximate solution becomes.

6.2 Software

Abaqus is a commercial software used for finite element analysis and computer-aided engineering [27], and was used to simulate the response of different CLT-panels for the work of this dissertation.

Python scripts were heavily utilised to construct FE-models in Abaqus in an efficient manner. Commands are issued internally by Abaqus/CAE after each operation performed in the graphical user interface. The Abaqus function *Macro Manager* allows the user to record Abaqus commands in a py.-file, where each command correlates to an interaction within Abaqus/CAE. By running the recorded py.-file with the Abaqus function *Run Script*, the macro reproduces the recorded sequence of interactions.

Commands were extracted after recording a sequence of interactions and adapted into Python scripts that after modifications yielded a highly parametric modelling process. This made it simple to construct any layer composition and geometry by changing a few values in the scripts. Parameters such as dimensions of the panel and material properties could also easily be modified. It was also possible to describe constraints between lamellas with the script which was very convenient as modelling these manually is a tedious process, especially for larger models. The Python scripts were also utilised to run several analyses in succession and extracting results, e.g. the natural frequencies and mode shapes of the panels.

6.3 Finite element approximations

Quadratic brick elements were used for the solid models. For the initial simulations, such as convergence studies and the pre-experimental numerical study, full integration was utilised, i.e. C3D20 elements according to the Abaqus naming convention. For the analyses conducted in Chapter 9, reduced integration was used, i.e. C3D20R elements, where the R denotes reduced integration. The reduced integration element uses $2 \times 2 \times 2$ integration points, in contrast to the full integration element which uses $3 \times 3 \times 3$ integration points. For the two-dimensional modelling, quadratic eight-node shell elements were used in Abaqus, i.e. S8R elements according to the Abaqus naming convention.

6.4 Finite element models

Three different modelling approaches were tested to determine the most appropriate approach for modelling CLT.

6.4.1 High-fidelity model

The most detailed model was the high-fidelity model, which was composed of solid elements, where all individual laminations were modelled and assembled, see Figure 6.1. The laminations were after assembly connected with tie-constraints on the top- and bottom surfaces of the laminations to mimic how CLT is manufactured, previously described in Section 3.2.

The high-fidelity model allowed for a high level of detail, such as modelling of gaps between boards and the possibility to apply different material properties for specific laminations in a layer. It was also possible to apply tie-constraints between adjacent laminations to create full interaction within the same layer. Glue could potentially have made its way in-between laminations during the manufacturing process, which in this model could be replicated with tie-constraints horizontally between laminations.

This level of flexibility does however come at a cost. For models with many surfaces bound together with tie-constraints, the computational demand quickly increases with the complexity of the model, resulting in increased computational time.

6.4.2 Layered model

The layered model was just like the high-fidelity model constructed with solid elements. Instead of several laminations per layer, one solid part was used for each layer, see Figure 6.2. The material orientations were defined for each individual layer. A comparison between the layered model and the fully tied high-fidelity model showed that both models produced similar natural frequencies, although the layered computed much faster, albeit not as fast as the composite model.

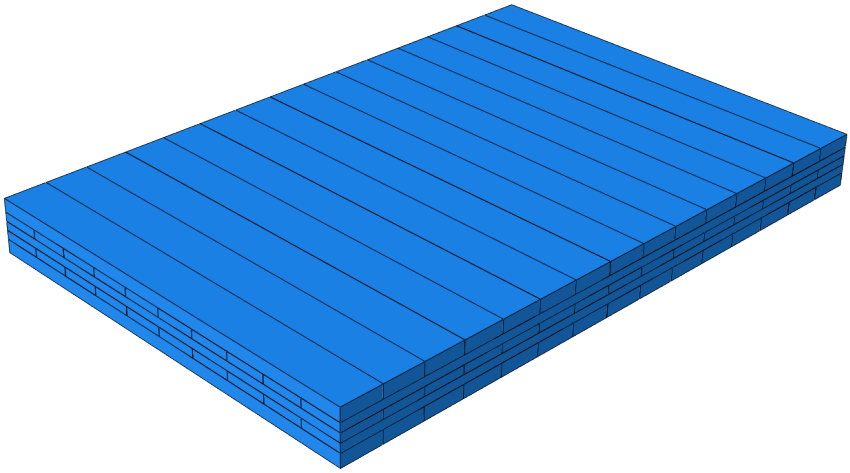

Figure 6.1: High-fidelity model.

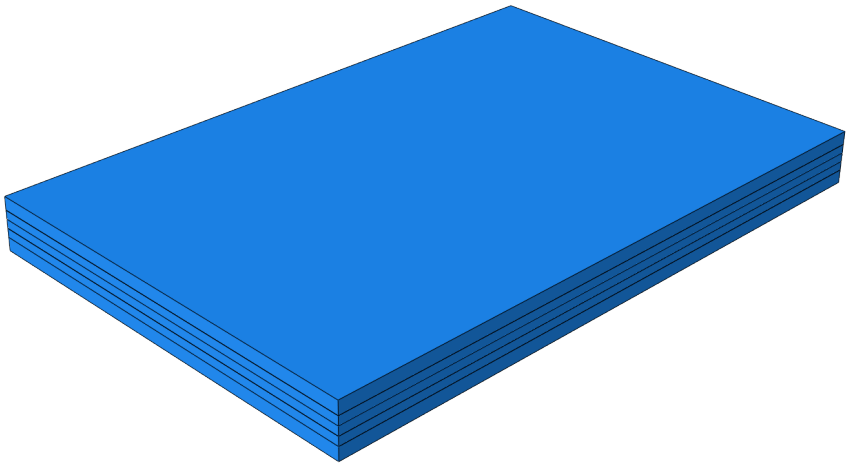

Figure 6.2: Layered model.

6.4.3 Composite model

In addition to the high-fidelity model and the layered model, a simpler two-dimensional composite model was constructed, see Figure 6.3. The composite model was modelled as a composite section using the Abaqus commands *Property* → *Create composite layup* for a 3D Planar-shell part. In the composite layup module, each layer is defined by its orientation, material properties and thickness. The composite model was by far the most efficient model regarding computational resources.

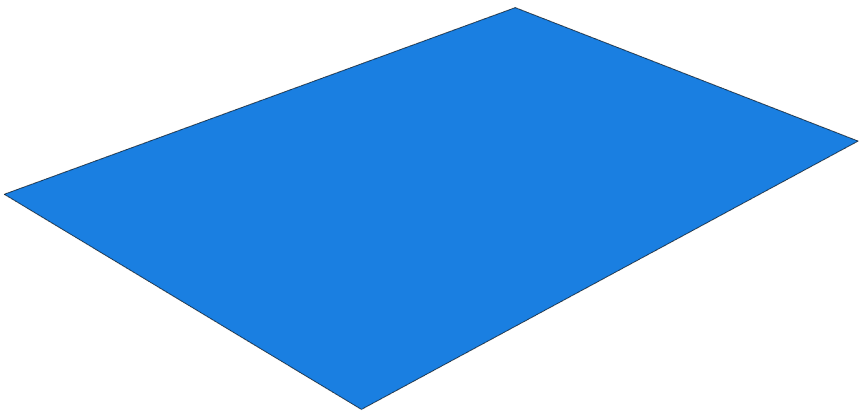

Figure 6.3: Composite model.

6.5 Mesh convergence analysis

A mesh convergence analysis was conducted to determine a suitable refinement of the mesh to use for the analysis with regard to precision and computational resources. The mesh convergence analysis was performed using the layered model with the same lay-up and dimensions as the tested CLT-panel, see Section 7.1. Modal analyses were performed for a range of mesh sizes. The natural frequencies of the first 12 modes from each considered mesh density were then compared to the natural frequencies of the most refined mesh to study the relative difference. The mesh size was deemed acceptable when two successive mesh sizes showed little variation in natural frequencies and the relative error compared to the finest mesh was low.

6.5.1 Elements per layer height

Up to three elements per layer height were tested to study how many elements were required per layer to accurately capture the modal behaviour. Quadratic elements (C3D20) were used for the evaluation and the mesh size in the horizontal plane were set to 50 mm. Figure 6.4 shows the relative difference for the natural frequencies of the first 12 modes. One element per layer height was sufficient to accurately capture the modal behaviour as the relative difference was less than 0.1% for all 12 modes. In addition, higher modes are more affected by the number of elements per layer height than lower modes.

6.5.2 Element size in horizontal plane

Mesh sizes ranging from 10 to 200 mm were tested. One element per layer height was used for the analysis based on the results from Section 6.5.1, which demonstrated that more than 1 per layer had minimal effect on the results when using quadratic

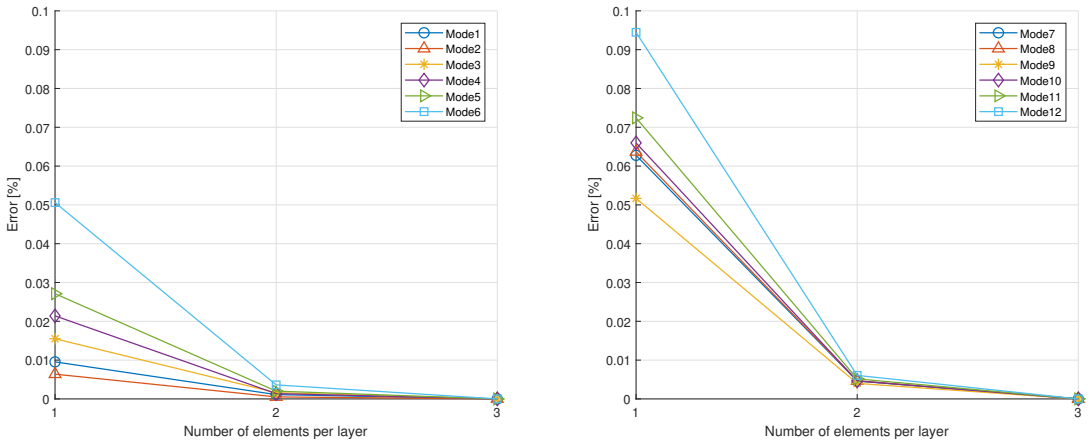

(a) Mode 1–6. **(b)** Mode 7–12.

Figure 6.4: Results from convergence analysis studying the effect on the number of elements per lamella height

elements. Figure 6.5 shows the relative difference for the natural frequencies of the first 12 modes. The relative error is not altered much as the mesh size is reduced below 100 mm, especially for lower modes. As with the convergence analysis of the number of elements per layer height, higher modes are generally more affected by change in mesh size than lower modes.

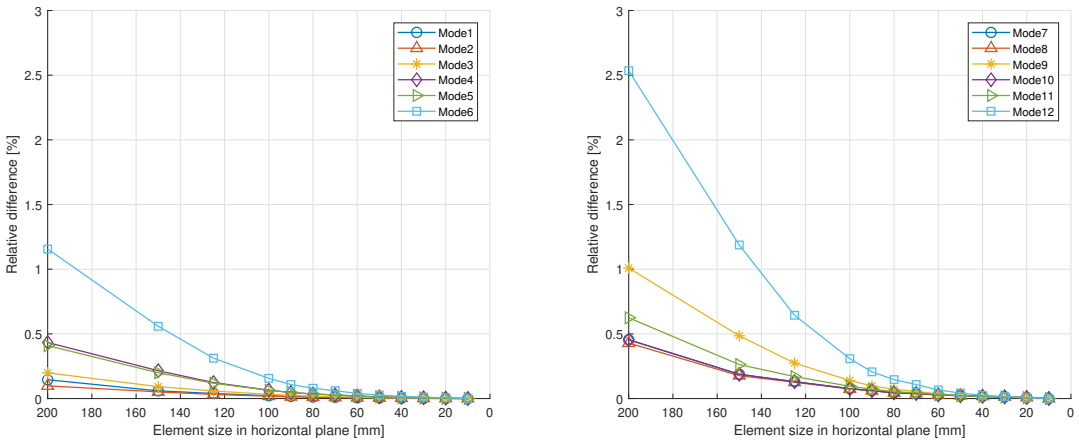

(a) Mode 1–6. **(b)** Mode 7–12.

Figure 6.5: Results from convergence analysis studying the effect of mesh size in horizontal plane.

7 Experimental approach

This chapter covers the experimental approach used to determine the natural frequencies, mode shapes, and damping of a real CLT panel. This includes a pre-experimental numerical study to design the experimental analysis. Governing theory of experimental modal analysis (EMA) is also included. The purpose of the experimental testing is to produce experimental data to determine the most appropriate modelling approach out of the three presented in Chapter 6. In addition, the experimental data was also used as a reference in Chapter 8 for the model validation.

7.1 Test specimen

A CLT-panel consisting of five layers, see Figures 7.1 and 7.2, was used as the test specimen. The outermost layers and the middle layer were orientated in the transverse direction in relation to the length of the panel. The remaining layers were oriented longitudinal in relation to the length of the panel. The dimensions of the panel were measured to $1.5 \times 1 \times 0.12$ m^3 and it weighed 86.9 kg. Based on the weight and the measured dimensions, the mass density was 479 kg/m^3.

7.2 Pre-experimental numerical study

A pre-experimental numerical study was conducted to design the experimental modal analysis. The models described in Chapter 6 were used for two objectives in the pre-experimental study: determining the frequency range of interest and the suitable number of measurement points and their positioning, i.e. the measurement grid.

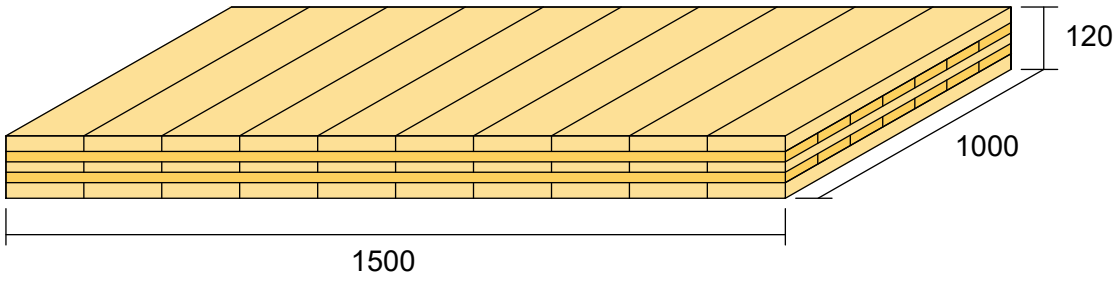

Figure 7.1: Geometry of the test specimen. Dimensions in mm.

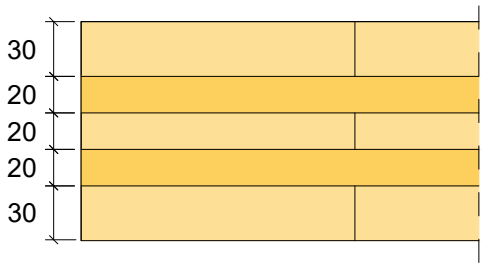

Figure 7.2: Illustration of the layer height of the test specimen. Dimensions in mm.

7.2.1 Determination of frequency range

100 Hz is previously well established as an upper limit of interest for what frequencies humans may perceive as disturbing. In addition, humans are more sensitive to low frequency noise ranging from roughly 2–8 Hz. Accordingly, a frequency range from 0.5–100 Hz was deemed reasonable for the pre-experimental numerical study. The lower limit 0.5 Hz was chosen to omit rigid body modes from the analyses.

The frequency range of interest for the experimental modal analysis was determined by comparing the mode shapes of two numerical models. One larger CLT-panel and one modelled after the test specimen panel. The dimensions of the larger CLT-panel were chosen arbitrarily to $6 \times 2.4 \times 0.15$ m^3. It consisted of five layers with a thickness of 30 mm each. The laminations of the outermost layers and the middle layer were orientated in the longitudinal direction, and the remaining layers in the transverse direction. A numerical modal analysis was then conducted, where modes appearing in the range 0.5–100 Hz were identified.

Consequently, a modal analysis was conducted on a FE-model of a CLT-panel with the same geometry as the test specimen. By identifying modes appearing in both models, and their corresponding natural frequencies, a frequency range of 0–500 Hz was deemed appropriate for the experimental modal analysis.

7.2.2 Determination of measurement grid

It is crucial to differentiate mode shapes from each other in modal analysis. In numerical analyses this is rarely a problem, due to the high level of discretization (i.e. mesh density) usually being high enough for no modal mixing to occur. However, in EMA, the test specimen might be discretized by as little as 5–10 measurement points depending on the geometry. Thus, by examining various sets of measurement grids numerically, with the use of an AutoMAC, a grid which could accurately depict the different mode shapes of interest could be determined.

Several different grids were examined, all which were uniform, or as uniform as the measurement grid allowed for. Sets with 9, 15, 18, 21, 24 and 30 nodes were created and examined. A maximum AutoMAC value of 7% was acquired for the grid with 30 measurement points. The sets with 18, 21 and 24 measurement points all yielded similar results, circa 12% as a max AutoMAC value. This was deemed as sufficiently accurate for a frequency range in-between 0 and 500 Hz. The AutoMACs for the measurement grid with 9, 15 and 18 nodes, respectively, are shown in Figure 7.4.

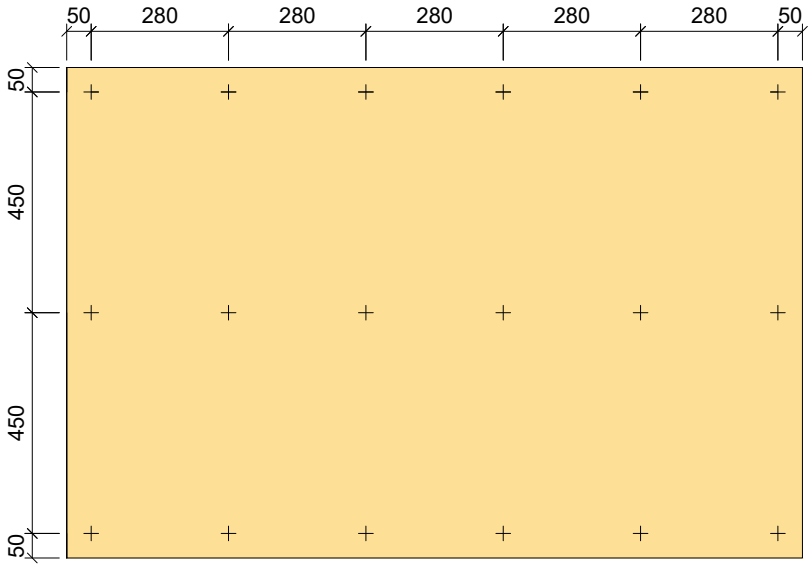

Figure 7.3: The measurement grid consisting of 18 evenly distributed points. Dimensions in mm.

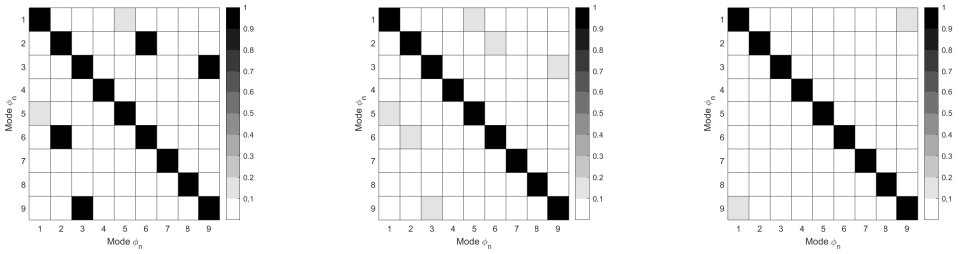

(a) **(b)** **(c)**

Figure 7.4: CrossMACs for three different measurement grids: 12 (a), 15 (b) and 18 (c) measurement points, respectively. Both the y-axis and the x-axis shows the mode number of the experimental model.

7.3 Experimental modal analysis

EMA was conducted to extract the natural frequencies, mode shapes and modal damping ratios of the CLT-panel. The flowchart in Figure 7.5 shows the main parts of EMA. These will be described further in this section.

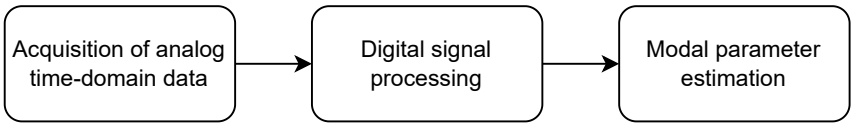

Figure 7.5: Flowchart of main parts of experimental modal analysis.

7.3.1 Acquisition of analogue time-domain data

To acquire analogue time-domain data, some type of test needs to be conducted. Generally, there are three types of modal tests: single input-multiple output, multiple input-single output, and multiple input-multiple output. For the experimental testing a multiple input-single output (MISO) test was conducted. For a MISO test, several pieces of equipment are needed:

- An excitation source, e.g. an impact hammer.
- An output transducer, e.g. an accelerometer.
- A dynamic analyser, e.g. a computer with data acquisition hardware, signal analysis software and modal analysis software.

An impact hammer (Brüel & Kjær Type 8208) was used to excite the structure in all measurement points and to measure impact forces during testing. The vibrations were measured with one piezoelectric accelerometer (Brüel & Kjær Type 4507-001) that was glued to the CLT at one of the corner measurement points, see Figure 7.3. Brüel & Kjær Type 3160-A-042 was used for data acquisition and BK Connect 2019 was used for signal processing.

7.3.2 Digital signal processing

After the analogue data has been acquired the data needs to be processed in a dynamic analyser. An important factor in digital signal processing is the ordinary coherence, which is the quotient between the input signal and the output signal. If there is no noise occurring, the coherence is equal to 1, i.e. the input is equal to the output. When performing the EMA the coherence was considered in BK connect for each measurement point. Each measurement point was excited three times, for which the average coherence was calculated. If the coherence was not sufficiently close to 1 for any given hammer hit, the hammer hit was repeated.

7.3.3 Modal parameter estimation

The modal parameter estimation is the final step in the EMA, where the different modal parameters can be determined: mode shapes, natural frequencies, and damping ratios. This is usually conducted by the means of curve-fitting FRFs. FFTs transform the analogue data from the time-domain to the frequency-domain.

The 18 FRFs obtained (one from each measurement point, see Appendix A), were curve-fitted both in BK Connect and in Matlab to yield stabilisation diagrams. The curve-fitting method used by BK Connect was the z-rational fractional polynomial method, whereas the method used in Matlab was the least squares complex exponential algorithm and the least square rational functional estimation method.

To explain what the stabilisation diagrams visualises it is first necessary to present some theory on the subject. FRFs are functions that consists of an amplitude and a

phase and can thus be expressed in a complex coordinate system. In this coordinate system, the amplitude has both a real and an imaginary part and the phase is the angle between said parts. The FRFs introduced in Equation 4.17 is in EMA usually expressed in partial-fraction (pole-residue) format [17]:

$$H_{u/p}(f) = \frac{A}{i\omega - \lambda_1} + \frac{A^*}{i\omega - \lambda_1^*} \tag{7.1}$$

where A and A^* are the *residues*, from which the mode shapes can be extracted. λ_1, λ_1^* are the *poles*, from which the eigenfrequencies, ω_n, and damping ratios, ζ, can be acquired:

$$\lambda_1, \lambda_1^* = -\zeta\omega_n \pm i\omega_n\sqrt{1-\zeta^2} = -\zeta\omega_n \pm i\omega_d \tag{7.2}$$

where ω_d is the forcing frequency.

EMA can be based on either real mode shapes or complex mode shapes. Real mode shapes implies that the structure is proportionally damped and that the dofs are vibrating in phase with each other. Complex mode shapes instead imply non-proportional damping (which is the case for most real structures) and dofs vibrating out-of-phase. In the dissertation, the modal parameter estimation has been based on the complex modes.

By curve-fitting the FRFs to Equation 7.1, modal parameters can be estimated. Iterations are performed with an increasing number of included modes, causing the pole values of the strictly physical eigenmodes to be very "stable", that is, they appear at an almost constant frequency. Obviously, whether the poles are stable or not is arbitrary and has to be defined. A common stability criterion according to [28] when comparing higher model order properties to a lower model order properties is the following deviating values:

- 1% for frequency stability
- 5% for damping stability
- 2% for eigenvector stability

The first two are what the curve-fitting methods provided in Matlab uses by default.

7.4 Experimental setup

The experimental test setup is shown in Figures 7.6 and 7.7. The full setup is illustrated in Figure 7.6a where the suspended CLT-panel can be seen together with the computer and interface setup.

As can be seen in Figure 7.6b, duct tape was utilised to minimise slip between the elastic bands and the CLT panel. Duct tape was also used to fasten the cable from the accelerometer and thus removing potential disturbance from the cable flailing against the panel, see Fig 7.6c. The elastic bands were connected to carbine hooks, which in turn were attached to the roof with steel wires, see Figures 7.7a and 7.7c.

7.4.1 Support conditions

Due to difficulty regarding support conditions and their impact on a structure's modal behaviour, the choice of these became an iterative process. Initially, simply supported support conditions tried to be reproduced by using wooden joists as supports. At one support rubber was placed in-between the panel and the support to hinder movement in the longitudinal direction. At the other support, several layers of plastic were placed to emulate a roller support. A problem with these conditions that became apparent after the first EMA was the non-rigidity of the supports, as the supported edges of the panel moved vertically. This is inconsistent with how these supports would be modelled in a FE software, where the nodes at the support would be prevented to move completely vertically. Consequently, these support conditions were deemed not suitable.

The next iteration of support conditions consisted of a rubber carpet that was folded twice and placed under each longitudinal end of the panel. The aim was to simulate free-free conditions, and thus not hinder movement in any direction. These conditions were emulated to a certain degree. However, the complexity for certain modes, and especially the higher modes, was fairly high.

The support conditions used for the third iteration is a well-established method, recommended in [17]. The aim was to emulate free-free conditions by suspending it in the air with elastic bands (see Figure 7.6a). These bands yielded the best results out of the three sets of support conditions investigated: in contrast to the other two support conditions, using bands during the measurements resulted in little modal complexity for the first 6 modes, the coherence between hammer strikes was acceptable, and sharp peaks in the stabilisation diagrams were obtained.

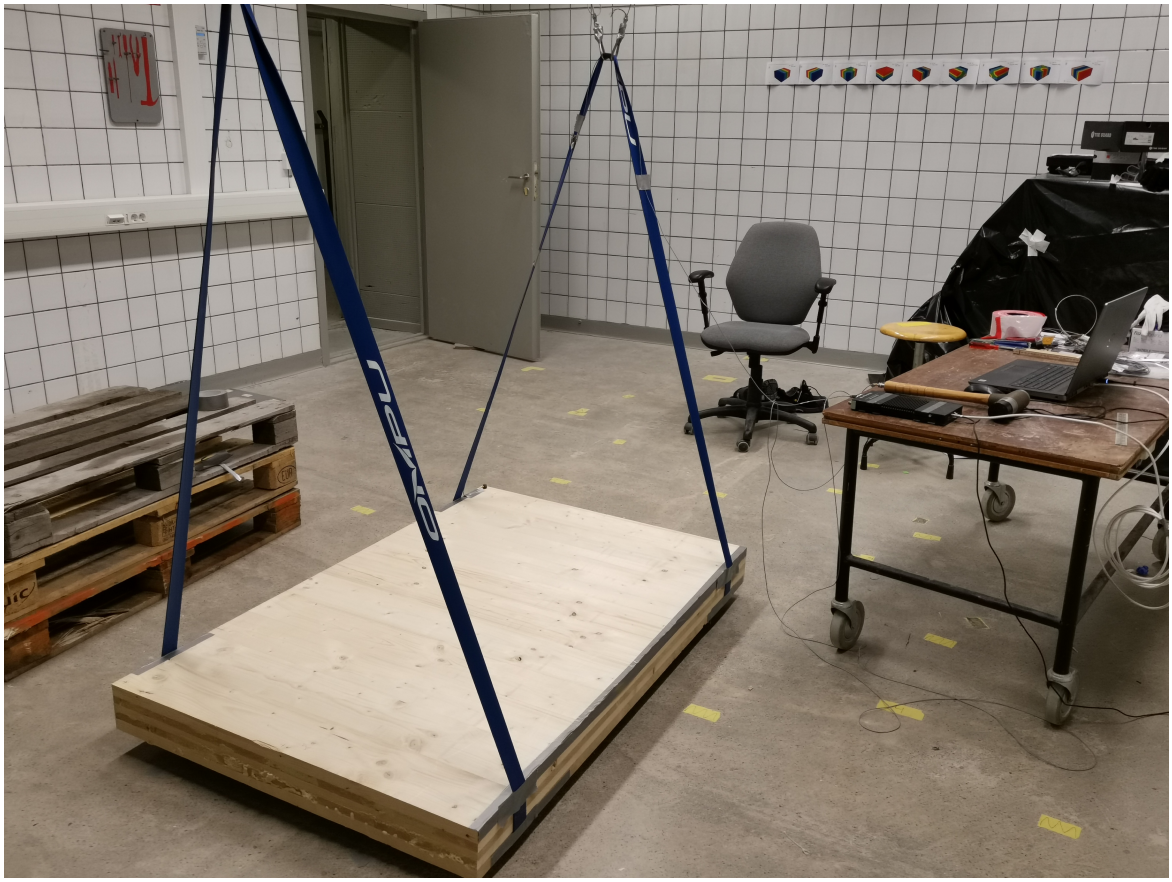

(a)

(b)

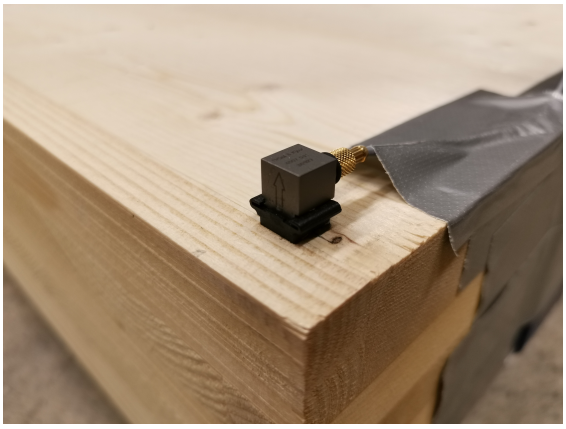

(c)

Figure 7.6: Experimental set–up.

(a)

(b)

(c)

Figure 7.7: Experimental set–up.

7.5 Experimental results

The natural frequencies determined with BK Connect are shown in Table 7.1, together with their damping ratio and complexity. Figure 7.8 shows the corresponding mode shapes. The experimental testing yielded values for the first 9 eigenmodes.

Table 7.1: Natural frequencies f_n, modal damping ratios ζ_n and complexity I acquired from the EMA.

Mode	f_n[Hz]	ζ_n [%]	I [%]
1	84.24	1.60	1.7
2	102.21	0.76	0.2
3	185.53	1.09	1.1
4	240.48	1.54	1.7
5	319.43	1.01	1.1
6	401.54	0.91	2.9
7	428.17	1.34	12.9
8	441.25	1.10	19.8
9	467.72	1.00	38.3

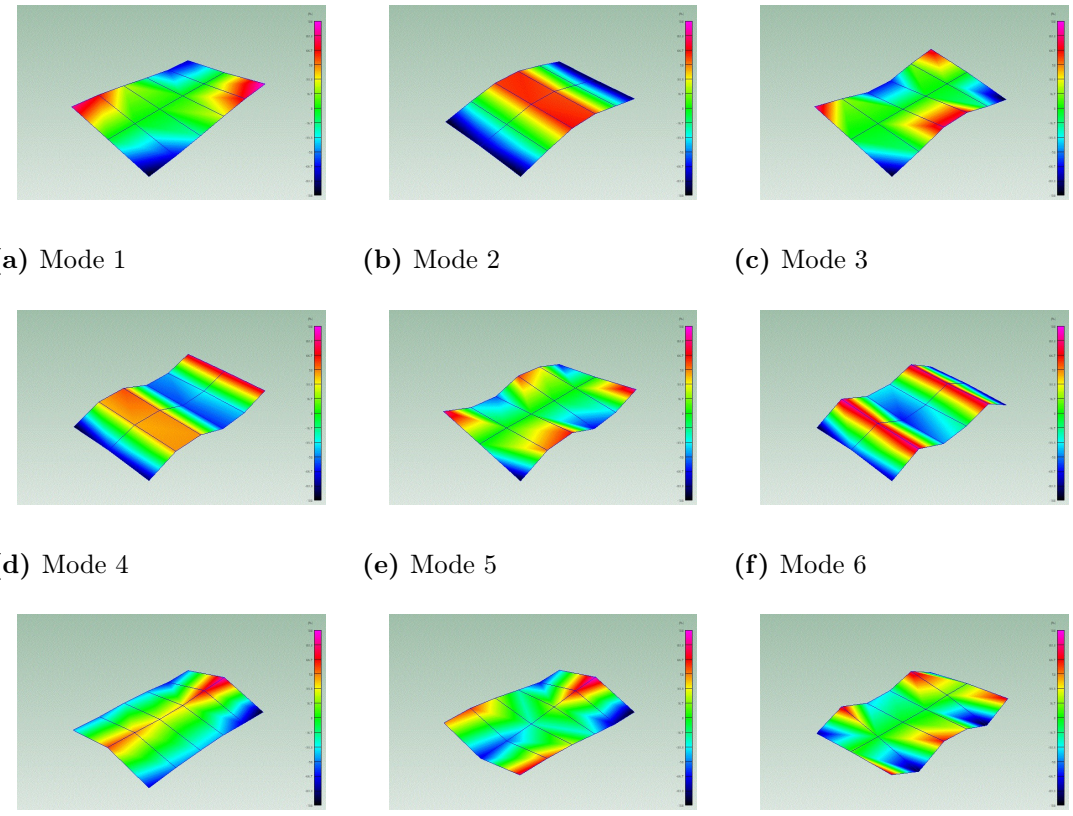

(a) Mode 1 **(b)** Mode 2 **(c)** Mode 3

(d) Mode 4 **(e)** Mode 5 **(f)** Mode 6

(g) Mode 7 **(h)** Mode 8 **(i)** Mode 9

Figure 7.8: Mode shapes of the first 9 modes from the experimental testing.

In Figure 7.9 the stabilisation diagram calculated in Matlab is shown. Values only stable in frequency are plotted as blue circles. Values not stable in frequency are plotted as blue dots. Values stable in both frequency and damping are plotted as pluses. The averaged response function can be seen as the red line. It can be seen that the first six modes are fairly stable, whereas the stability is not quite as good for the three highest modes. The same can be seen in the stabilisation diagram obtained directly from BK Connect, see Figure 7.10. The first six modes are very vertical, meaning the natural frequencies are occurring at the same frequency every iteration, whereas the three last modes start to lose some stability.

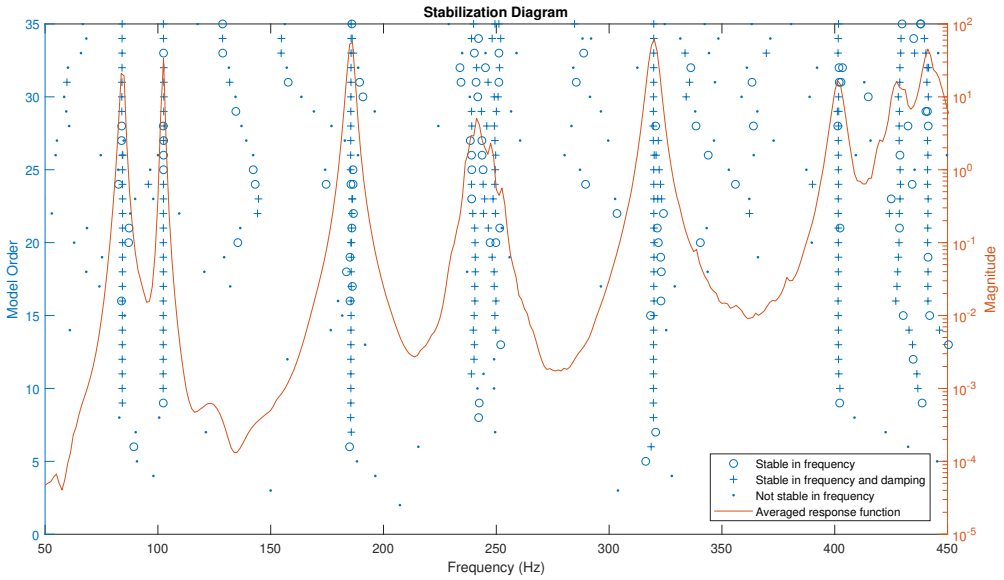

Figure 7.9: Stabilisation diagram calculated in Matlab with the least–square rational functional method. The model order (number of iterations) are on the left-most y-axis (blue) and the magnitude are on the right (red).

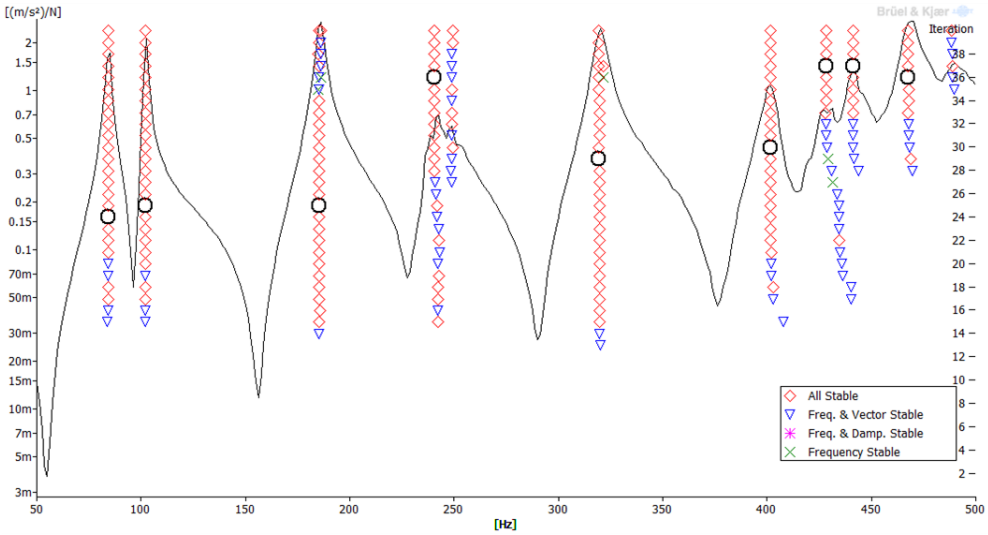

Figure 7.10: Stabilisation diagram calculated in BK Connect with the z-rational fractional polynomial method. The model order (number of iterations) are on the right y-axis and the magnitude on the left axis.

7.6 Comparison between experimental results and different modelling approaches

Figure 7.12 shows the natural frequencies of the three different models introduced in Chapter 6, using the same geometry and lay-up as the tested CLT panel and C24 material parameters, see Section 7.1. A mesh size of 50 mm and 1 element per layer height were used with quadratic elements for the analyses. As can be seen from the results, all models produce similar results, albeit with some differences. The layered model and the high-fidelity model with horizontal tie-constraints replicated the experimental results the best without any modifications. The layered model was however much quicker than the high-fidelity model. It was thus chosen as the model to be used for the case study, see Chapter 9.

The high-fidelity model does not assume full interaction between individual laminations within the same layer. Adding tie-constraints between adjacent laminations generally increased the natural frequency for all modes but had the largest effect on the twisting modes. A potential explanation for this is that the rotational stiffness is increased when stresses can be transferred between adjacent laminations and not only between layers.

For the composite model, full interaction between individual boards is assumed. This also holds true for the layered model. This became further evident when comparing the results from the modal analyses of the high-fidelity model with horizontal tie–constrains, with the layered model, as both produce almost identical results.

Shell elements are used for the composite model, meaning that all finite element calculations and integrations are performed along a single reference plane. Thus, the radial elastic modulus does not impact the composite model, contrary to the high-fidelity model and the layered model. In addition, shell theory assumes thin structures which might not be applicable for the tested panel, since it is relatively thick in relation to its length and width. If the tests were performed on a larger plate, the difference between the layered and the composite model could potentially be smaller.

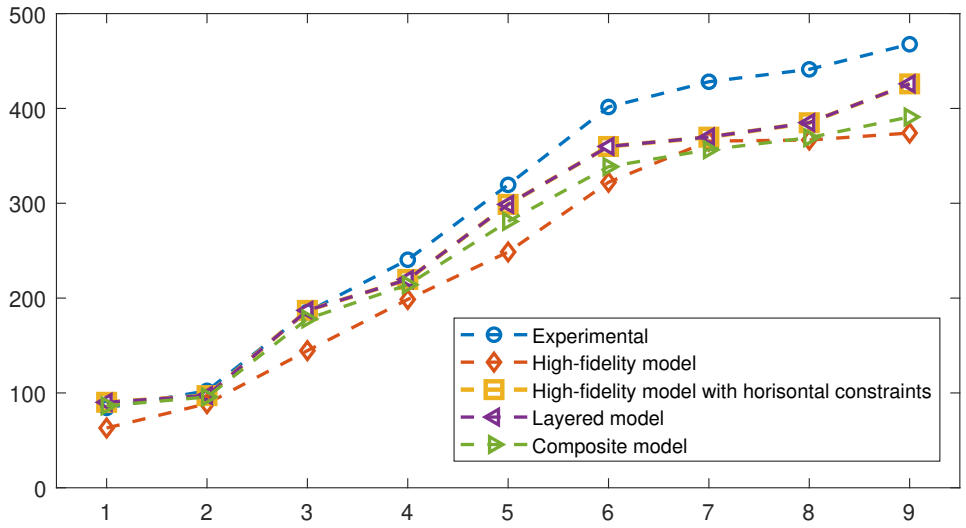

Figure 7.11: Comparison between the experimental natural frequencies and the natural frequencies obtained with the different modelling approaches.

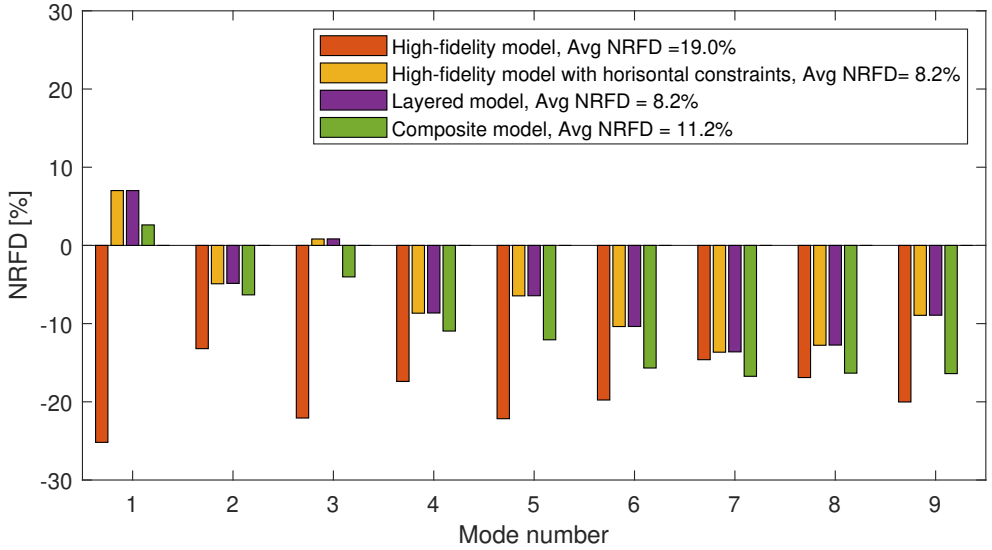

Figure 7.12: Comparison between the experimental natural frequencies and the natural frequencies obtained with the different modelling approaches.

8 Model validation

This chapters covers the general approach for validating the layered model described in Chapter 6 and calibration of the panels material parameters according to the experimental results in Chapter 7. In addition, the difference between the experimental results and the post-calibrated model is presented. The purpose of the chapter is to validate the modelling approach and thus confirm that the model could mimic a real panels behaviour arbitrarily well, using reasonable material parameters. It is rather difficult to draw this arbitrary line, which is why a rather extensive discussion is held on this subject later on.

8.1 General validation approach

To cite [29], model validation is "The process of determining the degree to which a model is an accurate representation of the real world from the perspective of the intended uses of the model." In engineering, it is of utmost importance to validate models, otherwise the result from simulations holds little to no value. The approach for model validation in structural dynamics described in [30] is what has been used in this dissertation. It presents the following step-by-step process for validating models.

1. **Specifying the purpose of the model**

   Determination of the model's application is important since all the following decisions is shaped by the fundamental use of the model. Thus, before modelling is initiated, the purpose and the use of the model has to be defined. In the dissertation, the purpose is defined in Chapter 1: the purpose of the model is to evaluate dynamic behaviour of cross-laminated timber panels.

2. **Specifying validation experiments**

   Validation experiments are intended to generate data for the model validation. The experimental modal analysis described in Chapter 7 was used as validation experiments. The analysis gave information about the natural frequencies, mode shapes and modal damping for the first nine modes of the tested CLT-panel.

3. **Specifying the conceptual model**

   The conceptual model holds all the fundamental modelling assumptions. Here, the following fundamental conceptual assumptions were made:

   - Linear-elastic response was assumed.
   - The panel was assumed to be homogenous in the sense that all individual laminations posses the same material properties.
   - The material was assumed to be orthotropic.

4. **Specifying the mathematical model**

   The mathematical model is the partial differential equations that can be derived analytically, i.e. the equations of motion. This model is not derived specifically in the dissertation, instead the reader is referred to [31].

5. **Specifying the computational model**

   This step introduces approximate numerical solutions to the previously mentioned mathematical models. As per the previous step, these are not explicitly derived in the dissertation, however the FE equations are introduced in Chapter 4. For a complete treatment, the reader is referred to [12].

6. **Specifying the physical system response measures of interest**

   The response measures are quantities that is to be measured. Here, it was the vertical accelerations occurring due to hammer excitation on the panel. These were measured with a one-dimensional accelerometer as described in Chapter 7.

7. **Specifying the validation metrics**

   The validation metrics are the mathematical evaluation methods for comparing experimental and numerical data, and thus evaluating the model's validity. The used validation metrics are introduced in Chapter 4: MAC (Section 4.6.2) and NRFD (Section 4.6.3).

8. **Specifying the domain of comparison**

   The domain of comparison refers to what types of values will be compared and in what range those values lie. The comparison domains were specified in Chapter 7 to the modal domain and a frequency range of 0–500 Hz.

9. **Specifying the calibration experiments**

   The calibration experiments are used for determining material parameters. Here, the chosen validation and calibration approach has been majorly influenced by the approach used in [24]. It consisted of three subsequent steps:

   - Sensitivity analysis.
   - Establishing an initial Newton optimisation guess.
   - Newton optimisation.

   These will be explained in depth later in this chapter.

10. **Specifying the adequacy criteria**

    The adequacy criteria decide how accurately the real physical phenomena should be modeled. It is desirable to mimic reality as accurately as possible, however this is limited by the introduced assumptions and simplifications made in the conceptual, mathematical, and computational models. In addition, computational demand is a limiting factor.

8.1.1 Newton optimisation

Newton optimisation was utilised for calibration of the model. To provide the reader with a fundamental understanding of this method of optimisation, the algorithm is thus derived in this section.

Consider a twice differentiable function f, which is assumed to be sufficiently smooth and for which a minimum is sought:

$$f = \mathbb{R}^n \to \mathbb{R} \tag{8.1}$$

By utilizing Taylor expansion around a current point $\boldsymbol{x}^{(k)}$, it is possible to acquire a quadratic approximation of the function f, if the terms of cubic order or higher are neglected. This yields:

$$f(\boldsymbol{x}) = f(\boldsymbol{x}^{(k)}) + (\boldsymbol{x} - \boldsymbol{x}^{(k)})\boldsymbol{g}^{(k)} + \frac{1}{2}(\boldsymbol{x} - \boldsymbol{x}^{(k)})^T \boldsymbol{H}(\boldsymbol{x} - \boldsymbol{x}^{(k)}) \triangleq q$$

where $\boldsymbol{g} = \boldsymbol{\nabla} f(\boldsymbol{x_t})$ is the gradient and $\boldsymbol{H} = \boldsymbol{\nabla}^2 f(\boldsymbol{x_t})$ the Hessian matrix. Differentiating with respect to $\boldsymbol{x}$ in conjunction with first order necessary conditions yields

$$\mathbf{0} = \nabla q(\boldsymbol{x}) = \boldsymbol{g}^{(k)} + \boldsymbol{H}(\boldsymbol{x}^{(k)})(\boldsymbol{x} - \boldsymbol{x}^{(k)})$$

and if the Hessian matrix is positive definite, i.e.:

$$\boldsymbol{H}(\boldsymbol{x}^{(k)}) > 0$$

the function q achieves a minimum at

$$\boldsymbol{x}^{(k+1)} = \boldsymbol{x}^{(k)} - \boldsymbol{H}(\boldsymbol{x}^{(k)})^{-1}\boldsymbol{g}^{(k)}$$

Thus, the algorithm assumes the form shown in Algorithm 1.

Algorithm 1 Newton optimisation

Initiate: $\boldsymbol{x}^{(0)}$, steplength, tolerance
while steplength $\geq$ tolerance **do**
  Calculate: $\boldsymbol{H}^{(k)}, \boldsymbol{g}^{(k)}$
  $\boldsymbol{\Delta x} = -\boldsymbol{H}^{-1}\boldsymbol{g}^{(k)}$
  $\boldsymbol{x}^{(k+1)} = \boldsymbol{x}^{(k)} + \boldsymbol{\Delta x}$
end while

A drawback with Newtons method is that there is no guarantee that the values in the iterations are descending to a minimum. If the first guess is not close enough to the minimum, the iteration might instead ascend, or the global minimum might not be found. Thus, it is important to establish a qualified first guess. In addition, due to the numerical nature of the model, it is difficult to determine the first and second order derivatives analytically, however they can instead be determined numerically according to the central difference method:

$$\frac{\partial f}{\partial x_1} = \frac{f(\boldsymbol{x} + \Delta\boldsymbol{x}) - f(\boldsymbol{x} - \Delta\boldsymbol{x})}{\delta} \tag{8.2}$$

$$\frac{\partial^2 f}{\partial x_1 \partial x_2} = \frac{f(\boldsymbol{x} + \Delta\boldsymbol{x}) - 2f(\boldsymbol{x}) + f(\boldsymbol{x} - \Delta\boldsymbol{x})}{\delta^2} \tag{8.3}$$

The objective function, f, i.e. the function to minimise, was chosen as the sum of the squared NRFD values for frequencies of interest:

$$f = \sum_{k=1}^{N} \left(\frac{f_{num} - f_{exp}}{f_{exp}}\right)^2 \tag{8.4}$$

where f_{num} denotes the numerically obtained natural frequency and f_{exp} the experimentally obtained natural frequencies. N is the number of modes included in the calibration.

8.2 Model calibration

This section covers the calibration process which was divided into three parts: sensitivity analysis, establishing an initial guess for Newton optimisation, and Newton optimisation.

8.2.1 Sensitivity analysis

To avoid unnecessary calibration of all material parameters, a sensitivity analysis was conducted to single out the most influential ones. Each parameter was varied individually and its influence on the modal order and natural frequencies was studied with CrossMACs and NRFDs. The intervals used for the material parameters were determined as a plausible range from the various collected stiffness parameters in Chapter 5. The lower and upper limits of the parameters are shown in Table 8.1, together with the reference values which were based on timber strength class C24. Five values were studied for each parameter.

Table 8.1: Lower and upper limits of material parameters for the sensitivity analysis, and the references values used. Moduli in MPa and mass density in kg/m^3.

	E_L	E_R	E_T	v_LR	v_LT	v_RT	G_LT	G_LR	G_RT	ρ
Lower limit	7 000	200	200	0.35	0.35	0.25	400	400	25	300
Upper limit	17 000	2 000	1 000	0.50	0.50	0.40	1 800	1 800	400	800
Ref. values	11 000	470	470	0.48	0.42	0.28	470	470	49	420

Effect on mode order

The CrossMACs showed that different values of E_T, v_LR, v_LT, v_RT, G_LR and ρ did not affect the mode order, and thus those CrossMACs are not included in the dissertation. E_L, E_R, G_LT and G_RT did however affect the mode order.

The effect on mode order of varying the longitudinal elastic modulus, E_L, is shown in Figure 8.1. The effect is not very large, except for the lowest value which causes three modes to shift compared to the reference model. In addition, the shift between modes 6 and 7 is not unanimous as can be seen by the higher MAC-value for mode 7.

The tangential elastic modulus, E_T, had a larger impact on the mode order than E_L, see Figure 8.2. For the first two values there are no deviation in mode order, however, for the third value modes 6 and 7 are switched, in addition to modes 9 and 10. For the two higher values, mode 6 has taken the place of mode 8 and mode 7 and 8 has taken the place of modes 6 and 7. The shift for modes 9 and 10 is still apparent.

The longitudinal shear modulus, G_LT, has a fairly large impact on the mode order for the three highest values, see Figure 8.3. Modes 1 and 2 are shifted for value 3, 4 and 5. An additional mode shift is introduced for value 4 and 5 where modes 3 and 4 are also shifted.

For the rolling shear modulus, G_RT, the impact on the mode order is rather minor, see Figure 8.4. Here, only the lowest value impacts the mode order. In addition, modes 9 and 10 are shifted.

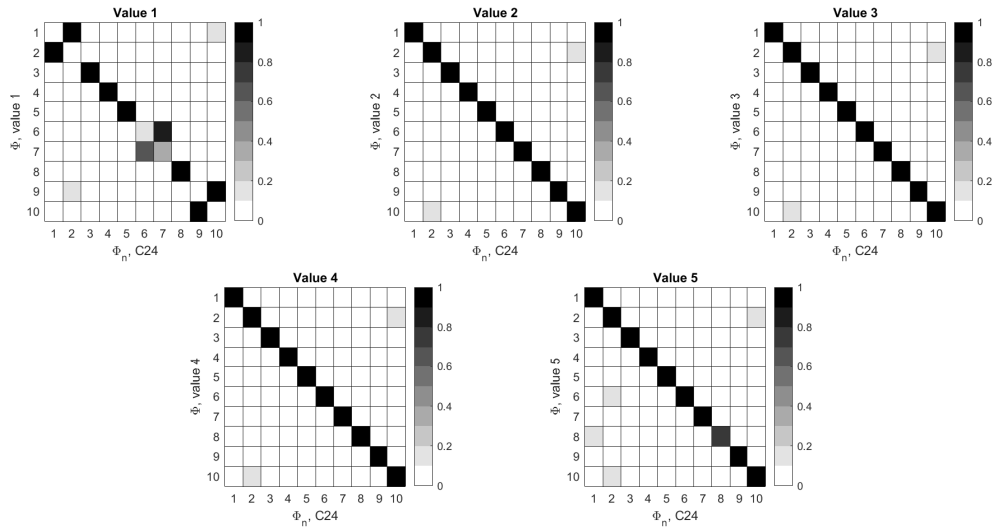

Figure 8.1: CrossMACs between C24 and different values of E_{L} according to Table 8.1.

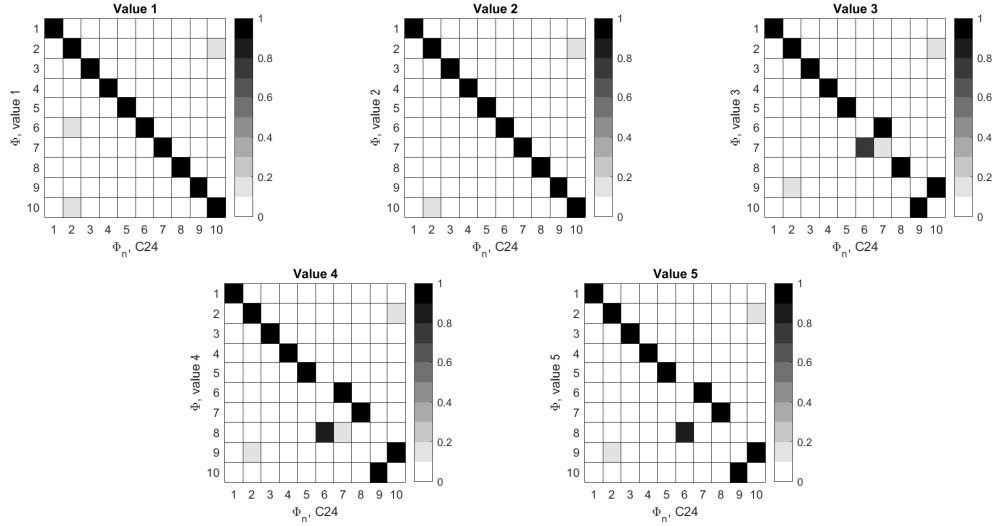

Figure 8.2: CrossMACs between C24 and different values of E_{T} according to Table 8.1.

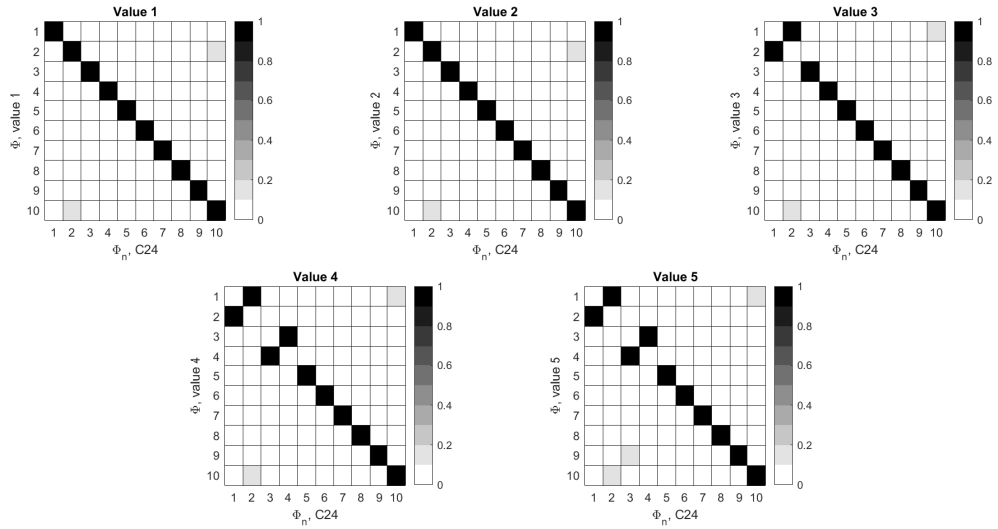

Figure 8.3: CrossMACs between C24 and different values of G_{LT} according to Table 8.1.

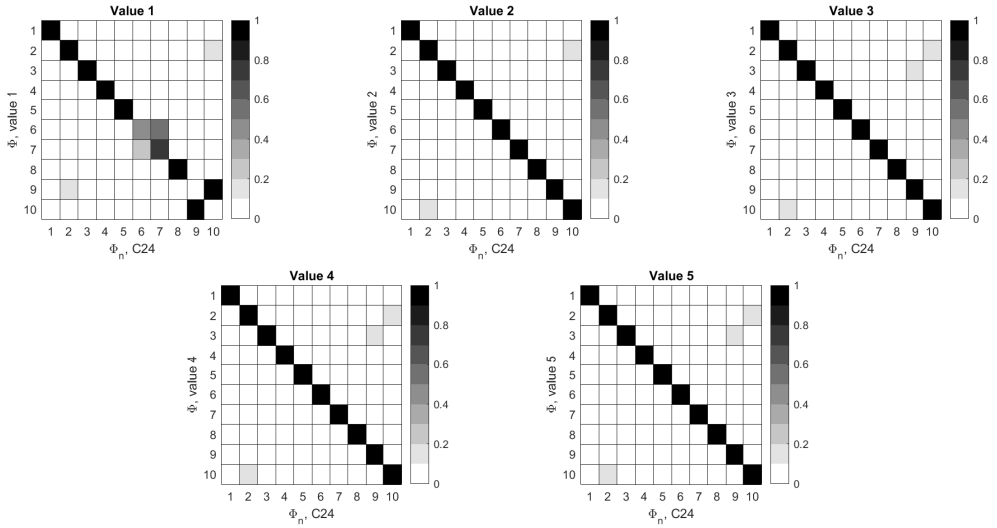

Figure 8.4: CrossMACs between C24 and different values of G_{RT} according to Table 8.1.

Effect on natural frequencies

In Figure 8.5, the NRFDs from the sensitivity analysis is shown. It should be noted that the previously explained shifts in mode order have been considered in these NRFDs, to only compare the natural frequencies of the same modes. In addition, only the parameters significantly affecting the NRFDs are shown. E_{L}, E_{R}, G_{LT}, G_{RT} and ρ were the parameters that had a major impact on the frequencies.

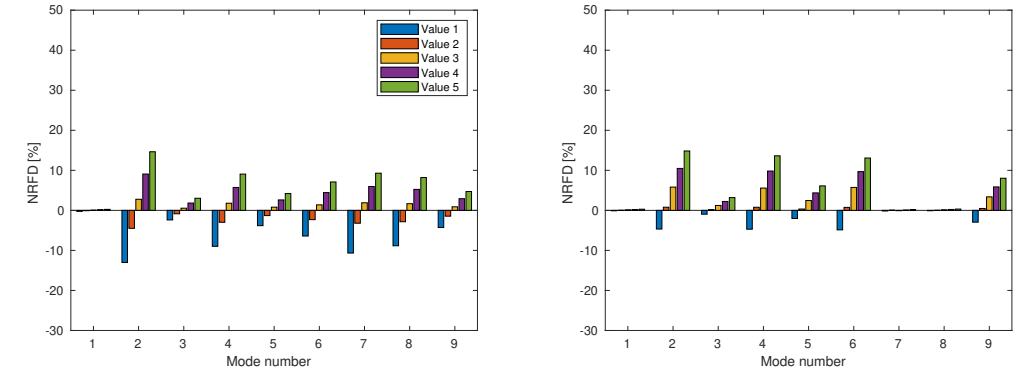

(a) E_{L} **(b)** E_{T}

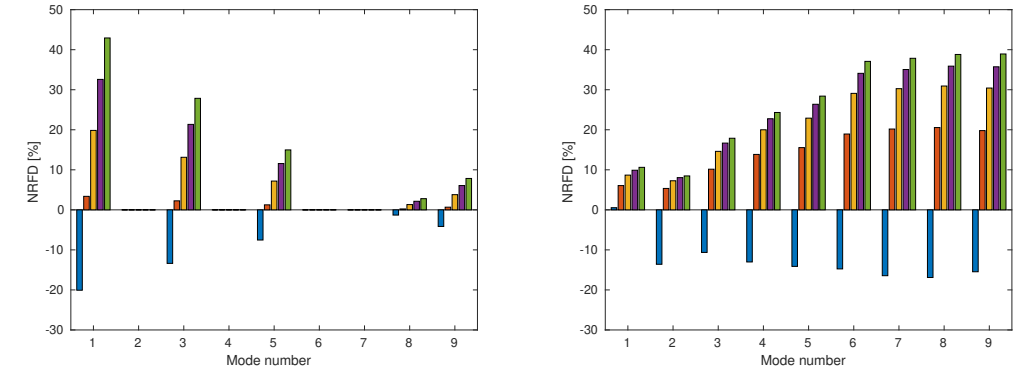

(c) G_{LT} **(d)** G_{RT}

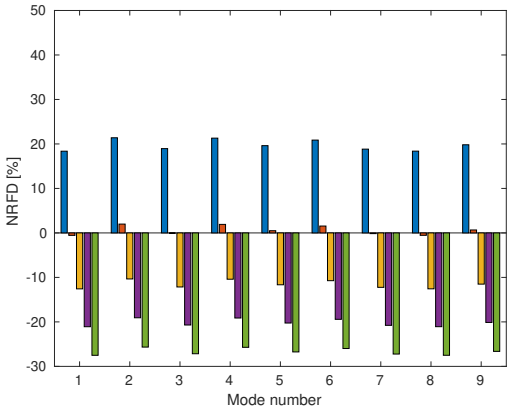

(e) ρ

Figure 8.5: NRFDs for the five parameters that had the largest effect on the frequencies in the sensitivity study. Remaining parameters had an impact of less than a few percent and are thus not shown. Five values were tested for each parameter, with C24 as reference. Legend in (a) valid for all subplots.

8.2.2 Establishing initial guess for Newton optimisation

Newton optimisation is dependent on an accurate first guess for the solution to converge towards a minimum. Such a guess can be established by various means, e.g. by performing a grid search where different combinations of material parameters are examined to gain an understanding of the appearance of the function. Excluding the mass density, four parameters did have a significant influence on the natural frequencies compared to the other parameters according to the sensitivity analysis. To analyse all combinations of the five values used in the sensitivity study for each influential parameter, 625 analyses would be required. The initial guesses were instead based on the material parameters of different strength classes of timber. For calibration 1–4, the material parameters of strength class C24 was used, as the timber of the CLT panel was specified to be C24. The initial guess for calibration 5 was established by comparing the weight of the tested panel with the different strength classes to see which it corresponds too. With a density of 479 kg/m^3, C40 was established as an initial guess for calibration 5.

8.2.3 Calibrations

Six different calibration runs were performed. Parameters which had less influence on the natural frequencies of the panel were omitted from the calibrations. However, the mass density did have a large effect on the natural frequencies but was not calibrated due to it already being known from measurements.

The calibrations were performed in iterations. For each iteration of calibration, the mode shapes of the numerical model were compared to the experimentally obtained mode shapes with CrossMACs. All diagonal CrossMAC values were consistently throughout the calibration 0.9 or higher, i.e. the modal resemblance between the numerical and experimental modes was high.

Calibration 1

For Calibration 1, two parameters were calibrated: E_{L} and G_{RT}, due to their relatively large effect on the natural frequencies. In addition, three modes were included in the objective function for this calibration, and thus the model was only calibrated to accurately capture the behaviour of the first 3 modes.

Calibration 2

For Calibration 2, E_{L} and G_{RT} were again calibrated. However, instead of only calibrating the model after three modes, it was instead calibrated after the first six modes.

Calibration 3

For Calibration 3, the same parameters as in Calibration 1 and Calibration 2 was once again calibrated, but instead nine modes were included in the calibration.

Calibration 4

Calibration 4 was performed in two runs. For the first run the model was first calibrated after two parameters, as previous calibrations. Nine modes were included in objective function during this calibration. G_{RT} was deemed to have the largest overall influence on all mode shapes and was thus considered appropriate to include in the first round of calibration. The same approach was considered when selecting the second parameter, E_{L}. The second round of calibration included calibration of E_{T} and G_{LT}.

Calibration 5

Calibration 5 was performed in the same manner as Calibration 4, but utilised C40 as an initial guess instead of C24.

8.2.4 Optimisation results

In Figure 8.6, the NRFDs for the first nine modes are shown for Calibration 1–5. From Calibration 1–3 the average NRFD improved with an increasing number of modes included. In addition, the average NRFD also improved by including an additional two parameters in the calibration, as shown by Calibration 4.

In Table 8.2, the initial guesses for the various calibration runs are shown together with the parameters after calibration. The first round corresponds to calibrating E_{L} and G_{RT}, and the second round to the E_{T} and G_{LT}. In addition, the calibrated parameters are marked in bold.

When calibrating four parameters with C24 as an initial guess (Calibration 4), the average absolute NRFD was determined to 0.8% with fairly reasonable material parameters, see Table 8.2. The longitudinal elastic modulus was calibrated to 14 216 MPa, which is higher than the actual parameter of C24, which is 11 000 MPa. The rolling shear modulus was calibrated to 88.9 MPa, which is also higher than the initial guess.

Calibration of four parameters with C40 as an initial guess (Calibration 5) yielded a higher average absolute NRFD value of 2.8% compared to when C24 was used as an initial guess. However, for this calibration, the calibrated parameters reflected the parameters of the initial guess (C40) more accurately, see Table 8.2. The longitudinal elastic modulus was calibrated to 15 770 MPa, compared to the actual value of C40, which is 14 000 MPa. The remaining three calibrated parameters was fairly close to their initial values after calibration.

Table 8.2: Initial guess and final material parameters for the five calibrations. Moduli in MPa and mass density in kg/m^3. Calibrated parameters are marked in bold.

	E_L	E_T	E_R	G_LT	G_LR	G_RT	ρ
Calibration 1, initial guess	**11 000**	370	370	690	690	**49**	480
Calibration 1, final results	**15 216**	370	370	690	690	**58.2**	480
Calibration 2, initial guess	**11 000**	370	370	690	690	**49**	480
Calibration 2, final results	**14 340**	370	370	690	690	**82.8**	480
Calibration 3, initial guess	**11 000**	370	370	690	690	**49**	480
Calibration 3, final results	**14 234**	370	370	690	690	**88.4**	480
Calibration 4 - round 1, initial guess	**11 000**	370	370	690	690	**49.0**	480
Calibration 4 - round 1, results	**14 216**	370	370	690	690	**88.9**	480
Calibration 4 - round 2, initial guess	14 216	**370**	370	**690**	690	88.9	480
Calibration 4 - round 2, final results	14 216	**380**	370	**626**	690	88.9	480
Calibration 5 - round 1, initial guess	**14 000**	470	470	880	880	**63.0**	480
Calibration 5 - round 1, results	**15 770**	470	470	880	880	**66.0**	480
Calibration 5 - round 2, initial guess	15 770	**470**	470	**880**	880	66.0	480
Calibration 5 - round 2, final results	15 770	**490**	470	**665**	880	66.0	480

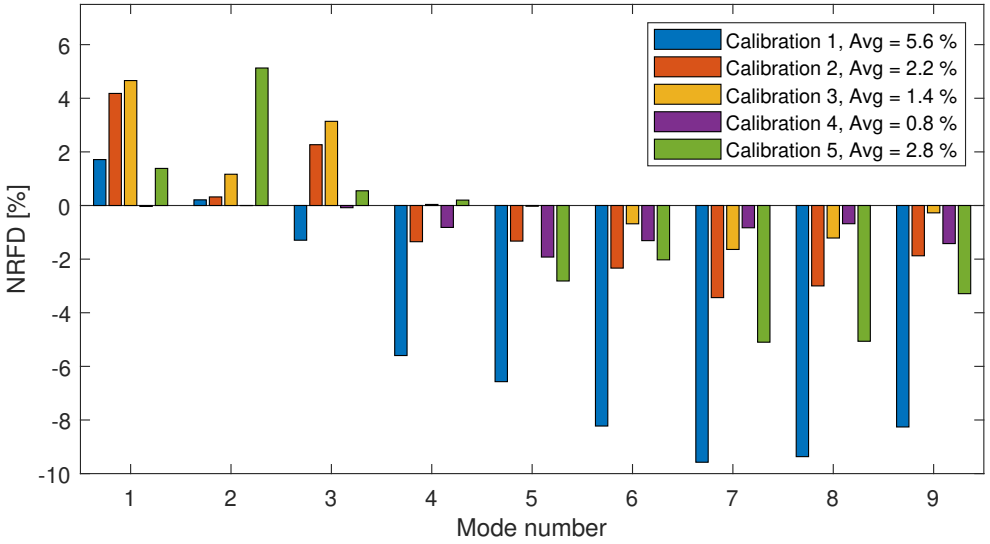

Figure 8.6: NRFDs for Calibration 1–5. In addition, the average absolute NRFD value of the first nine modes are included in the legend.

8.3 Mode shapes comparison

The CrossMAC between the layered and experimental model after Calibration 4 is shown in Figure 8.7. The modal resemblance proved to be very good, with diagonal MAC values all higher than 0.9. In the off-diagonals most MAC values were below 0.1, except for one outlier where the MAC-value was circa 0.12.

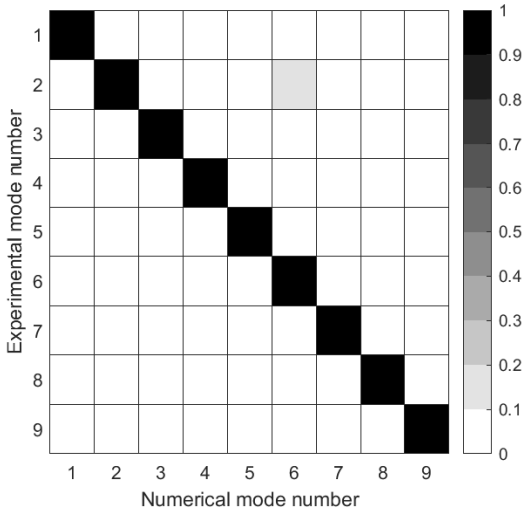

Figure 8.7: CrossMAC between the layered model and the experimental model for calibration 4.

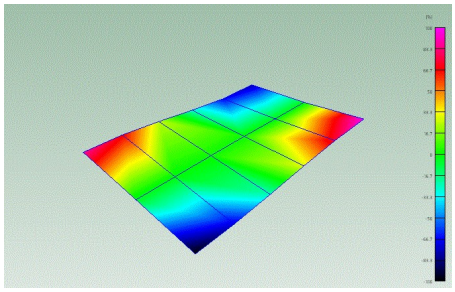

(a) Experimental mode 1

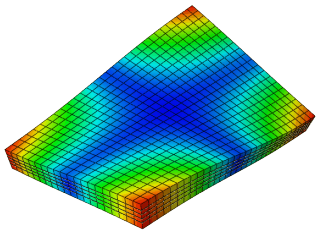

(b) Numerical mode 1.

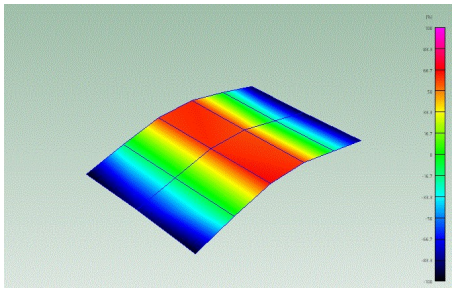

(c) Experimental mode 2

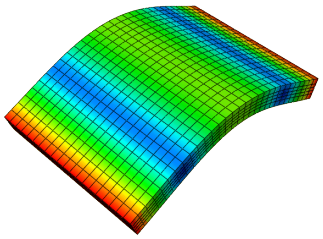

(d) Numerical mode 2.

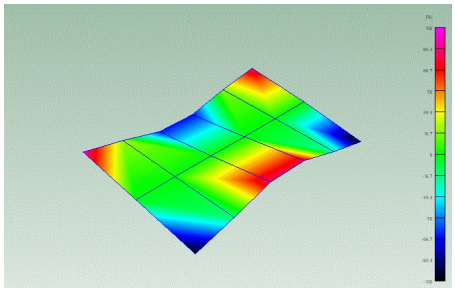

(e) Experimental mode 3

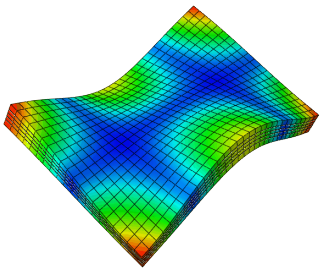

(f) Numerical mode 3.

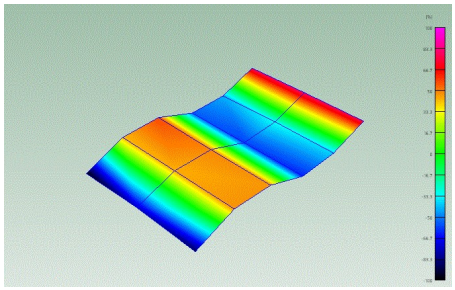

(g) Experimental mode 4.

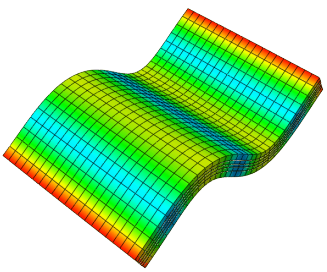

(h) Numerical mode 4.

Figure 8.8: Experimental mode shapes 1–4 in the left column and numerical mode shapes 1–4 in the right column.

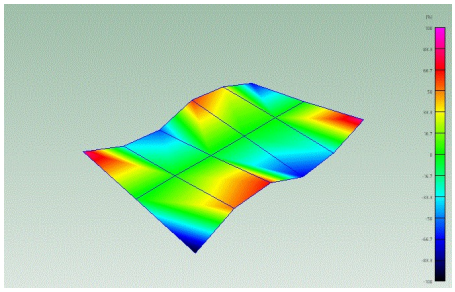

(a) Experimental mode 5.

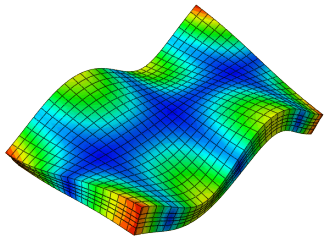

(b) Numerical mode 5.

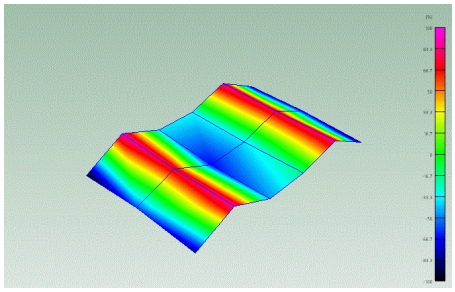

(c) Experimental mode 6.

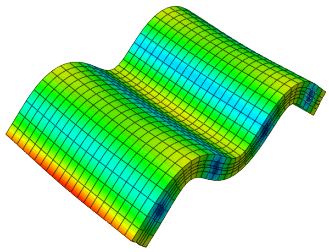

(d) Numerical mode 6.

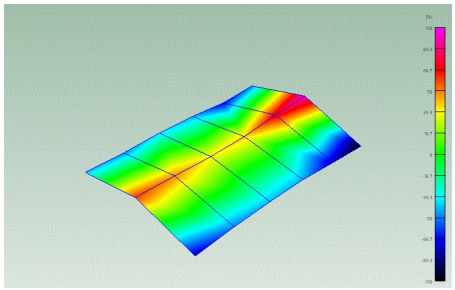

(e) Experimental mode 7.

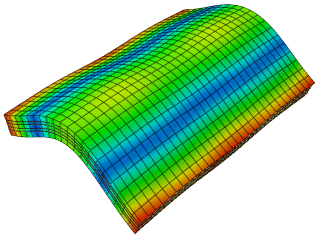

(f) Numerical mode 7.

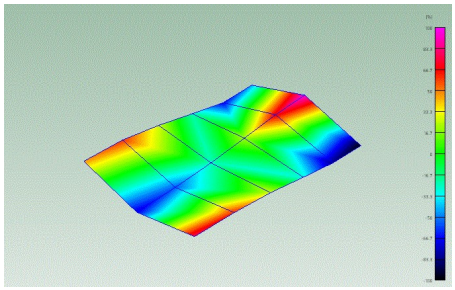

(g) Experimental mode 8.

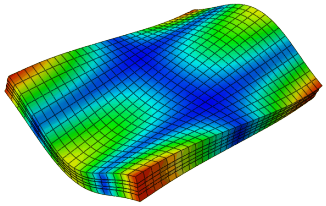

(h) Numerical mode 8.

Figure 8.9: Experimental mode shapes 5–8 in the left column and numerical mode shapes 5–8 in the right column

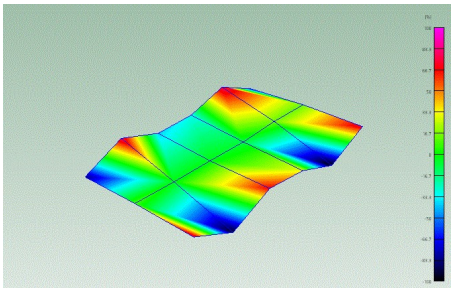

(a) Experimental mode 9.

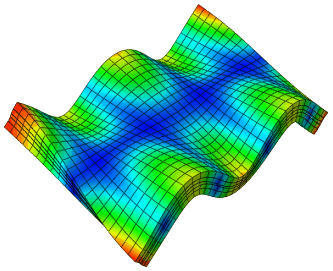

(b) Numerical mode 9.

Figure 8.10: Experimental mode shape 9 in the left column and numerical mode shape 9 in the right column

9 Case study – wood species

In this chapter, the effects of utilising different wood species in CLT are presented in the form of a case study which compares the dynamic response of different CLT floor panels using the following evaluation metrics:

- Natural frequencies (Section 4.3)
- Modal assurance criterion (Section 4.6.2).
- Normalised relative frequency difference (Section 4.6.3).
- Frequency response function (Section 4.5).
- Transient response from walking over the slab (Section 9.3).

The analyses were performed on three floor panels with different spans and lay-ups to evaluate the change in dynamic response as a result of material choice in floor panels of different sizes. The reason for testing three differently sized panels was to evaluate if the panel size affected the change in dynamic behaviour. The panels used for the analyses were 5, 7, and 9 m long, respectively, and 2.4 m wide. These will henceforth be referred to as the small-, medium-, and large floor panel, respectively, see Figure 9.1. The small floor panel consists of 5 layers of 30 mm thick laminations, the medium floor panel of 7 layers of 40 mm thick laminations, and the large floor panel of 7 layers of 45 mm thick laminations, see Figure 9.2. The two outer layers of the medium and large floor panels are oriented parallel with the length of the panels.

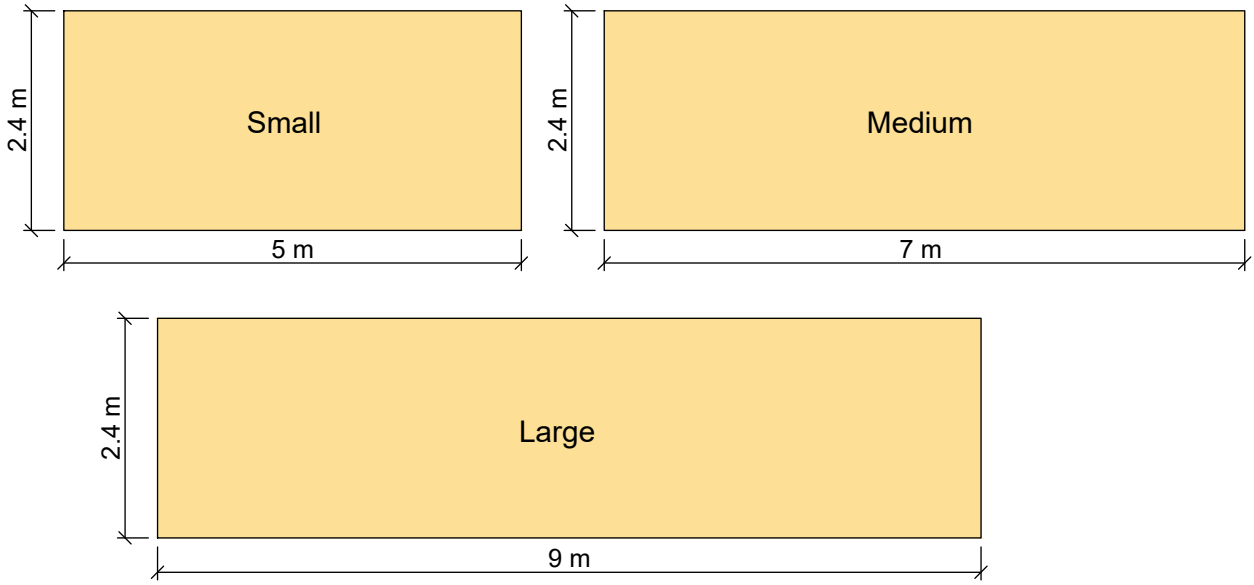

Figure 9.1: Illustration of the small-, medium-, and large floor panel, respectively.

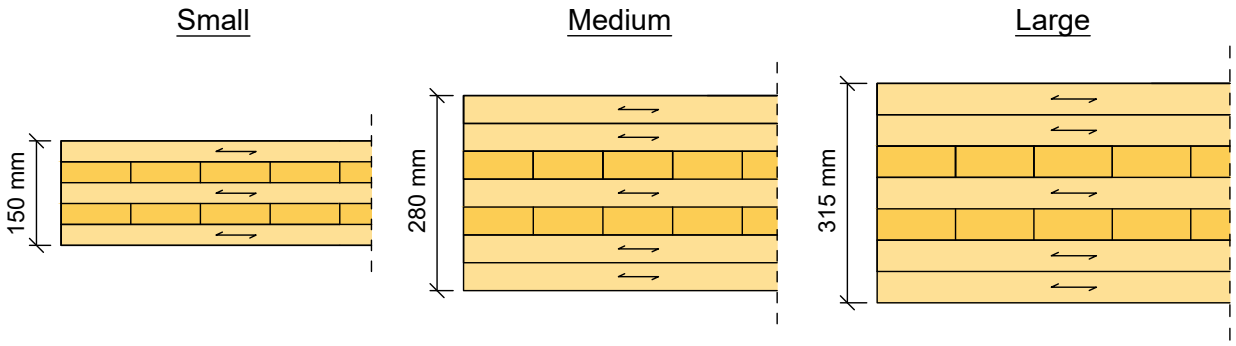

Figure 9.2: Lay-ups of the three different floor panels used for analysis.

To ensure that the analyses have practical relevance, the three panels were verified according to the design methods presented in the CLT-Handbook by Swedish Wood [13], which are based on SS-EN 1995-1 [11] and national adaptations for Sweden found in EKS 10 [32]. The panels are assumed to be made of strength class C24 timber and the control was performed for service class 1 and safety class 3. The panels were verified for maximum moment- and shear force in the ultimate limit state. They were also verified to fulfil the following serviceability limit state conditions:

- Quasi-permanent deflection less than $L/300$, where L is the length of the panel.
- Fundamental frequency higher than 8 Hz to avoid a detailed investigation of the acceleration response.
- Deflection from a static point load of 1 kN acting in the middle of the panel did not exceed the largest permitted value of 1.5 mm (nationally adopted value used in Sweden).

Simply supported boundary conditions were used for all analyses. At one support, the floor panel was prevented to move in all directions along a line located in the middle of the cross section, see dashed line in Figure 9.3, whereas at the other support, it was only prevented to move in the y- and z-directions.

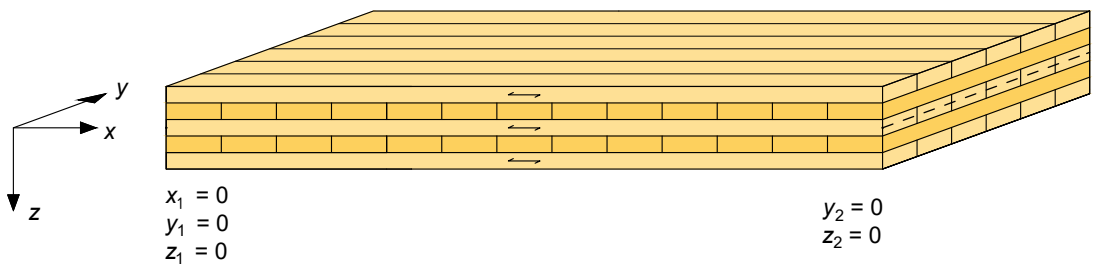

Figure 9.3: Illustration of the boundary conditions used, prescribed along a line at both ends, see dashed line.

Table 9.1: Material sets used for the analysis. Moduli in MPa and mass density in kg/m^3.

	E_L	E_R	E_T	G_{LT}	G_{LR}	G_{RT}	ρ
Spruce	10 991	716	435	682	693	43	390
Low birch	13 000	1 100	620	850	850	175	510
High birch	16 500	1 260	650	850	850	180	830
Low beech	10 000	1 310	460	1 240	940	350	540
High beech	18 000	1 510	730	1 240	940	380	910

The analyses were performed using the material parameters of spruce, birch, and beech. Spruce was included as the reference case using the material parameters presented in [19], where an average set of parameters for spruce was determined. Birch and beech were included in the analysis as birch is the most common hardwood species in Sweden and beech is the most common hardwood species in Europe. For birch and beech, both low- and high values were included to highlight possible variations in material parameters, see Table 9.1. The Poisson's ratios were set to the same values for all material sets, due to their negligible impact on modal behaviour, shown in Chapter 8.

9.1 Effect on modal properties

In this section, the results from the modal analyses are presented in the form of CrossMACs, natural frequencies and NRFDs for the small-, medium-, and large panels, respectively, considering the five sets of material parameters given in Table 9.1. Spruce was used as reference for the NRFDs and the CrossMACs.

9.1.1 Small panel

The small panel showed little change in modal order for the first nine modes. However, a shift in mode order for modes 6 and 7 could be identified for high beech, as is shown in the CrossMAC in Figure 9.4. Mode 6 is the 3rd bending mode with 3 bays in the longitudinal direction, see Figure 9.7f. Mode 7 is the 3rd torsional mode with 3 bays in the longitudinal direction and 2 bays in the transverse direction, see Figure 9.7g.

The natural frequencies were slightly shifted in frequency by changing material parameters, see Figure 9.5. The high values of birch and beech reduce most of the natural frequencies, whereas the low values generally increase the frequencies. This behaviour is also demonstrated by the NRFDs, shown in Figure 9.6, where the low values of birch and beech generally results in an increased NRFD, whereas the high values results in a decreased NRFD. However, some exceptions exist. For example, all natural frequencies are decreased by all sets of material values for mode 1, which is the 1st bending mode (Figure 9.7a).

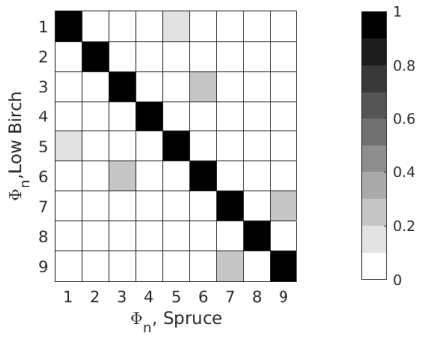

(a) CrossMAC between low value of birch and spruce.

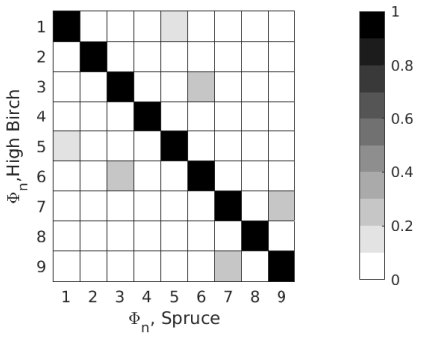

(b) CrossMAC between high value of birch and spruce.

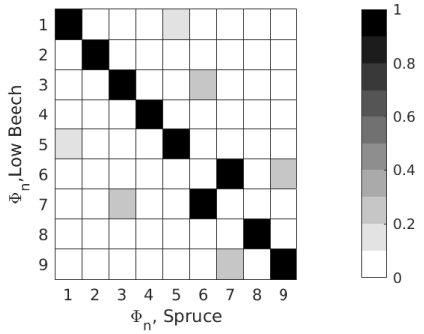

(c) CrossMAC between low value of beech and spruce.

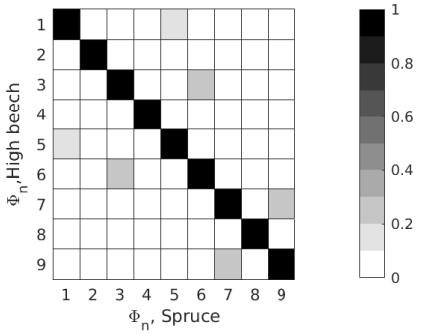

(d) CrossMAC between high value of beech and spruce.

Figure 9.4: CrossMACs for the different wood species for the small panel.

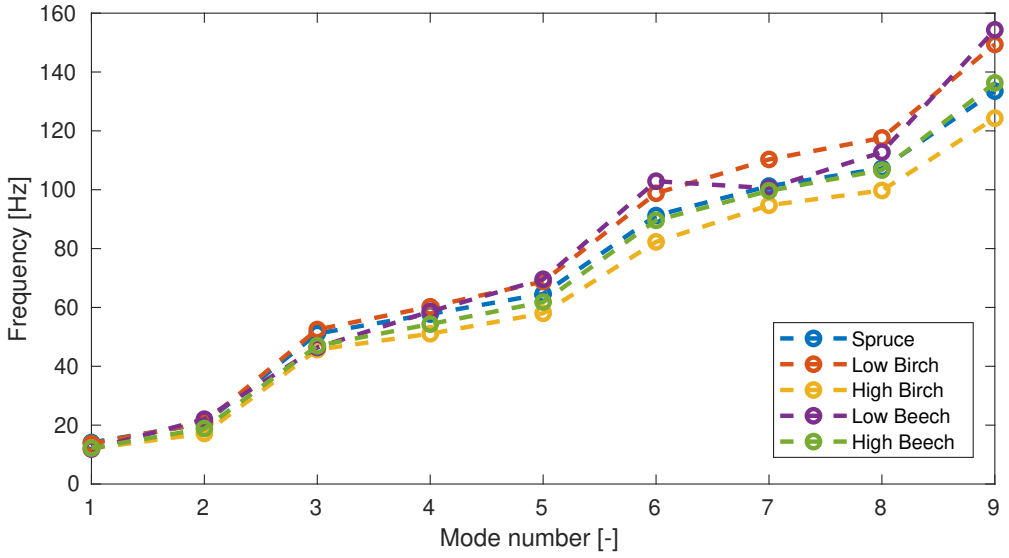

Figure 9.5: Natural frequencies for spruce, and low- and high values for birch and beech for the small panel.

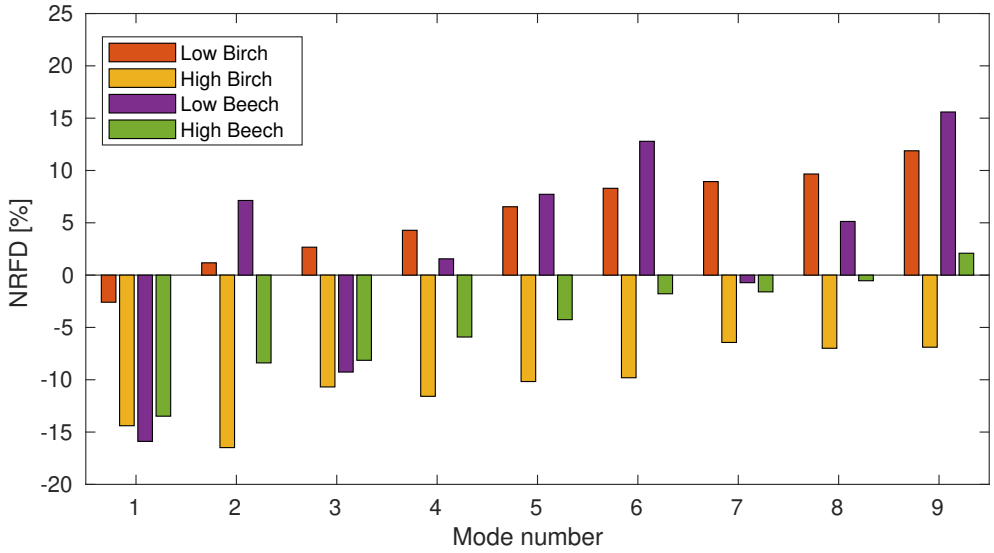

Figure 9.6: NRFDs for the low- and high values for birch and beech for the small panel, with spruce as reference.

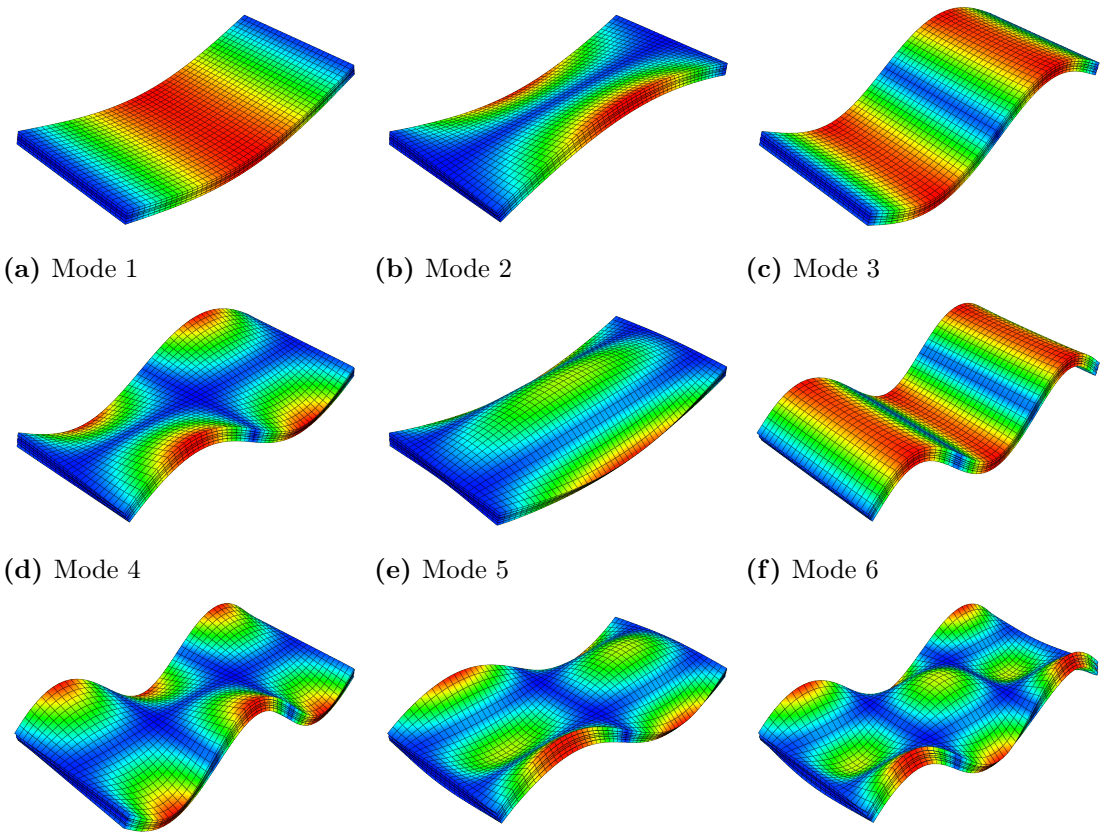

(a) Mode 1 **(b)** Mode 2 **(c)** Mode 3

(d) Mode 4 **(e)** Mode 5 **(f)** Mode 6

(g) Mode 7 **(h)** Mode 8 **(i)** Mode 9

Figure 9.7: Mode shapes of the first 9 modes for the small panel using spruce.

9.1.2 Medium panel

The medium-sized panel did not show large alteration in mode order with the different wood species. The only noticeable shift for the first 9 modes is modes 6 and 7, which are shifted for all sets of material parameters. Here, mode 6 is the 3rd torsional mode (Figure 9.11f) and mode 7 is the first bending mode in the transversal direction (Figure 9.11g).

With regard to the natural frequencies, see Figure 9.9, it can be seen that low birch and beech generally increases the natural frequencies. The high values of birch are the only material set which lowers most natural frequencies. The increase in natural frequencies for the low material values are fairly high, ranging from 10% up to over 20%, see Figure 9.10. As for the small slab, the fundamental frequency is decreased significantly for all material sets except low birch, which leaves it mostly unchanged.

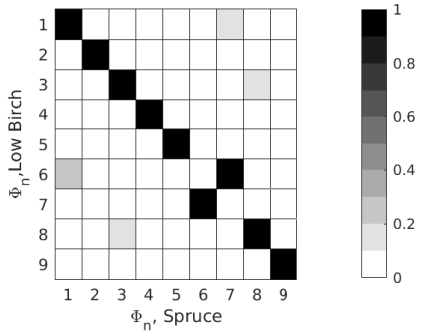

(a) CrossMAC between low value of birch and spruce.

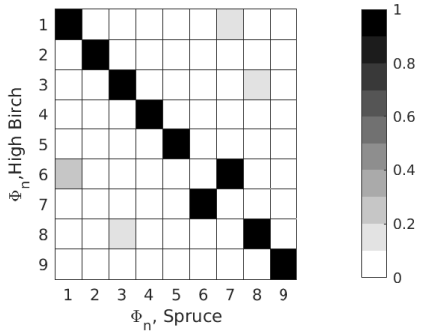

(b) CrossMAC between high value of birch and spruce.

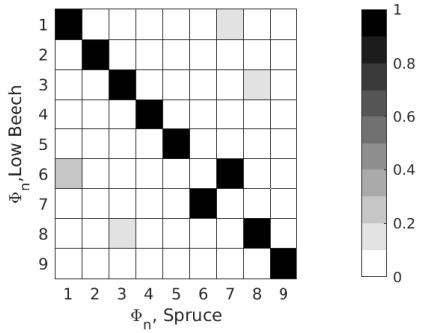

(c) CrossMAC between low value of beech and spruce.

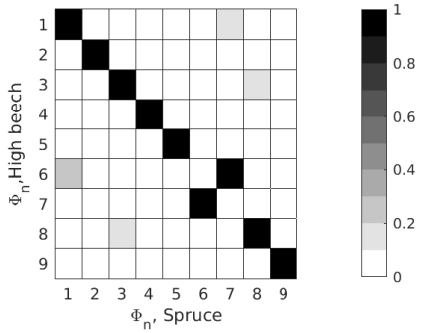

(d) CrossMAC between high value of beech and spruce.

Figure 9.8: CrossMACs for the different wood species for the medium panel.

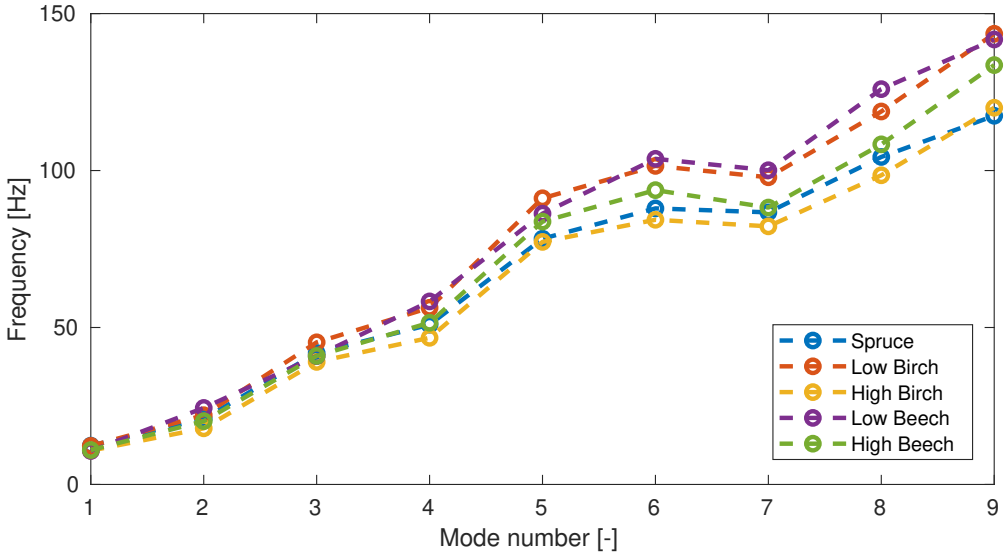

Figure 9.9: Natural frequencies for spruce, and low- and high values for birch and beech for the medium panel.

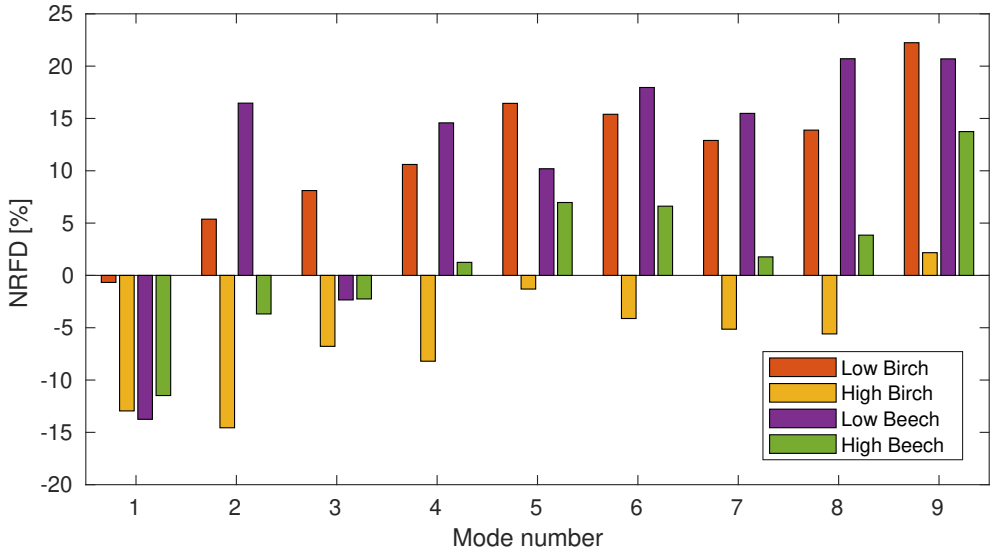

Figure 9.10: NRFDs for the low- and high values for birch and beech for the medium panel, with spruce as reference.

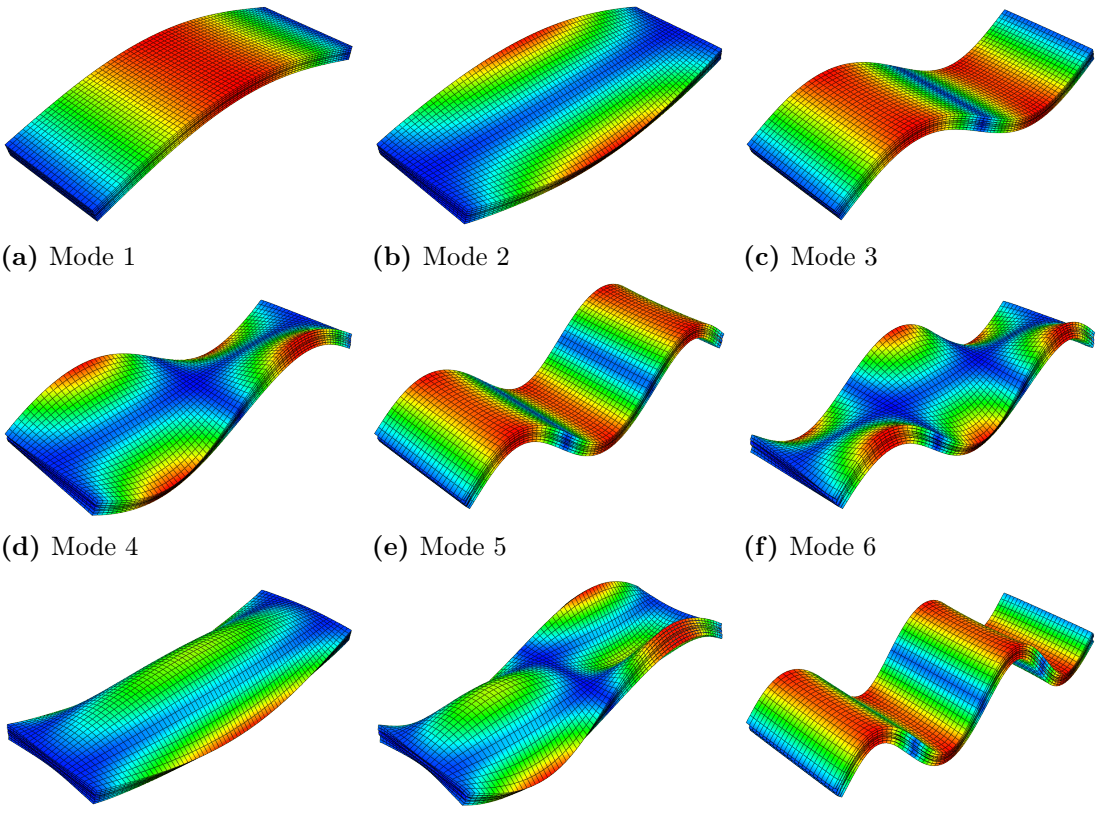

(a) Mode 1 **(b)** Mode 2 **(c)** Mode 3

(d) Mode 4 **(e)** Mode 5 **(f)** Mode 6

(g) Mode 7 **(h)** Mode 8 **(i)** Mode 9

Figure 9.11: Mode shapes of the first 9 modes for the medium panel using spruce.

9.1.3 Large panel

The large panel did not show any significant change in modal order other than a modal shift in between modes 7 and 8 for the low value of beech. Here, mode 7 is the 4th bending mode in the longitudinal direction, with 4 bays in its lengthwise direction (Figure 9.15g). Mode 8 is the first bending mode in the transversal direction (Figure 9.15h).

As shown in Figure 9.13, the low values do increase the natural frequencies, together with the high value of beech. The high value of birch slightly reduces most of the natural frequencies, see Figure 9.14, whereas the high value of beech lowers the first three, and increases the last five, leaving the fourth unchanged. As for the two previous panels, the fundamental frequency is reduced significantly for all material values except low birch, which only slightly reduces it.

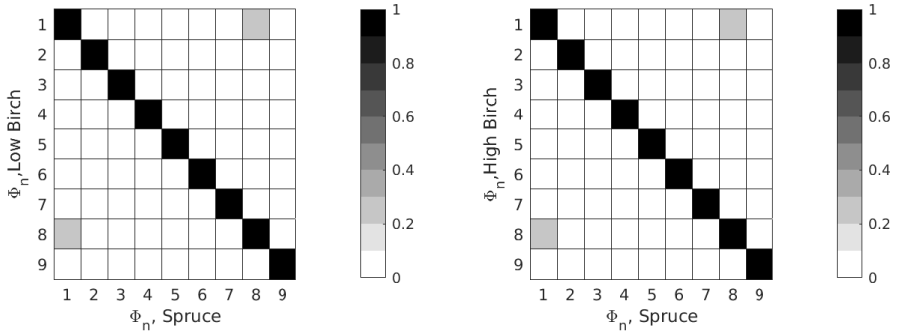

(a) CrossMAC between low value of birch and spruce.

(b) CrossMAC between high value of birch and spruce.

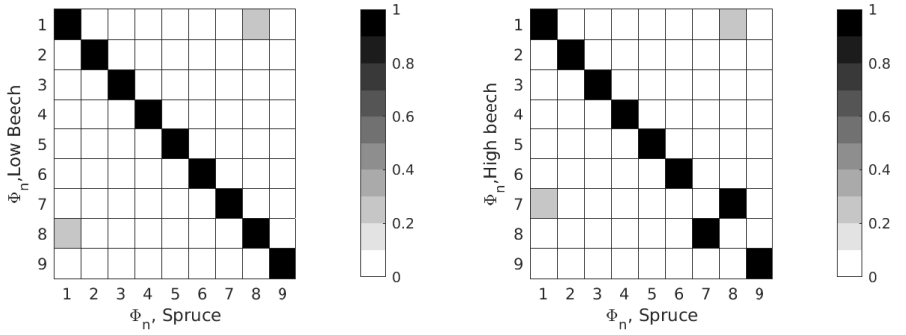

(c) CrossMAC between low value of beech and spruce.

(d) CrossMAC between high value of beech and spruce.

Figure 9.12: CrossMACs for the different wood species for the large panel.

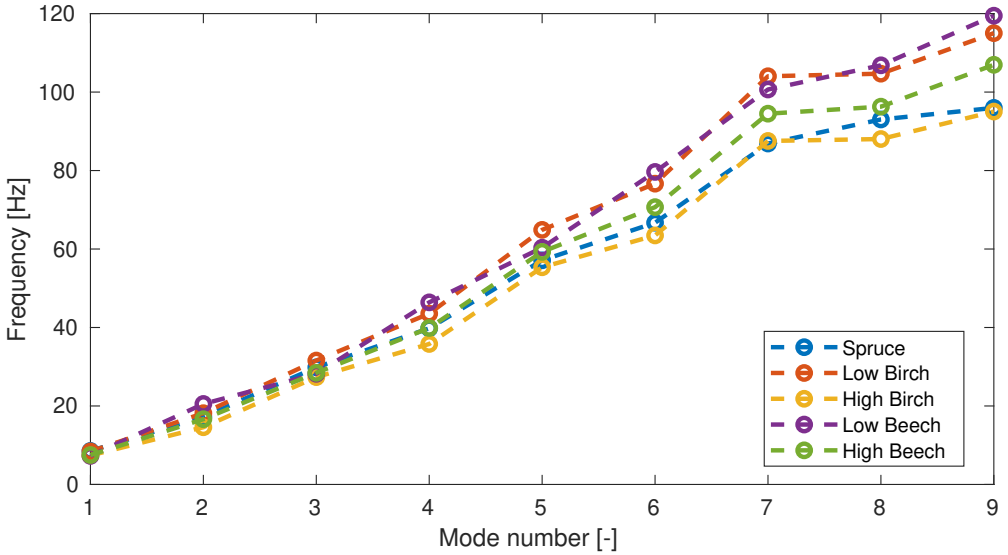

Figure 9.13: Natural frequencies for spruce, and low- and high values for birch and beech for the large panel.

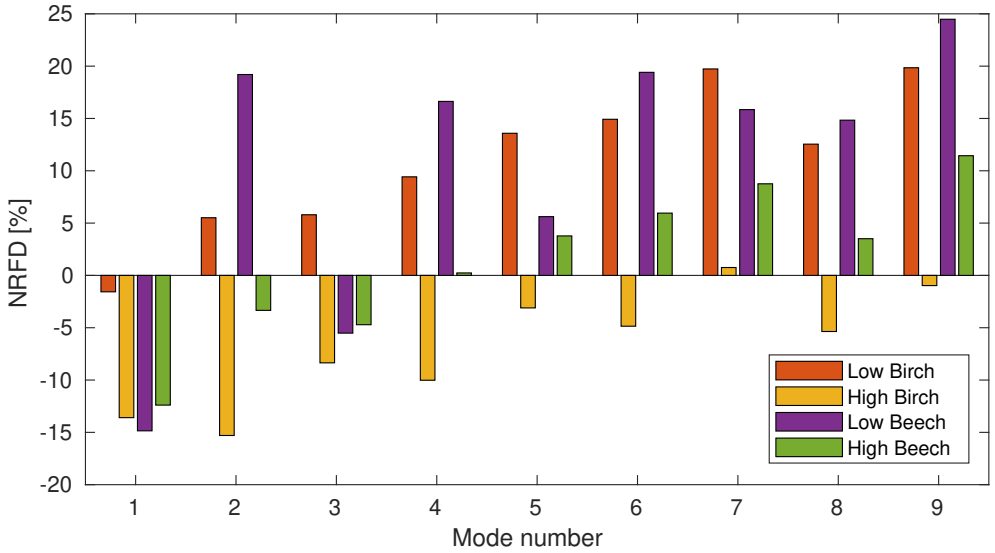

Figure 9.14: NRFDs for the low- and high values for birch and beech for the large panel, with spruce as reference.

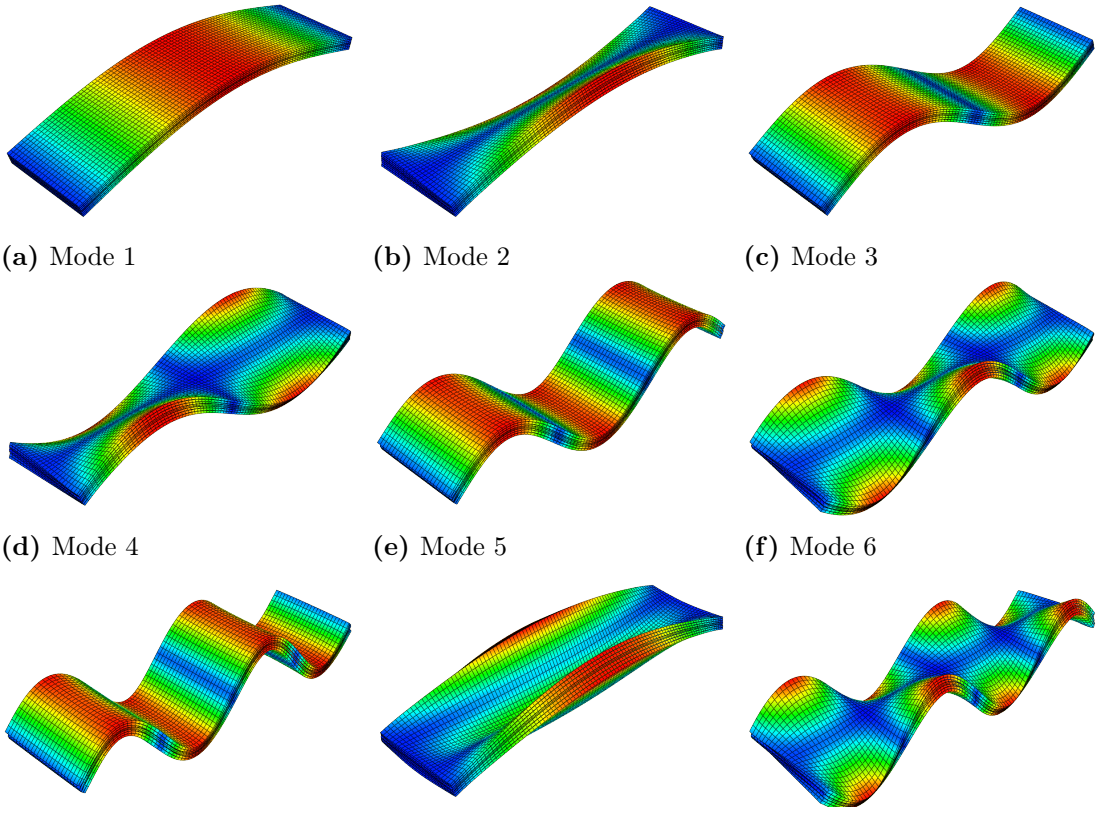

(a) Mode 1 **(b)** Mode 2 **(c)** Mode 3

(d) Mode 4 **(e)** Mode 5 **(f)** Mode 6

(g) Mode 7 **(h)** Mode 8 **(i)** Mode 9

Figure 9.15: Mode shapes of the first 9 modes for the large panel using spruce.

9.2 Effect on frequency response functions

The effect on the FRFs was evaluated using Abaqus with the step *Steady-state dynamics, Modal*, which is used to calculate the steady-state dynamic linear response of a system subjected to harmonic excitation. The frequency range of interest was set to 0.1–100 Hz and 1% damping was utilised for the entirety of the chosen frequency range. A unit force of 1 N was applied at excitation point E1, and the acceleration response was evaluated at measurement point M1, which is located at the opposite corner of the excitation point, see Figure 9.16. The point of excitation and measurement was chosen so that all modes within the frequency range would be excited. The change in magnitude of the FRFs is also demonstrated in the form of a root mean square value which has been normalised to the reference case spruce.

Figures 9.17a, 9.18a and 9.19a show the FRFs, and 9.17b, 9.18b and 9.19b the corresponding normalised RMS values for the small, medium, and large panels, respectively. The resonance frequencies have shifted and that the number of modes occurring below 100 Hz varies for the different materials for all panels. There is also a notable change in magnitude at the resonances of the frequency response functions, as the magnitude is lower than the reference case spruce for both the low- and high values of birch and beech for all panels.

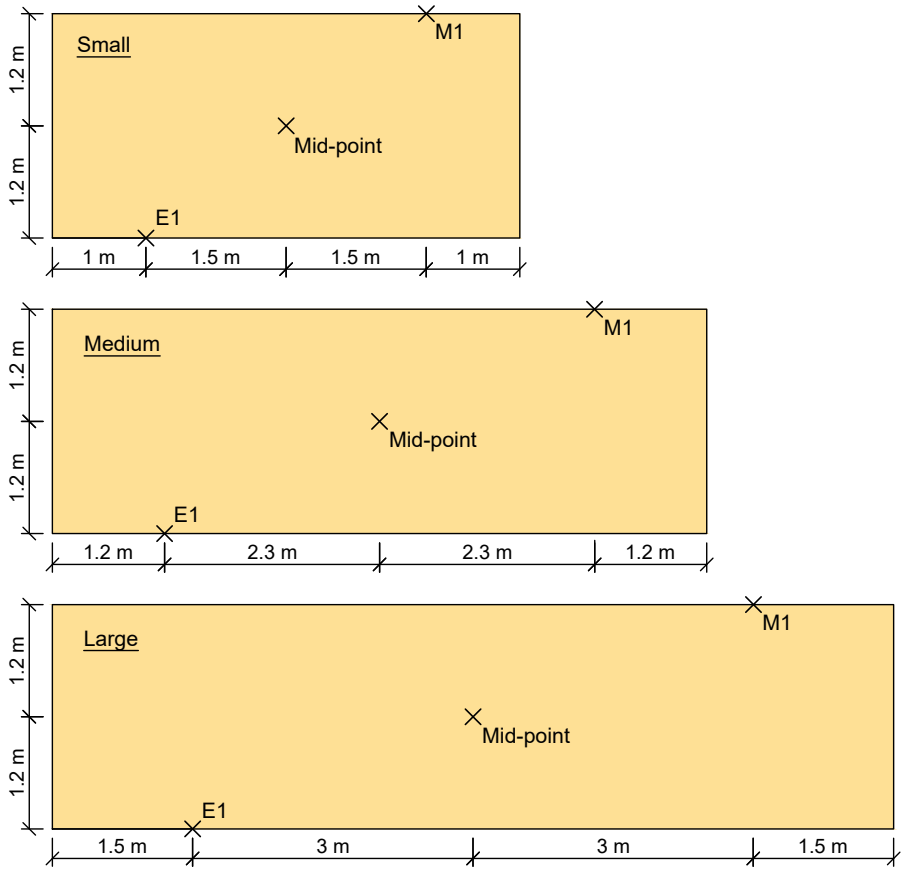

Figure 9.16: Placement of excitation- and measurement points on the small-, medium-, and large panels.

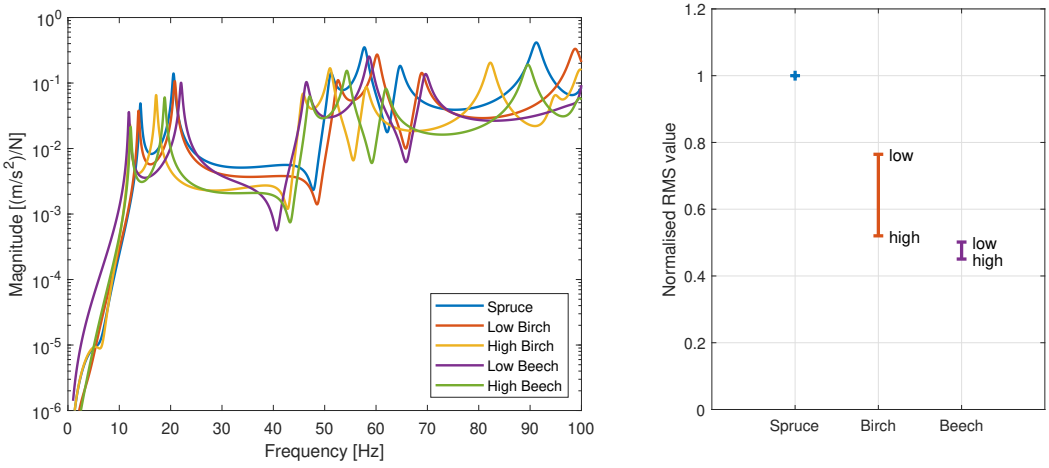

(a) **(b)**

Figure 9.17: Accelerance FRFs (a) and normalized RMS values of the FRFs (b) for different materials for the small panel.

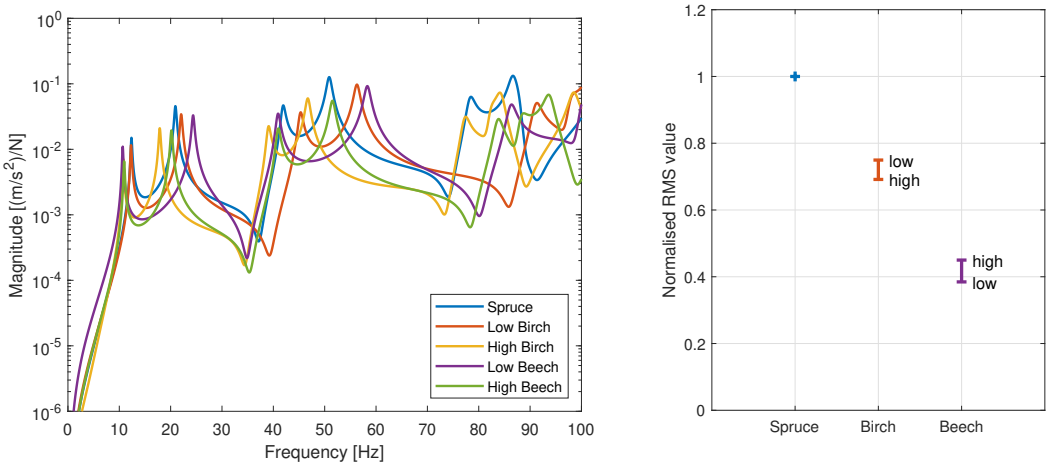

(a) **(b)**

Figure 9.18: Accelerance FRFs (a) and normalized RMS values of the FRFs (b) for different materials for the medium panel.

The fundamental frequency is lowered with high values of birch and the low- and high value of beech when compared to the reference case spruce. This effect was however not as obvious for the low value of birch, although still prevalent.

The normalised RMS values shows a reduction in magnitude when testing birch and beech for all panels. For the small panel, birch reduced the magnitude to 52–76% of the reference case and beech to 45–50%. For the medium panel, birch reduced the magnitude to 69–75% of the reference case and beech to 39–45%. For the large panel, birch reduced the magnitude to 44–65% of the reference case and beech to 37–62%. Utilisation of beech reduces the RMS values more than birch for all tested panel sizes. This is especially obvious for the medium panel, where there is a large distinction between the two intervals, as opposed to for the small and large panel, where the difference between birch and beech is more subtle.

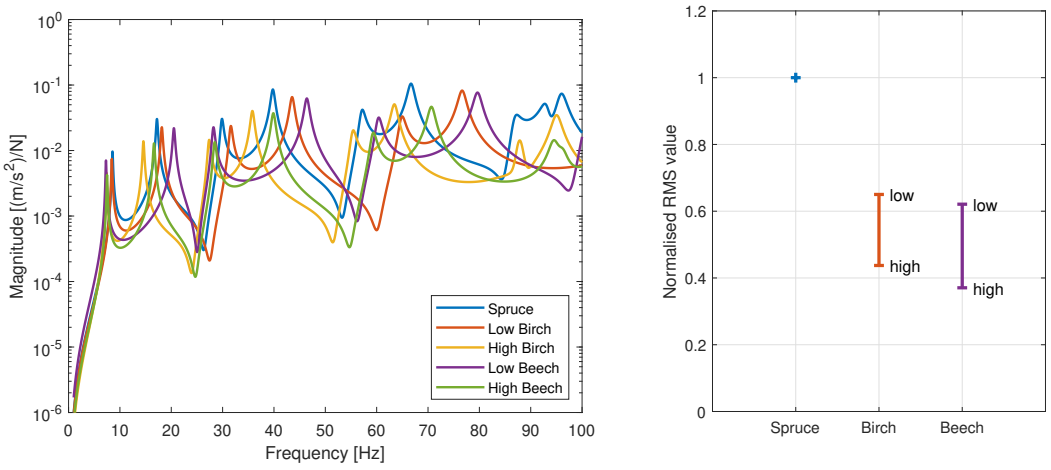

(a) **(b)**

Figure 9.19: Accelerance FRFs (a) and normalized RMS values of the FRFs (b) for different materials for the large panel.

9.3 Effect on footfall response

In this section the following are presented: an introduction to human induced vibration and a description of the approach used for modelling footfalls on the panel, including theory on stride length, stride width, load placement, and load history. In addition, a convergence study conducted to ensure sufficient time-step size and number of modes included in the modal truncation for the transient analysis is presented. Lastly, the result from the transient analyses for the three differently sized panels are presented for 10 different walking frequencies.

9.3.1 Human induced vibrations

Human activities are the most common source of dynamic excitation of floor panels in occupied buildings. These can be from walking, running, or jumping, with walking being the most common and thus the most relevant for this study.

Walking frequencies are typically in the range of 1.2 to 2.4 Hz. Studies have shown that up to the third or fourth harmonic of the walking frequency can cause resonance in floors: with harmonics meaning a multiplication of the frequency of applied force. For example, the third harmonic of a walking frequency of 2.0 Hz would be 6.0 Hz. Thus, resonant vibrations can occur if low-frequency floors (natural frequencies below 8–10 Hz) coincide with harmonics of the walking frequency. High-frequency floors (natural frequencies above 8–10 Hz), however, are not excited by this to the same extent, as they instead dampen out each successive impact between the steps [33, 34].

An increase in walking frequency generally results in increased load magnitude, walking speed and stride length [35]. Equations describing the relationship between the mentioned parameters have been established and are utilized in many design guidelines. The equations used to model footsteps for the transient analysis are described in Section 9.3.2.

9.3.2 Modelling of footfall

Three typical normalized load histories for a single footstep can be seen in Figure 9.20. The first peak occurs when the foot makes initial contact with the ground and the self-weight of the person and inertial components are transferred to the ground. The trench between the two peaks represents a weight shift to the other leg during walking. The second peak occurs when the foot pushes off from the ground before the whole foot leaves the floor. In case of hard soles, the heel-strike from walking may result in a sharp additional peak in the reaction force curve when the foot makes contact with the ground [35]. However, modelling of the described additional peak is not considered in the chosen footfall modelling approach.

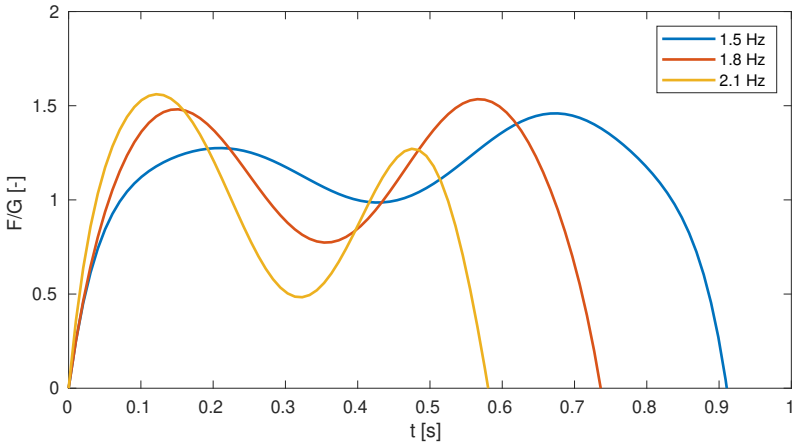

Figure 9.20: Normalised load history for a single footstep for walking frequencies 1.5, 1.8, and 2.1 Hz.

Human-induced loads can be modelled analytically either as frequency-domain models or time-domain models, with time-domain models being the most commonly used for simulation purposes according to [36]. For the present work, a time-domain approach presented in [36] was used, where the footfall force induced by a single footfall is expressed with an 8th order polynomial according to Eq. 9.1:

$$F(t) = G(K_1 t + K_2 t^2 + K_3 t^3 + K_4 t^4 + K_5 t^5 + K_6 t^6 + K_7 t^7 + K_8 t^8) \tag{9.1}$$

where the coefficients K_1 to K_8 are dependent on the step frequency according to Table 9.2. $F(t)$ is the induced force and G is the weight of the person.

Stride length and width

The stride length was determined based on a relationship between walking frequency and velocity proposed by Bachmann and Ammann in [37], where v is the walking velocity (m/s) and f_s the walking frequency (Hz).

Table 9.2: Coefficients K_1 to K_8 depending on walking frequency according to [36].

	$f_s \leq 1.75$ Hz	$1.75 \leq f_s \leq 2.00$ Hz	$f_s \geq 2.00$ Hz
K_1	$-8f_s + 38$	$24f_s - 18$	$75f_s - 120$
K_2	$376f_s - 844$	$-404f_s + 521$	$-172f_s + 3\ 153$
K_3	$-2\ 804f_s + 6\ 025$	$4\ 224f_s - 6\ 274$	$17\ 055f_s - 31\ 936$
K_4	$6\ 308f_s - 16\ 573$	$-29\ 144f_s + 45\ 468$	$-94\ 265f_s + 175\ 710$
K_5	$1\ 732f_s + 13\ 619$	$109\ 976f_s - 175\ 808$	$298\ 940f_s - 553\ 736$
K_6	$-24\ 648f_s + 16\ 045$	$-217\ 424f_s + 353\ 403$	$-529\ 390f_s + 977\ 335$
K_7	$31\ 836f_s - 33\ 614$	$212\ 776f_s - 350\ 259$	$481\ 665f_s - 888\ 037$
K_8	$-12\ 948f_s + 15\ 532$	$-81\ 572f_s + 135\ 624$	$-174\ 265f_s + 321\ 008$

$$v = 1.67f_s^2 - 4.83f_s + 4.5 \tag{9.2}$$

With the walking velocity known, the stride length l_s could be determined as:

$$l_s = v/f_s \tag{9.3}$$

The stride width is the perpendicular distance between the heels of two steps and was set to 100 mm.

Load application on model

For the transient analysis, a load case simulating five consecutive steps walking straight across the length of the CLT in a centre line were modelled/studied with the third step always located in the middle of the panel, see Figure 9.21. The load induced by footfalls was applied to the structure as pressure distributed over a square surface of 100×100 mm^2. Pressure was used instead of concentrated force to avoid excessive local deformations. Figure 9.21 shows how the loads were applied to the CLT panels in Abaqus. The time history of the load and the stride length were changed based on what walking frequency was currently being studied according to Equation 9.1 and 9.3.

9.3.3 Time-step and modal decomposition

Mode-superposition was deemed an appropriate approach for determining the transient response of the panels due to linear-elastic conditions being assumed. As mode-superposition includes an arbitrary number of eigenmodes in the analysis, a sufficient number of modes to include had to be determined. The time convergence and modal

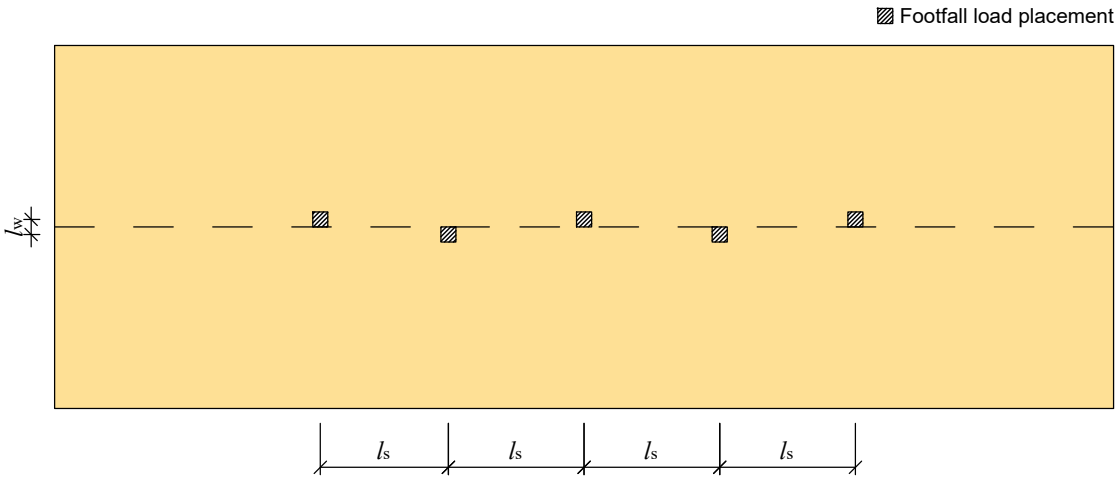

Figure 9.21: Load application for the transient analysis.

decomposition were examined using the response in measurement point M1 of the medium panel, see Figure 9.16. If point M1 shows sufficient convergence for the time-step and the modal decomposition is accurate, the mid-point will also show sufficient convergence with the same modal decomposition, since all modes excited at the mid-point are also excited at point M1. The analyses were performed in Abaqus with the *Modal Dynamics* step, which uses mode super position, thus reducing computational time compared to implicit dynamic time-integration.

First, an implicit dynamic analysis, step *Dynamic (Implicit)* in Abaqus, was performed for three different time-steps with a walking frequency of 2.0 Hz. The acceleration response in M1 is shown in Figure 9.22 where it can be seen that the response overall is larger for the larger time-step of 5 ms. For time-steps of 1 and 2 ms the response is however sufficiently similar, i.e. the response has converged using 2 ms with regard to the size of the time-step of 1 ms.

In Figure 9.23, a comparison between the response of the implicit analysis and a mode-superposition analysis with 10 modes with 1% modal damping are shown. The response is captured fairly well with 10 modes, however when all steps are finished at 2.5 seconds the truncated response includes much more noise. When 12 modes instead are included in the truncated response, see Figure 9.24, the noise in the second half of the time-history is reduced and the response from the implicit analysis is captured very well throughout the entire time span of the analysis.

9.3.4 Transient analysis

The vertical transient acceleration response was measured at the mid-point since the highest response was expected at that point. The point M1 was also considered, but it did not show higher response than the mid-point, and thus the mid-point was chosen as the evaluation point for the analysis. Ten walking frequencies were analysed, ranging from 1.5 to 2.4 Hz, for the different sets of material parameters, see Table 9.1. Based on the convergence analysis, the time-step was set to 1 ms, and 12 modes were included in the analysis. The footfall amplitude time-history and stride length varied depending on the walking frequency according to Equations 9.1 and 9.3. The response was measured for a period of five seconds for all tests.

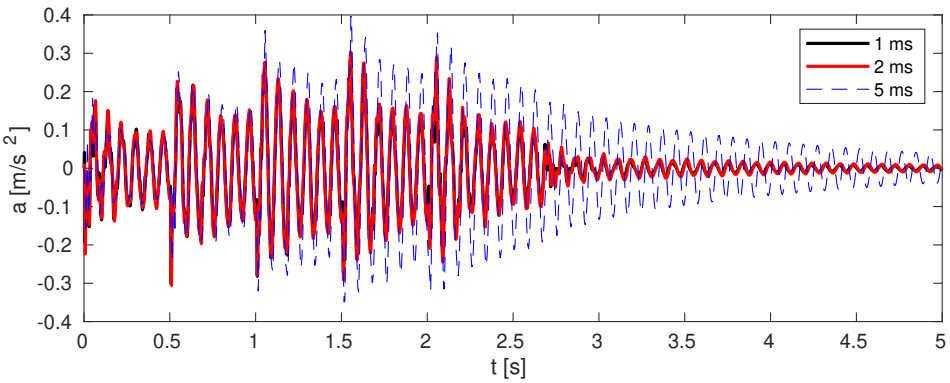

Figure 9.22: Acceleration response in M1. Three different time-steps are shown: 1 ms, 2 ms and 5 ms.

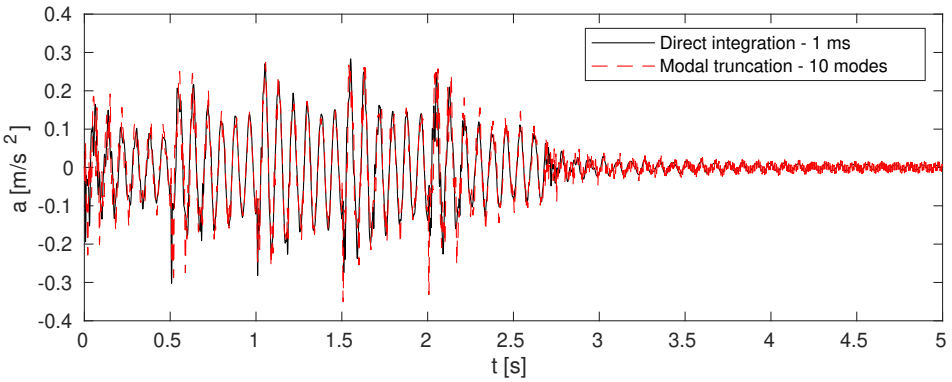

Figure 9.23: Transient acceleration response for direct integrated implicit integration with a time-step of 1 ms compared to the truncated transient modal response with 12 modes included.

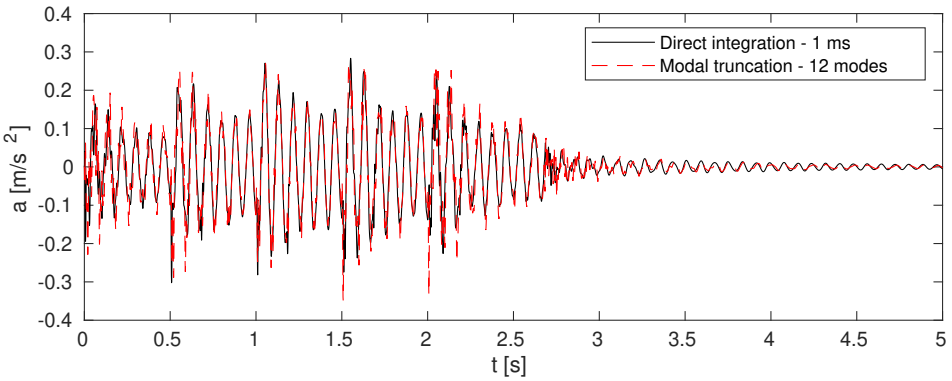

Figure 9.24: Transient acceleration response for direct integrated implicit integration with a time-step of 1 ms compared to the truncated transient modal response with 12 modes included.

Appendices B, C, and D show the results of the analyses for all tested walking frequencies and wood species for the small, medium, and large panel, respectively. The left column of subplots shows the transient acceleration response at mid-point for the whole measurement period. The 1 s of highest response was determined by calculating the RMS value for all 1 s intervals during the entire five second measurement period and choosing the highest, shown as a red coloured box. The right column of subplots shows a FFT of the transient response, the harmonics of the walking frequency (red dashed line), and the fundamental frequency (blue dashed line). The FFT was performed to examine the frequency content of the transient response and to identify potential correlation between harmonics and fundamental frequency.

Since acceleration response in the time-domain is difficult to evaluate by itself, the effect on human-perceived disturbance in the floor panels was evaluated with root mean square values. These are presented in the upper subplot of Figures 9.25, 9.26, and 9.27. In addition, the RMS from all ten walking frequencies for each wood species were averaged. This averaged RMS value was calculated both for the 1 s of highest response and for the whole measurement period. These are presented in the lower subplot of Figures 9.25, 9.26, and 9.27.

Small panel

The RMS values for the small panel shows a large variation in response depending on the material selection and also for the ten different walking frequencies, see Figure 9.25. For spruce, the worst responses are found for the following walking frequencies: 1.6, 2.0, 2.3 and 2.4 Hz. In Figures B.1 and B.2, it can be seen that the four walking frequencies with the worst response all have a harmonic of the walking frequencies that matches the panel's fundamental frequency well. For walking frequency 1.6 Hz, it is the 9th harmonic that matches well, for 2.0 Hz it is the 7th harmonic, and for 2.3 and 2.4 Hz it is the 6th harmonic. Even though the response is the largest for walking frequencies 2.3 and 2.4 Hz, the match between a harmonic and fundamental frequency is slightly closer for the 1.6 and 2.0 Hz walking frequencies.

For birch, the response is lower than spruce for most walking frequencies, see Figure 9.25. This is also highlighted by the averaged RMS values, which shows that the highest average RMS value for both the low- and high values of birch is less than 50% of that of spruce. Low birch experiences the highest response for walking frequencies 1.7 and 2.3 Hz. In the same manner as spruce, a harmonic of the walking frequency matches very well with the panels fundamental frequency for these two cases, see Figures B.3 and B.4. The high birch response is slightly lower or equivalent to low birch for most walking frequencies, except 1.5 and 2.0 Hz, where the response is slightly higher than low birch. This might be explained by the 8th harmonic matching the fundamental frequency of the high birch very well, whereas low birch in comparison did not match as well, see Figure B.5 and B.6. The equivalent can be identified for the walking frequency of 2.0 Hz, where the match between walking harmonic and fundamental is closer for high birch than for low birch.

The response of the beech panel shows more deviation than birch between the low- and high values. Low beech shows the highest response of all tested materials for the small panel, whereas the high beech value shows the lowest response. Low beech experiences the worst response for the walking frequencies 1.5, 2.0, 2.3 and 2.4 Hz. Again, this can largely be explained by harmonics and fundamental frequencies matching well, see Figure B.7 and B.8. A harmonic of 2.0 and 2.4 Hz matches the fundamental frequency well. However, for 2.3 Hz, the match is not quite as close, but the response is still very large. For high beech, the response is low for all walking frequencies, especially in comparison to low beech and spruce. Harmonics of the walking frequency matches the fundamental frequency fairly well for walking frequencies 1.5, 2.0 and 2.4 Hz for high beech, but neither produce a high RMS value, see Figure B.9 and B.10.

The averaged RMS-response for the small panel, see Figure 9.25, show the same patterns as the previously discussed RMS values. Both values of birch are showing lower response, whereas there is a large interval between the high and low value of beech. The difference in between using the worst 1 s average or the average for the full time of the analysis, is rather insignificant.

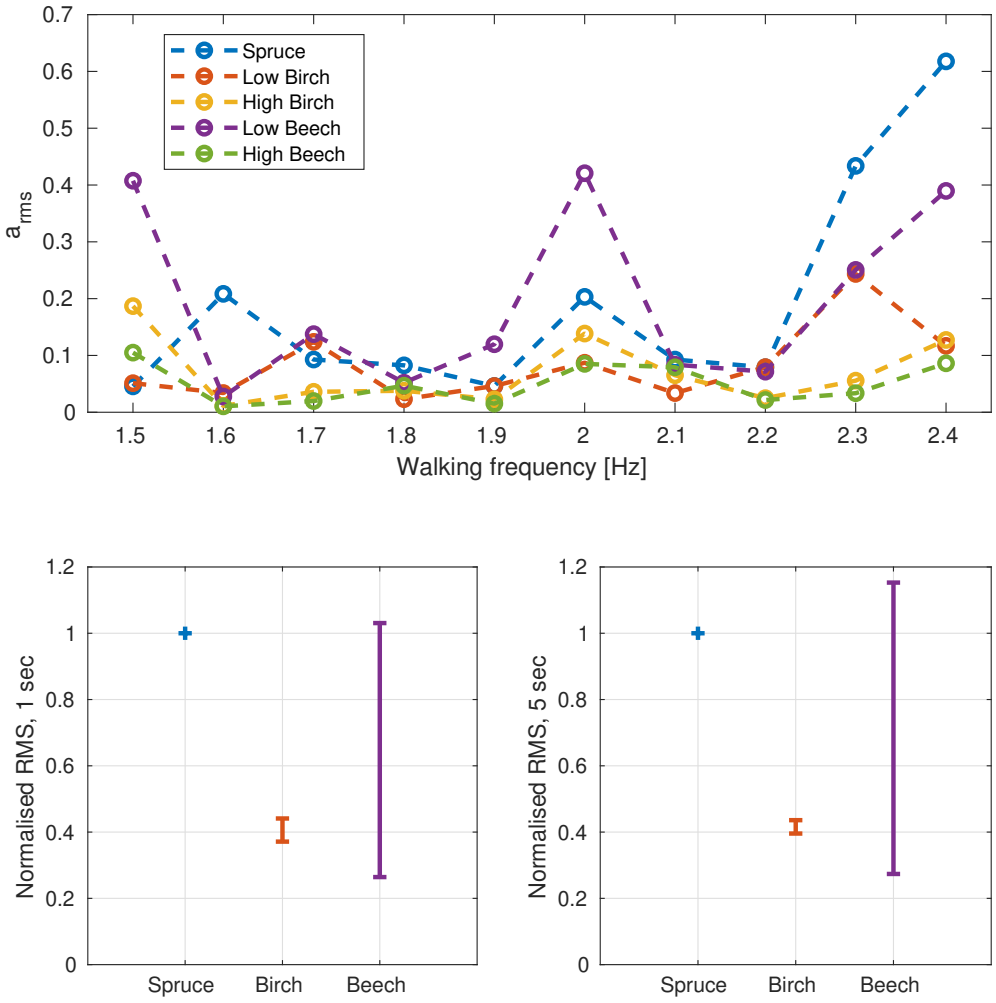

Figure 9.25: RMS acceleration response, a_{RMS}, for walking frequencies in between 1.5 and 2.4 Hz (top), and normalised averaged RMS values for the worst second of response (lower left) and for the full simulated time (lower right). Plots valid for the small panel.

Medium panel

For the medium panel constructed with spruce, the response is the worst for walking frequencies 1.8 and 2.1 Hz, see Figure 9.26. Just like for the small panel, these walking frequencies have harmonics that matches the fundamental frequency of the panel well. For 1.8 Hz, the 7th harmonic matches well, whereas for 2.1 Hz, the 6th harmonic matches well, see Figure C.1 and C.2.

For both the low- and high values of birch, the response is reduced when compared to spruce. For low birch, the harmonics of the walking frequencies do not match the fundamental frequencies very well for any of the tested walking frequencies. However, the walking frequencies 1.5, 2.0, 2.1 and 2.4 Hz have harmonics which matches the fundamental frequency to some extent, and in turn show higher response than the remaining walking frequencies, see Figure C.3 and C.4. For the walking frequency 2.2 Hz, the fundamental frequency falls almost exactly in between two harmonics which in turn results in a very small response. High birch shows higher response than low birch for most walking frequencies for the medium panel. This is especially noticeable for walking frequencies 1.8 and 2.2 Hz, where high birch has a harmonic closer to the fundamental frequency than low birch, and in turn the response is higher, see Figures C.5 and C.6.

The low value of beech produces the highest overall response for the medium panel. Two notable peaks occur at 1.8 Hz and 2.1 Hz, see Figure 9.26. The harmonics for these walking frequencies match the fundamental frequency well, see Figure C.7 and C.8. However, a harmonic of walking frequency 1.5 Hz also matches the fundamental frequency in a similar fashion but does not acquire the same magnitude in response. When examining the acceleration response in the time-domain, an explanation might be found. For the lower walking frequency, 1.5 Hz, the response is more impulsive. The response is being damped out in between the walking strikes, whereas for 1.8 and 2.1 Hz, the response is much more resonant, meaning the response increases for as long as the steps are occurring and not decreased until after the last step. An interesting comparison can also be made between 2.1 and 2.4 Hz, where there is a large difference in response. For 2.4 Hz, the fundamental frequency falls almost perfectly in the middle of two harmonics and in turn the response is largely reduced. For 2.1 Hz, a harmonic of the walking frequency matches the fundamental frequency almost perfectly. High beech shows large improvement in comparison to the low values of beech. Even though some of the harmonics match well with the fundamental frequency (e.g 1.8 Hz and 2.2 Hz) the response is significantly lower than that of low beech.

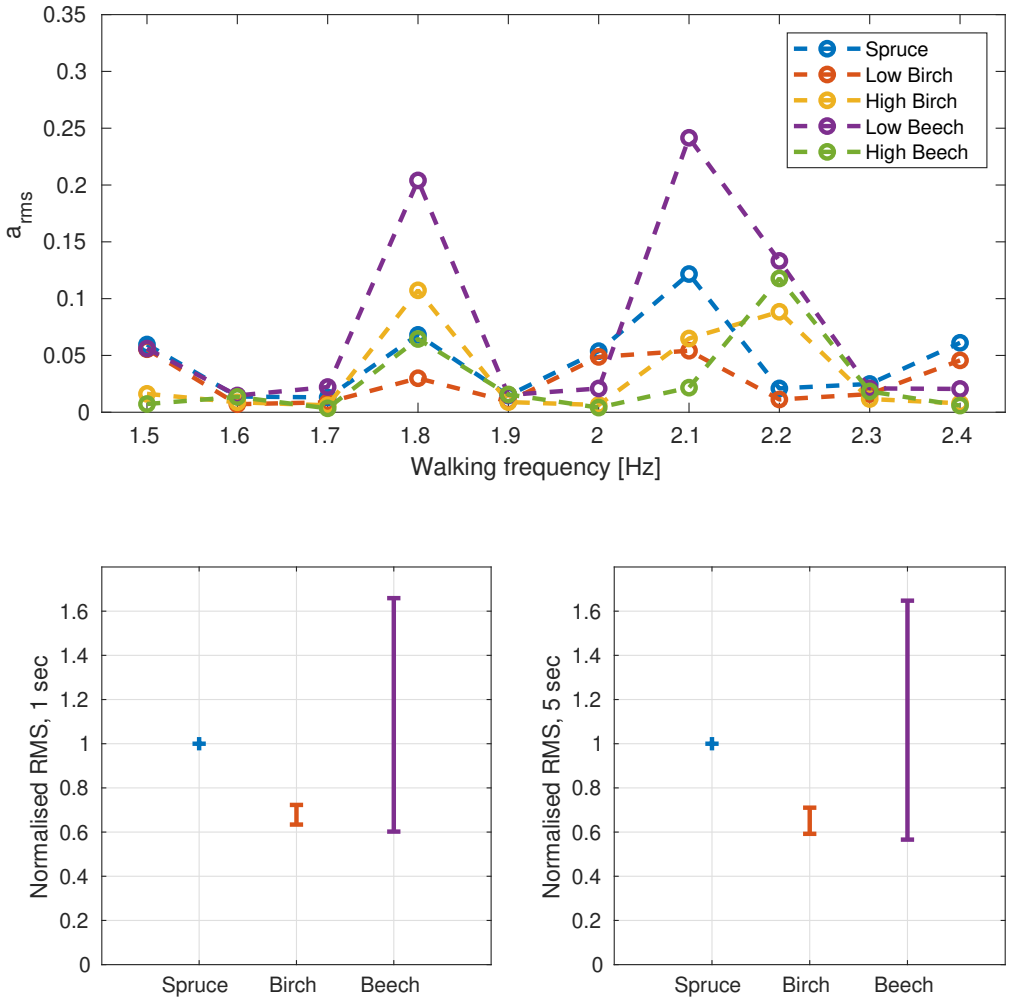

Figure 9.26: RMS acceleration response, a_{RMS}, for walking frequencies in between 1.5 and 2.4 Hz (top), and normalised averaged RMS values for the worst second of response (lower left) and for the full simulated time (lower right). Plots valid for the medium panel.

Large panel

The RMS values for the large panel are largely influenced by material selection and walking frequencies, as for the small and medium panels, see Figure 9.27. In general, the response is the largest for spruce, with the exceptions of walking frequencies 1.5 and 2.4 Hz. The same is also indicated from the averaged RMS values in the same figure, where the response for spruce is markedly higher than the response for birch and beech. For spruce, the highest response occurs for walking frequencies of 1.7, 2.1 and 2.2 Hz. As can be seen in Figures D.1 and D.2, at 1.7 and 2.1 Hz a harmonic and the fundamental frequency matches well. At 2.2 Hz the match is fairly good, but not quite as good as the previously mentioned frequencies, which might explain the lower response compared to 1.7 and 2.1 Hz. For the remaining walking frequencies for spruce, there are no other close matches, and most fundamental frequencies fall in between two harmonics, which in turn results in a low response.

For the low values of birch, the response is lower than spruce for most walking frequencies, but some minor peaks occur for 1.7, 2.1 and 2.2 Hz where the 5th harmonic of the walking frequency matches the fundamental frequency very well, see Figures D.3 and D.4. For high birch, the response is low for all walking frequencies except for 1.5 Hz, where the 5th walking harmonic matches the fundamental frequency well, see Figure D.5. Walking frequencies 1.8, 1.9 and 2.4 Hz also matches the fundamental frequency fairly well (Figure D.6). However, the match is not as good as for 1.5 Hz, which might be the reason why no peaks occur for these frequencies. For a walking frequency of 1.5 Hz, the response of low birch is lower than for high birch. However, a harmonic of the walking frequency matches the fundamental frequency closer for high birch.

For beech, the response is very similar to high birch, especially for high beech. High beech has more or less an identical RMS response as high birch and the value for the first walking frequency 1.5 Hz is peaking due to the exceptional match between the 5th walking harmonic and the fundamental frequency, see Figure D.9. The same is also valid for low beech, where a peak occurs at 1.5 Hz, see Figure D.7 In addition, high beech shows an increased RMS response for the two highest walking frequencies, as the 5th harmonic matches the fundamental frequency well.

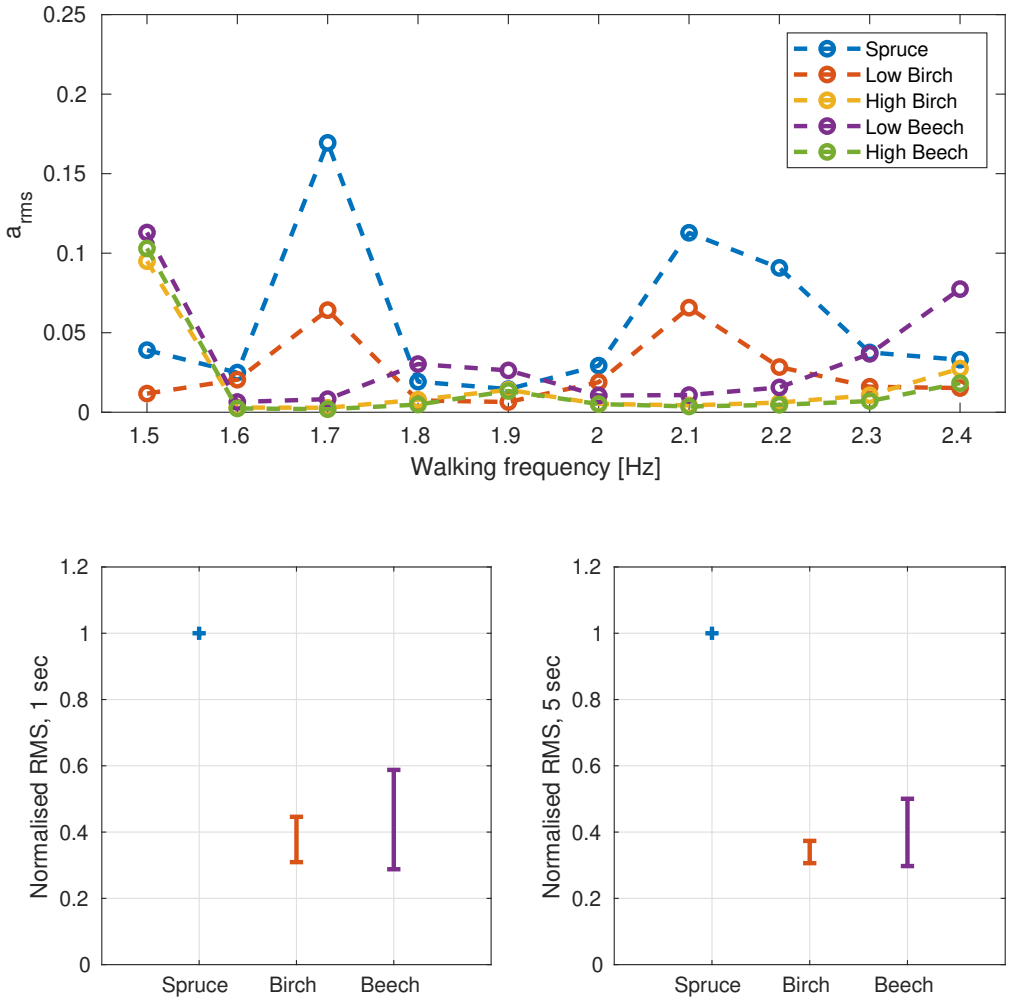

Figure 9.27: RMS acceleration response, a_{RMS}, for walking frequencies in between 1.5 and 2.4 Hz (top), and normalised averaged RMS values for the worst second of response (lower left) and for the full simulated time (lower right). Plots valid for the large panel.

10 Discussion

This chapter presents a discussion on the validity of the chosen method of modelling CLT and on the results presented for the case study. Simplifications and approximations made throughout the dissertation will be repeated in the forthcoming sections for the sake of a collected discussion.

10.1 Availability of stiffness parameters of hardwood

During the collection of stiffness parameters for various wood species it was discovered that they are not as widely available for hardwoods as they are for spruce. In general, the rolling shear modulus was the least available parameter. This might be because it is difficult to determine in comparison to for example the longitudinal elastic modulus. In addition, the rolling shear modulus has not historically been used much when designing timber constructions until CLT was invented.

For design purposes, E_{R} is usually set to the same value as the E_{T} which is lower. A probable reason for this is that there are variations in how the annual rings of the laminations are oriented. This was not considered when selecting the material parameters for the case study, where instead the actual values of E_{R} were used. It could have been interesting to use the same approach as for design purposes, where the lower value of E_{R} and E_{T} is used for both. Another approach could be to use an average value of E_{R} and E_{T} to account for variations in annual ring orientation of the laminations. Both approaches could influence the results.

10.2 Numerical modelling

The layered model used for the analyses introduces several approximations. For example, full interaction was introduced in between individual laminations. In addition, the model used for the analyses also assumes homogeneous material distribution throughout the panel, i.e. every lamination, or in this case every layer, had the same material orientation and material parameters.

The panels tested in the case study have been modelled as simply supported. Displacement boundary conditions could largely influence the dynamic behaviour of a floor panel, meaning errors might arise due to the chosen approach to model boundary conditions. An alternative and more in-depth approach could be to also model the connecting walls and columns that the panel is connected to, and thus capturing the contributing stiffness properties of the supports. However, this approach requires information about the building and the results would be specific to one type of building/wall/clamping construction. In contrast to the present work, which aim has been

to study the general effect of utilising hardwood in floor panels, this might be more interesting when considering conditions in a specific building.

10.3 Model validity

Determining when a model is sufficiently accurate is a challenging task. In the present work, three different models were initially created, as described in Chapter 6. The model that produced the best initial results compared to the results of the experimental modal analysis was the layered model. The high-fidelity model with constraints between laminations produced similar results as the layered model, however with much longer computational time as a consequence. The layered model was thus chosen early on as the best modelling approach, from a perspective of accuracy and computational time required.

It should be noted that for the comparison between the three models and the experimental results in Section 7.6, material parameters of strength class C24 were used. Using C40, which corresponds well to the weight of the tested panel, might have resulted in another model matching the experimental results more accurately.

The test specimen panel used in the experiments was rather small, 1.0×1.5 m^2, and thus rather thick in comparison to its width/length in contrast to the larger panels evaluated in the case study. This might be a reason why the layered model produced the most accurate results when compared with the experimental results initially. It performed better than the composite model, which in general is a very good modelling approach for thin plates. For the analyses performed in Chapter 9 it is thus difficult to assess if the layered model is the best modelling approach, since the modelling choice is based on the smaller test specimen, but it is at least an adequate approach.

It is important to remember that the experimental testing was performed on a single CLT panel. Testing of multiple panels reduces the risk of potential specimen outliers and faulty measurements. With an average NRFD of 0.8% for the first 9 modes, the calibration showed that the layered model could accurately describe the dynamic behaviour of the CLT panel used for experimental testing.

10.4 Effect of wood species on modal properties

The largest panel acquired the lowest natural frequencies. It could be observed that the mode order was not influenced much by the material choice. At most, one mode shift per set of parameters was observed. In general, the natural frequencies are increased with the low material values of birch and beech. A clear trend for the high values cannot as easily be identified. The results indicate that there is a high possibility to move natural frequencies by utilising different materials, which was also concluded in [3]. The present work also indicates a low possibility of alternating the mode order by utilising different materials. This is strengthened by [3] where the same conclusion was made.

10.5 Effect of wood species on FRFs

The FRFs showed that the fundamental frequencies for birch and beech were lower than for spruce. It was established in the sensitivity study in Chapter 8 that increasing the mass density resulted in lower natural frequencies. The increase in mass is thus likely the reason for why the fundamental frequencies are lower for the high values of birch and the low- and high value of beech. The other material parameters are generally higher than spruce which should lead to a stiffer panel, except for low beech which has a lower value of longitudinal elastic modulus E_{L} when compared to the reference case spruce, 10 000 vs 10 991 MPa. The fundamental frequency is not changed by a substantial amount for low birch compared to spruce. Intuitively, the frequency would be reduced by the increase in mass, 510 vs 390 kg/m^3. However, low birch also has an increased E_{L} compared to spruce, 13 000 vs 10 991 MPa, which might explain why the fundamental frequency does not change much. The same cannot be seen for the high values of birch and beech, which might be because the mass density has a higher effect on the fundamental frequency than the other parameters.

In [3], a detailed sensitivity study of the different material parameters effect on transfer mobility functions (velocity FRFs) was conducted. The study showed that four parameters generally had the largest effect: Density ρ, longitudinal elastic modulus E_{L}, shear modulus G_{LT} and the rolling shear modulus G_{RT}. The magnitude of the velocity FRFs was shown to be primarily affected by the density ρ and rolling shear modulus G_{RT}. The study also showed that natural frequencies increase as longitudinal elastic modulus E_{L} and shear modulus G_{LT} is increased, with the longitudinal elastic modulus having the greatest effect of the two. A reason for why beech generally slightly outperforms birch when it comes to magnitude might be because beech not only has higher density than birch, but also a higher rolling shear modulus G_{RT}. This agrees well with [3], where the density was shown to have the highest impact on the magnitude of the FRFs, and the rolling shear modulus the second highest impact on the magnitude.

10.6 Effect of wood species and walking frequencies on footfall response

Ten different walking frequencies were evaluated for every panel and every wood species. The RMS response from footfall loading show large variation in result depending on how well a harmonic of a walking frequency matches the fundamental frequency. This was in general apparent for all panels and all materials, with some exceptions. Previous research and design codes usually mentions the first four harmonics of the walking frequency to be of extra importance, but the present work indicates that even the 8th or 9th harmonic might cause an amplification of the RMS-value.

It should be noted however, that if more walking frequencies were tested, e.g. 100 frequencies in between 1.5 and 2.4 Hz, panels which did not experience any large response due to the absence of matching frequencies, would be more likely to acquire a higher response. With 10 frequencies, this might be missed. For example, the medium

panel with spruce did not experience any close match resulting in a low response, whereas some values of beech did experience a close match, and thus acquiring a higher response than spruce. If more walking frequencies would have been tested, spruce might have acquired a higher response than low beech. In other words, the results could be affected due to the discretization of walking frequencies.

From the averaged RMS responses, it could be observed that the variation in response between the low- and high values of beech compared to the low- and high values of birch is fairly different. Beech shows large intervals, whereas birch generally has intervals much smaller. This could be a direct consequence of the material parameters, see Table 9.1, where there are much larger spans for the beech parameters, e.g. 10 000–18 000 MPa for beech compared to 13 000–16 600 for birch. It could also be due to the aforementioned lack of discretization of walking frequencies.

The measurement point used for evaluating the highest acceleration response was in the middle of the panel since it is expected that the first bending mode might be the primary excited mode. This seemed to hold true when comparing the acceleration response of the middle point with the acceleration response of the point at the edge, previously referred to as point M1, see Figure 9.16. This, despite the middle point being a zero node for several modes, meaning that some modes do not contribute to any acceleration response there. An alternative point that potentially could have shown a larger response is the mid-point in the length direction, but closer to the edge in the width direction of the panel. For such a point the acceleration response could be higher than for the mid-point, as both bending and twisting could contribute to the response.

When comparing the response of the different panels, it is noticeable that the acceleration response is markedly lower for the larger panel compared to the small panel. This might be due the weight of the large panel being significantly higher than the small panel, thus mitigating the vibration response.

Footfall modelling is the only load case evaluated in the transient analysis. As was seen in the results, the footfall loading primarily excited the first mode. Other loads, such as loads from a washing machine, or traffic loads, might excite higher-frequency modes, in turn causing a different response. For such a case, the effect of birch and beech could be different. For example, in the sensitivity study, see Chapter 8, the rolling shear modulus affected all modes, but the largest effect was found for higher modes. Thus, since especially beech has a substantially larger rolling shear modulus, the potential positive effect might be greater for other types of loads.

The footfall modelling is, as is all modelling, an approximation of reality. In the present work, footfall was modelled as evenly distributed pressure on a quadratic surface. This approximation might not completely mimic reality, where a footstep might have longer length in comparison to the width. It is possible to model the footsteps in more detail, even using real footprints and spending a substantial time on meshing said parts. This was however deemed outside the scope of the dissertation.

11 Main conclusions

The aim of the present work was to evaluate the dynamic response of cross-laminated timber floor panels made of non-conventionally used species, e.g. birch and beech. The main conclusions are presented in this chapter, followed by propositions of future work. The conclusions are as follows:

- The layered model, in conjunction with deterministic material parameters, is a viable approach for modelling the dynamic properties of cross-laminated timber panels. The modal behaviour is captured accurately for such a model.
- Stiffness parameters for hardwood are not widely available, especially the rolling shear modulus.
- Changing material from spruce to birch and beech had little effect on the modal order for all panels considered in the present work.
- The material choice has an effect on the natural frequencies of floor panels. The fundamental frequency is generally lowered by utilising hardwoods compared to spruce.
- The walking frequency largely influences the dynamic response of CLT floor panels. Due to this, design methods considering only a single walking frequency might result in misrepresentation of the actual dynamic response.
- For a floor subjected to footfall loading, the response in the frequency domain is largely dominated by the first mode.
- Walking harmonics above the 4th influence the dynamic response of floor panels. In the present work, harmonics as high as the 9th harmonic might amplify the response.
- Changing material from spruce to birch and beech generally reduces the RMS of both the FRFs and the transient acceleration response. This effect was more prevalent for the higher material values of birch and beech.
- A potential reduction in acceleration response by utilising birch and beech in CLT is shown to be more apparent for longer spans.

11.1 Further work

In this section, propositions for further work are presented.

- Study and determine material parameters for hardwood species.
- Continue studying how the order of harmonic impacts the amplification of the response.
- Study more walking frequencies, i.e. 100 or 1000 values in a plausible range, to eliminate the risk of bad matches for certain walking frequencies.
- Conduct a study using other measurement points and walking patterns than those used in transient study of this dissertation. This to excite and capture modes which could not be captured by measuring response at mid-point.
- An interesting continuation of work from a modelling perspective would be to perform experimental testing on a larger panel, and conduct Newton optimisation for all three different models to asses which modelling approach might ultimately be the best for a panel which is of a more practical size.

Bibliography

[1] Kirsi Jarnerö. 'Vibrations in timber floors : Dynamic properties and human perception'. PhD thesis. Linnaeus University, Department of Building and Energy Technology, 2014, p. 64. ISBN: 9789187925238.

[2] Beatrice Bartolucci, Andrea Rosa, Chiara Bertolin, Filippo Berto, F. Penta, Anna Siani, Citation Bartolucci, De Rosa, A Bertolini, C Berto and F Siani. 'Mechanical properties of the most common European woods: a literature review'. In: *Frattura ed Integrità Strutturale* 14 (Aug. 2020), pp. 249–274. DOI: 10.3221/IGF-ESIS.54.18.

[3] Peter Persson, Ola Flodén, Henrik Danielsson, Andrew Peplow and Lars Vabbersgaard Andersen. 'Improved low-frequency performance of cross-laminated timber floor panels by informed material selection'. In: *Applied Acoustics* 179 (2021), p. 108017. ISSN: 0003-682X. URL: https://www.sciencedirect.com/science/article/pii/S0003682X21001109.

[4] Liaison Unit Bratislava Ministerial Conference on the Protection of Forests in Europe FOREST EUROPE. 'FOREST EUROPE, 2020: State of Europe's Forests 2020.' In: (2020). URL: www.foresteurope.org.

[5] Skogskunskap. *Björk (Betula spp.)* sv. URL: https://www.skogskunskap.se/skota-lovskog/om-lov/vara-lovtrad/bjork-betula-spp/ (visited on 19/05/2022).

[6] John M. Dinwoodie. *Construction Materials, their nature and behaviour*. E & FN, 1994. ISBN: 0 419 15470 1.

[7] Emil Nilsson. 'Characterisation of Cross Laminated Timber Properties'. In: (July 2021).

[8] Per Gunnar Burström and Kjell Nilvér. *Byggnadsmaterial. Tillverkning, egenskaper och användning. 3'e upplagan*. Studentlitteratur, 2019. ISBN: 978-91-44-05755-2.

[9] Swedish Wood. *Design of timber structures Volume 1 Edition 2:2016*. ISBN: 978-91-980304-8-8.

[10] *Standard - Träkonstruktioner - Konstruktionsvirke - Hållfasthetsklasser SS-EN 338:2016*. sv. (Visited on 05/04/2021).

[11] *Standard - Eurokod 5: Dimensionering av Träkonstruktioner - Del 1-1: Allmänt - Gemensamma Regler och Regler förr Byggnader SS-EN 1995-1-1:2004*. sv. URL: https://www.sis.se/produkter/byggnadsmaterial-och-byggnader/byggnadsindustrin/tekniska-aspekter/ssen1995112004/ (visited on 28/02/2022).

[12] Niels Ottosen. *Introduction to the Finite Element Method*. New York: Prentice Hall, 1992. ISBN: 978-0-13-473877-2.

[13] Swedish Wood. *The CLT Handbook*. May 2019. ISBN: 978-91-983214-4-3.

[14] Sven Thelandersson. *Timber Engineering*. John Wiley & Sons, 2003. ISBN: 9780470844694.

[15] FPInnovations. *Canadian CLT Handbook 2019 Edition, Volume 1*. ISBN: 978-0-86488-592-0.

[16] Chopra K. Anil. *Dynamics of structures*. Pearson Education Limited, 2017. ISBN: 1978-1-29-224918-6.

[17] Craig R. Roy. *Fundamentals of structural dynamics*. New Jersey: John Wiley & Sons, 2006. ISBN: 978-0-471-43044-5.

[18] T. Ehrhart and R. Brandner. 'Rolling shear: Test configurations and properties of some European soft- and hardwood species'. In: *Engineering Structures* 172 (2018), pp. 554–572. ISSN: 0141-0296. URL: https://www.sciencedirect.com/science/article/pii/S0141029617338142.

[19] Kristian Dahl. 'Mechanical properties of clear wood from Norway spruce'. In: (Jan. 2009).

[20] Simon Aicher, Zachary Christian and Maren Hirsch. 'Rolling shear modulus and strength of beech wood laminations'. In: *Holzforschung* 70.8 (2016), pp. 773–781. URL: https://doi.org/10.1515/hf-2015-0229.

[21] Gerhard Schickhofer Georg Jeitler Manfred Augustin. 'Mechanical properties of Glued Laminated Timber and Cross Laminated Timber produced with the wood species birch'. In: *World conference on timber engineering; Vienna, Austria 2016* (2016).

[22] Hans Holmberg. and Dick Sandberg. *Structure and Properties of Scandinavian Timber*. 1997.

[23] Marija Milojević, Emilija Damnjanović, Marija Nefovska-Danilovic and Miroslav Marjanović. 'Effects of material uncertainties on vibration performance of cross laminated timber floors'. In: *Gradjevinski Materijali i Konstrukcije* 64 (Aug. 2021), pp. 153–157. DOI: 10.5937/GRMK2103153M.

[24] Ola Flodén, Kent Persson and Göran Sandberg. 'A multi-level model correlation approach for low-frequency vibration transmission in wood structures'. In: *Engineering Structures* 157 (2018), pp. 27–41. ISSN: 0141-0296. URL: https://www.sciencedirect.com/science/article/pii/S0141029616316753.

[25] Peter Niemz, Tomasz Ozyhar, Stefan Hering and Walter Sonderegger. 'Zur Orthotropie der physikalisch-mechanischen Eigenschaften von Rotbuchenholz'. In: *Bautechnik* 92.1 (2015), pp. 3–8. URL: https://onlinelibrary.wiley.com/doi/abs/10.1002/bate.201400079.

[26] Thomas Volkmer, Thomas Lorenz, Philipp Hass and Peter Niemz. 'Influence of heat pressure steaming (HPS) on the mechanical and physical properties of common oak wood'. In: *European Journal of Wood and Wood Products* 72(2) (2018), pp. 249–259. DOI: 10.1007/s00107-014-0777-9.

[27] Dassault Systemés Simulia Corp. *Abaqus/CAE*. Version 2019.

[28] Jenny Lau, Jeroen Lanslots, Bart Peeters and Herman Van der Auweraer. 'Automatic modal analysis. Reality or myth?' In: *Sound & vibration* (Jan. 2007).

[29] Christopher J. Freitas. 'Standards and Methods for Verification, Validation, and Uncertainty Assessments in Modeling and Simulation'. In: *Journal of Verification, Validation and Uncertainty Quantification* 5.2 (June 2020). 021001. ISSN: 2377-2158. URL: https://doi.org/10.1115/1.4047274.

[30] Thomas Lee Paez. 'Introduction to Model Validation.' In: (Nov. 2008). URL: https://www.osti.gov/biblio/1142730.

[31] Niels Saabye Ottosen and Matti Ristinmaa. 'The Mechanics of Constitutive Modeling'. In: ed. by Niels Saabye Ottosen and Matti Ristinmaa. Oxford: Elsevier Science Ltd, 2005. ISBN: 978-0-08-044606-6. URL: https://www.sciencedirect.com/science/article/pii/B9780080446066500047.

[32] Boverket. *BFS 2015:6, EKS 10*. 2015.

[33] G. Pernica. 'Dynamic Load Factors for Pedestrian Movements and Rhythmic Exercises'. In: *Canadian Acoustics* 18.2 (1990), p. 3. URL: https://jcaa.caa-aca.ca/index.php/jcaa/article/view/618.

[34] J.H. Rainer and G. Pernica. 'Vertical dynamic forces from footsteps'. In: *Canadian Acoustics* 14.2 (1986), 12–21. URL: https://jcaa.caa-aca.ca/index.php/jcaa/article/view/559.

[35] Yuanzhi Cai, Guobin Gong, Jun Xia, Jiale He and Jianli Hao. 'Simulations of human-induced floor vibrations considering walking overlap'. In: *SN Applied Sciences* 2 (Jan. 2020). DOI: 10.1007/s42452-019-1817-1.

[36] European Commission, Directorate-General for Research, Innovation, C Butz, G Sedlacek and C Heinemeyer. *Generalisation of criteria for floor vibrations for industrial, office, residential and public building and gymnastic halls*. Publications Office, 2006.

[37] Hugo Bachmann and Walter Ammann. *Vibrations in structures - Induced by Man and Machines*. IABSE-AIPC-IVBH, 1987. ISBN: 3-85748-052-X.

A FRFs from experimental testing

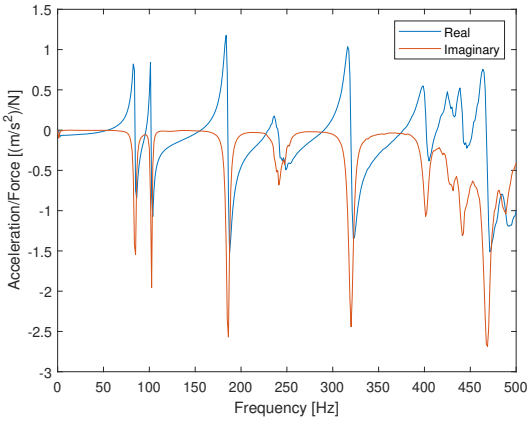

(a) Real and imaginary FRF for measurement point 1.

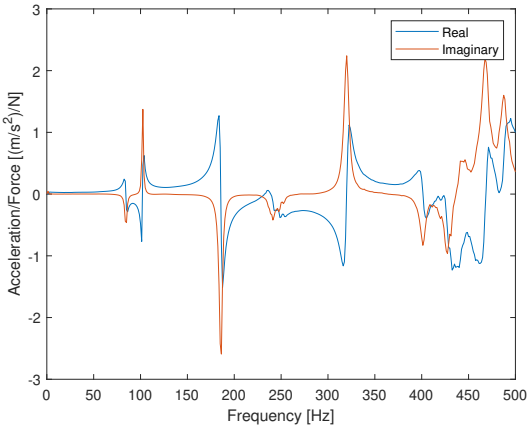

(b) Real and imaginary FRF for measurement point 2.

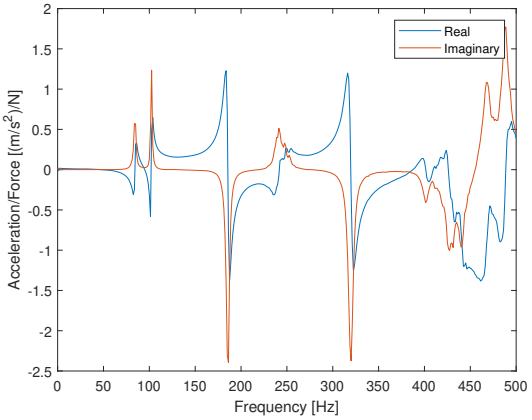

(c) Real and imaginary FRF for measurement point 3.

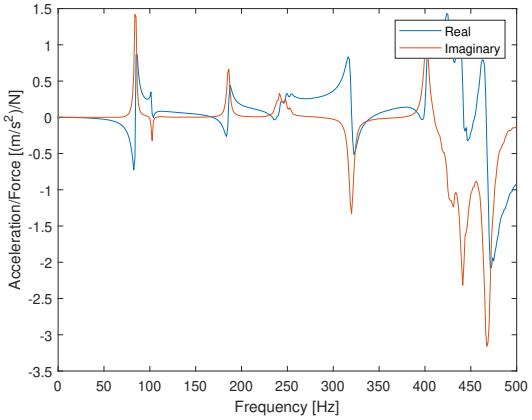

(d) Real and imaginary FRF for measurement point 4.

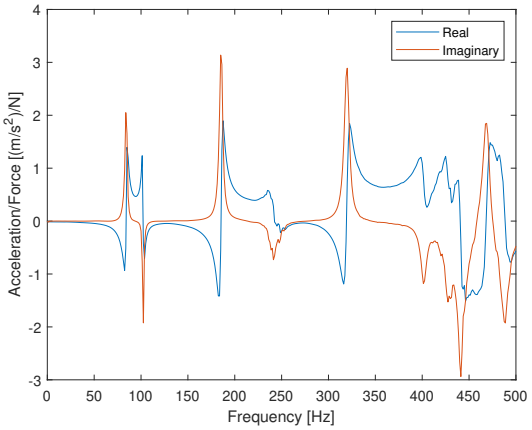

(e) Real and imaginary FRF for measurement point 5.

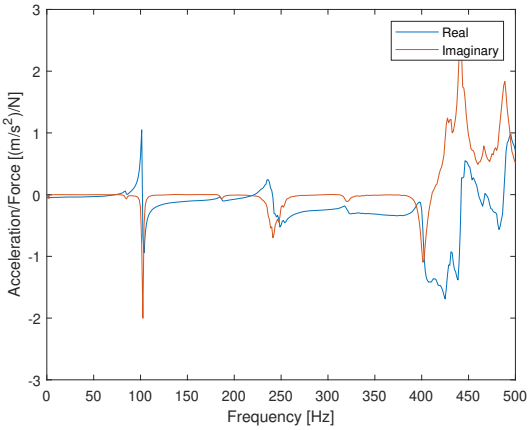

(f) Real and imaginary FRF for measurement point 6.

Figure A.1: FRFs acquired from BK Connect after experimental testing. Both real and imaginary components of the FRFs are shown.

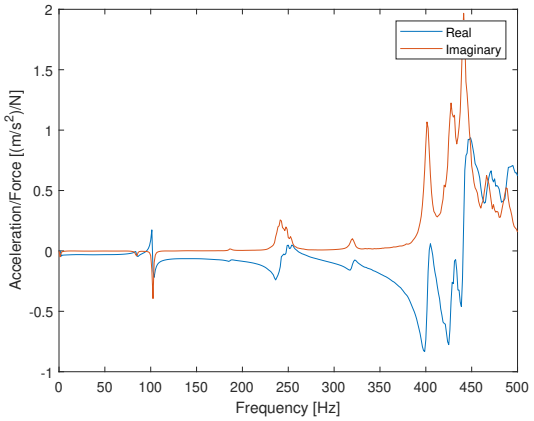

(a) Real and imaginary FRF for measurement point 7.

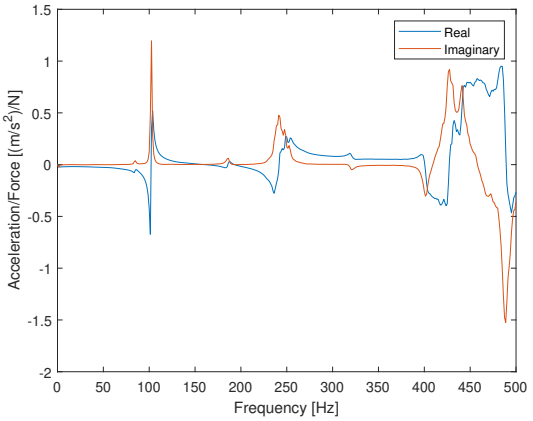

(b) Real and imaginary FRF for measurement point 8.

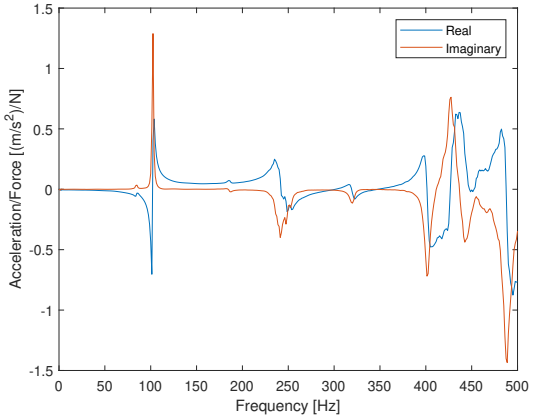

(c) Real and imaginary FRF for measurement point 9.

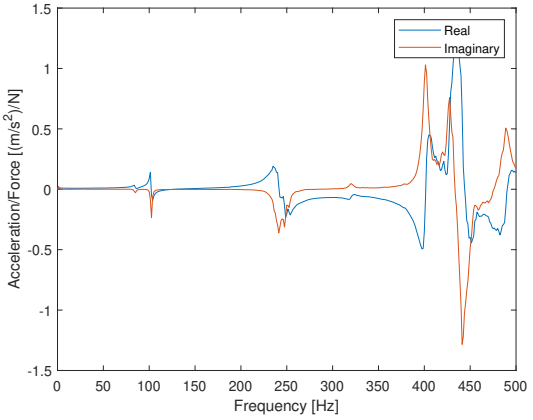

(d) Real and imaginary FRF for measurement point 10.

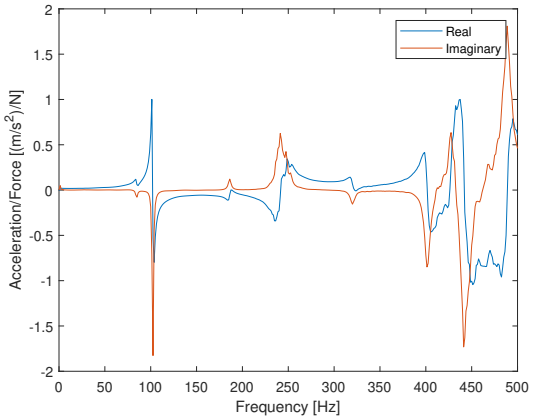

(e) Real and imaginary FRF for measurement point 11.

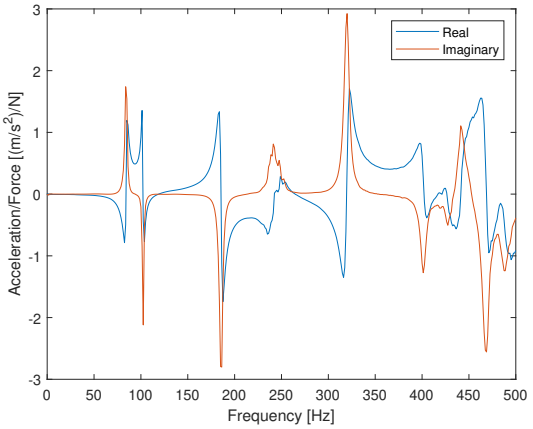

(f) Real and imaginary FRF for measurement point 12.

Figure A.2: FRFs acquired from BK Connect after experimental testing. Both real and imaginary components of the FRFs are shown.

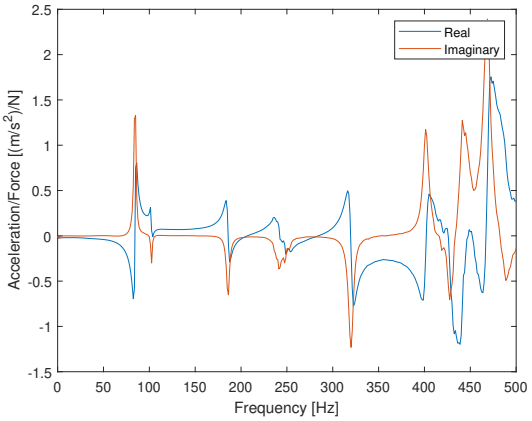

(a) Real and imaginary FRF for measurement point 13.

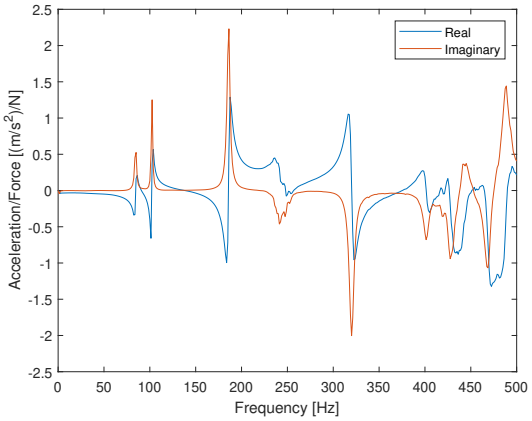

(b) Real and imaginary FRF for measurement point 14.

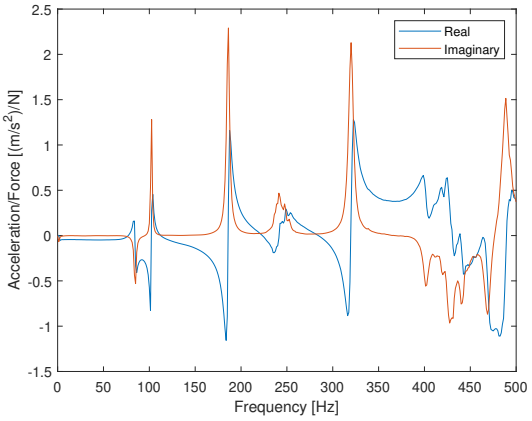

(c) Real and imaginary FRF for measurement point 15.

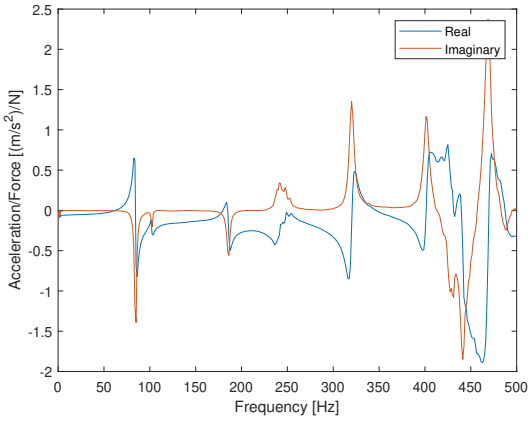

(d) Real and imaginary FRF for measurement point 16.

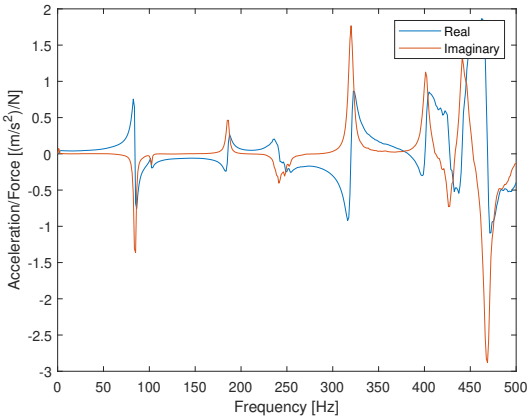

(e) Real and imaginary FRF for measurement point 17.

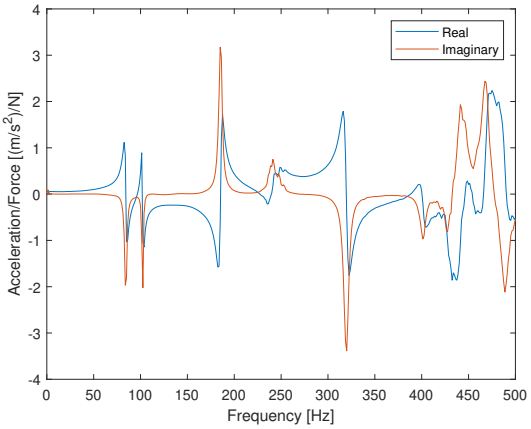

(f) Real and imaginary FRF for measurement point 18.

Figure A.3: FRFs acquired from BK Connect after experimental testing. Both real and imaginary components of the FRFs are shown.

B Acceleration response and FFTs of small panel

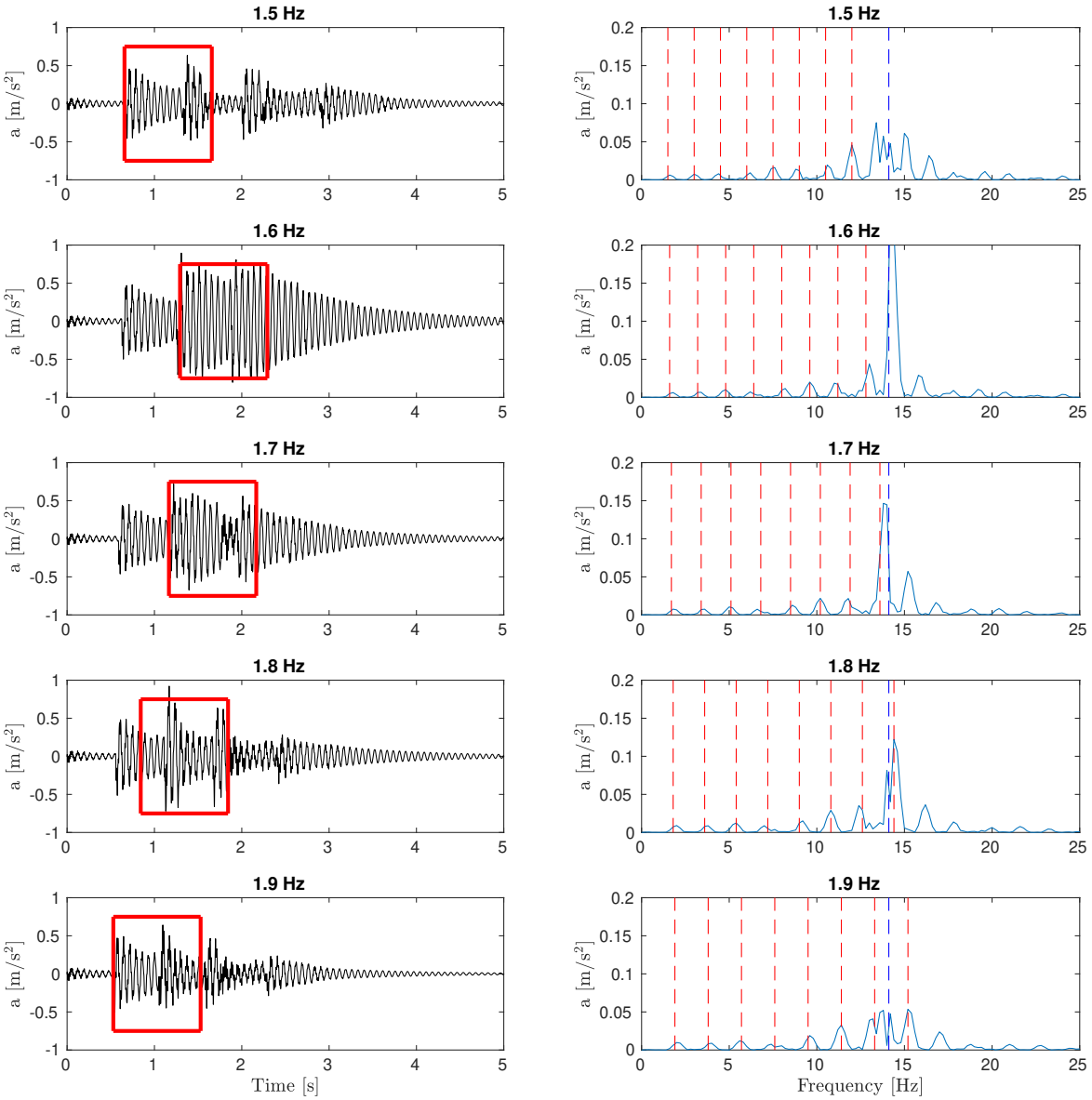

Figure B.1: Acceleration response (left column) and FFT of acceleration response (right column) walking frequencies between 1.5 to 1.9 Hz for spruce. Dashed red lines are walking harmonics, and dashed blue line the fundamental frequency.

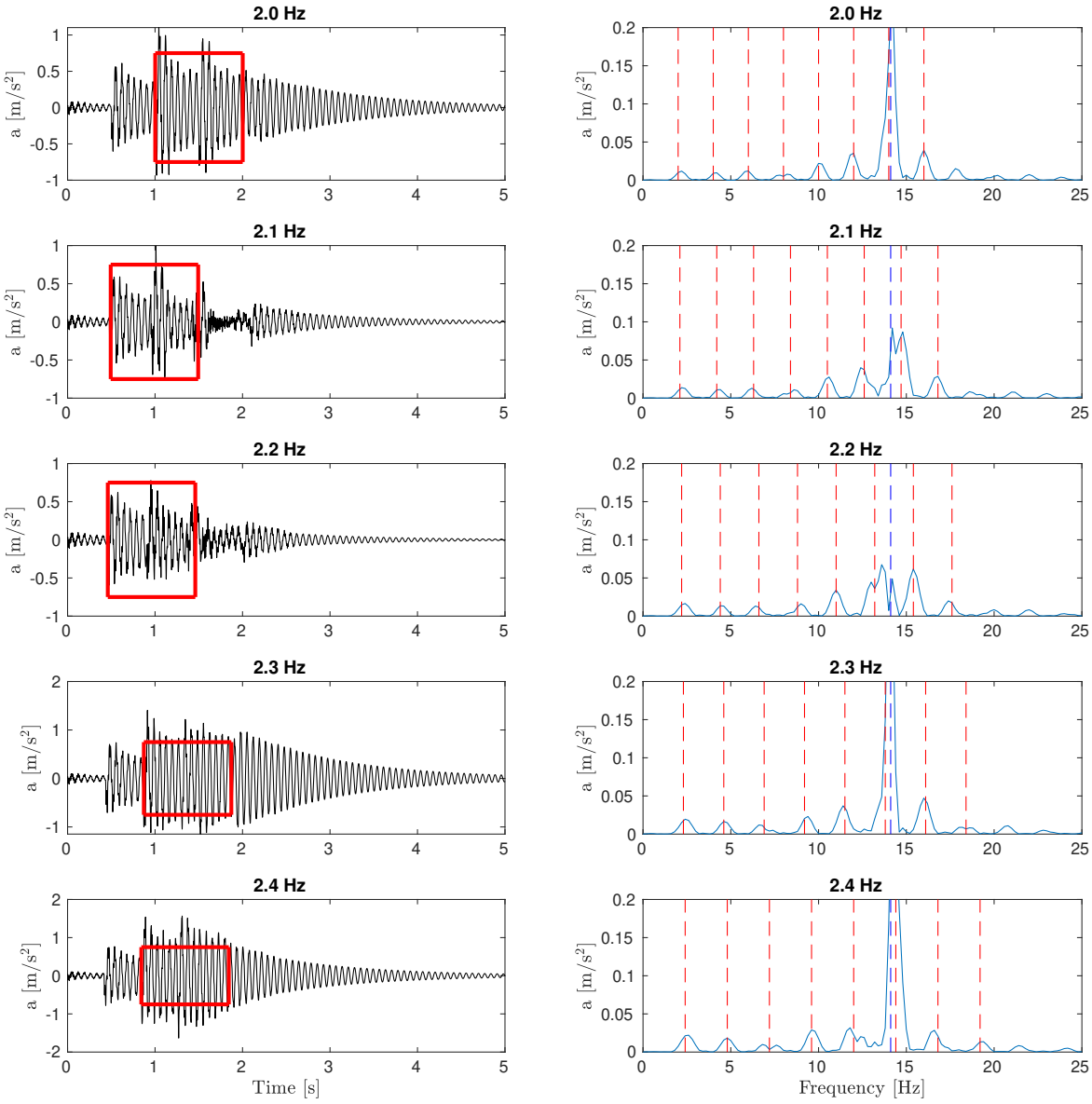

Figure B.2: Acceleration response (left column) and FFT of acceleration response (right column) walking frequencies between 2.0 to 2.4 Hz for spruce. Dashed red lines are walking harmonics, and dashed blue line the fundamental frequency.

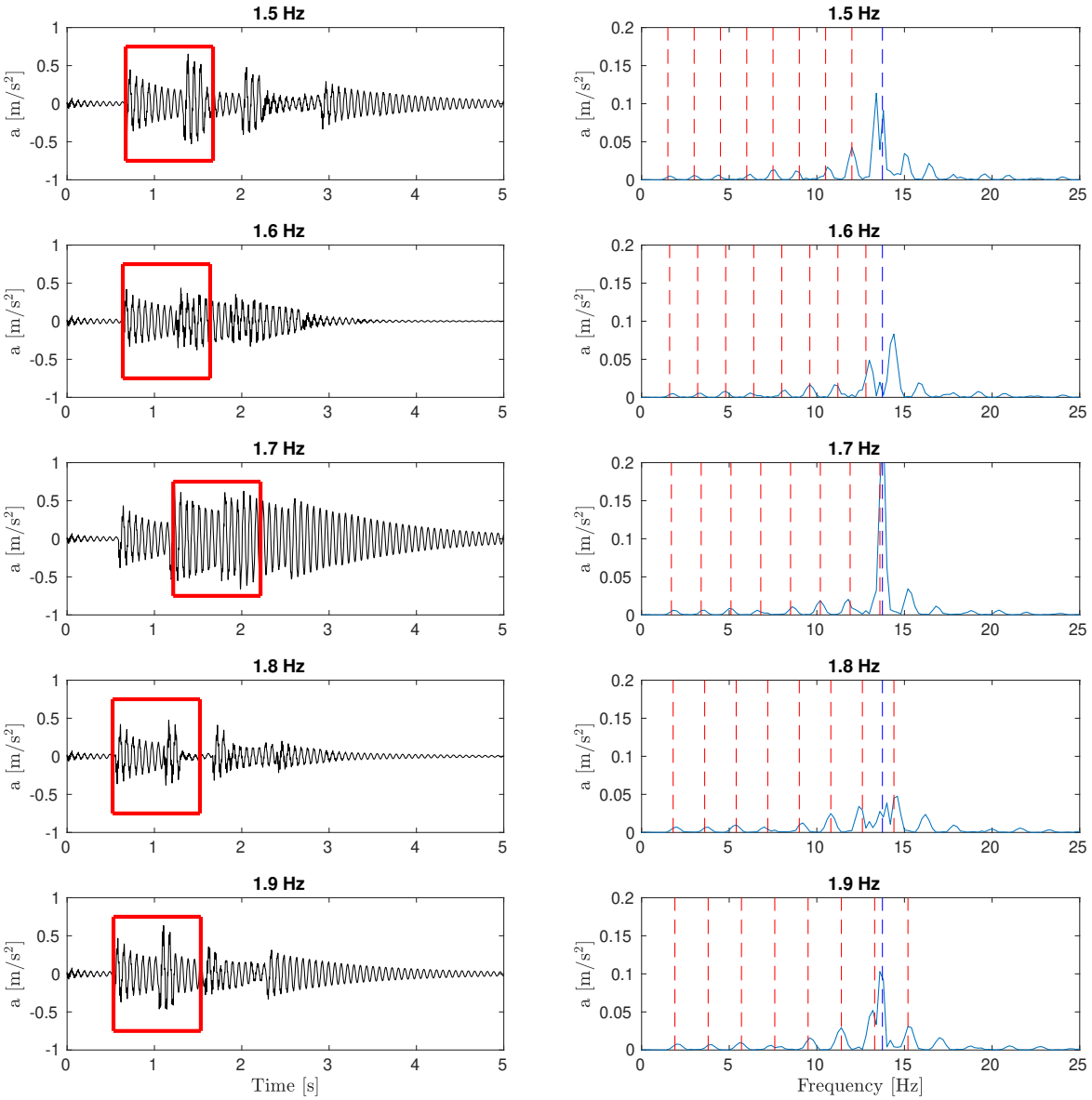

Figure B.3: Acceleration response (left column) and FFT of acceleration response (right column) walking frequencies between 1.5 to 1.9 Hz for low birch. Dashed red lines are walking harmonics, and dashed blue line the fundamental frequency.

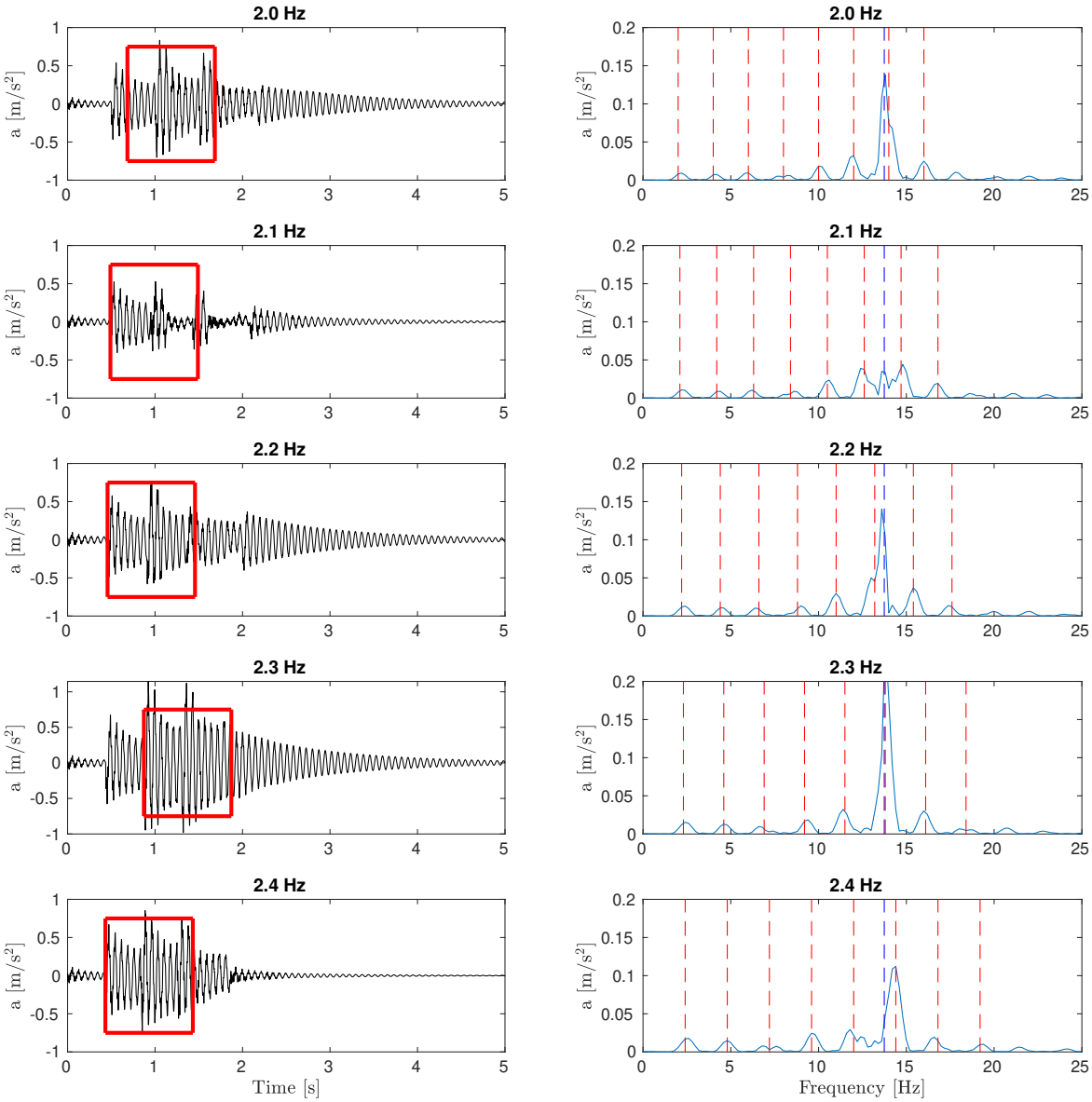

Figure B.4: Acceleration response (left column) and FFT of acceleration response (right column) walking frequencies between 2.0 to 2.4 Hz for low birch. Dashed red lines are walking harmonics, and dashed blue line the fundamental frequency.

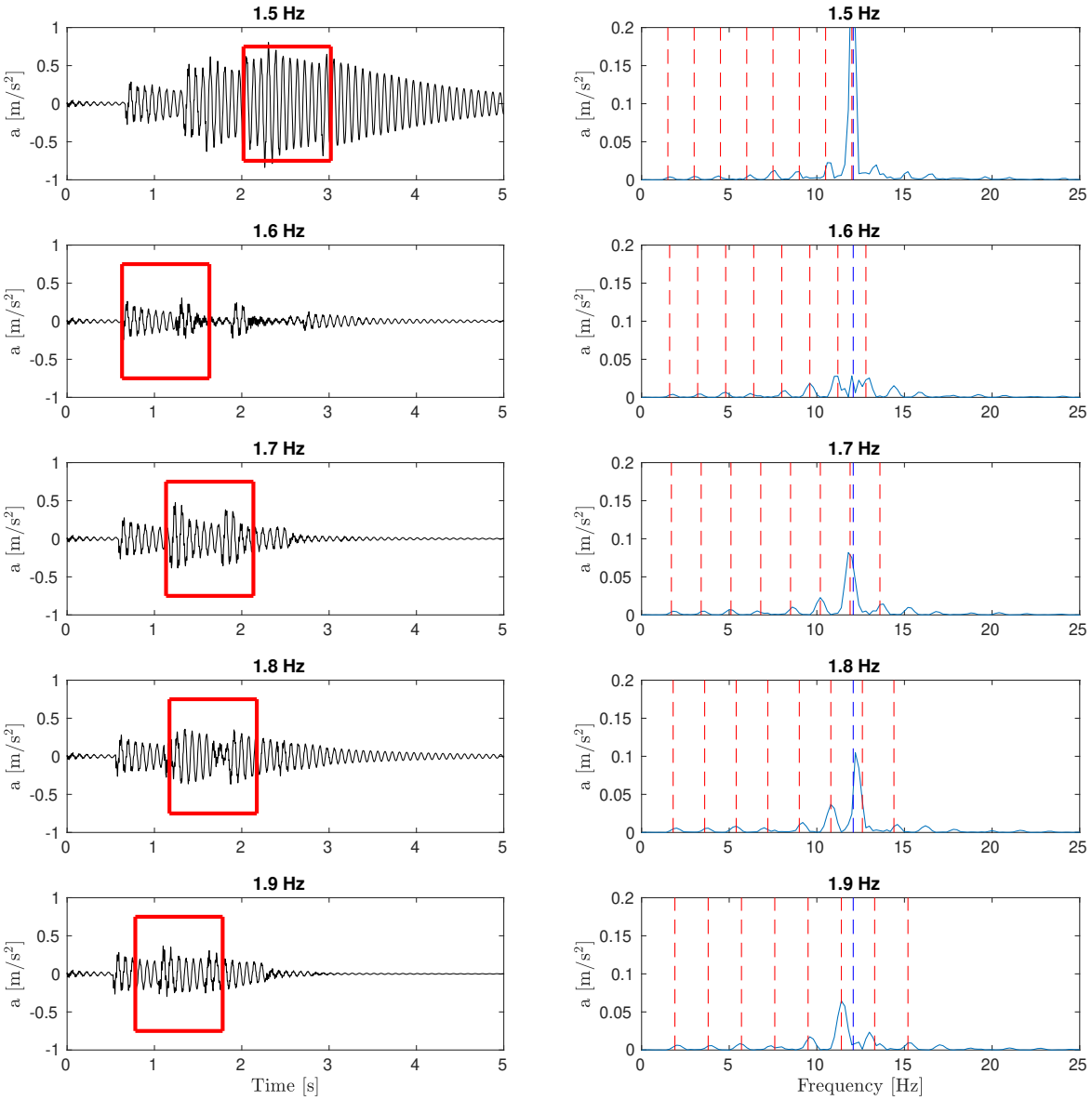

Figure B.5: Acceleration response (left column) and FFT of acceleration response (right column) walking frequencies between 1.5 to 1.9 Hz for high birch. Dashed red lines are walking harmonics, and dashed blue line the fundamental frequency.

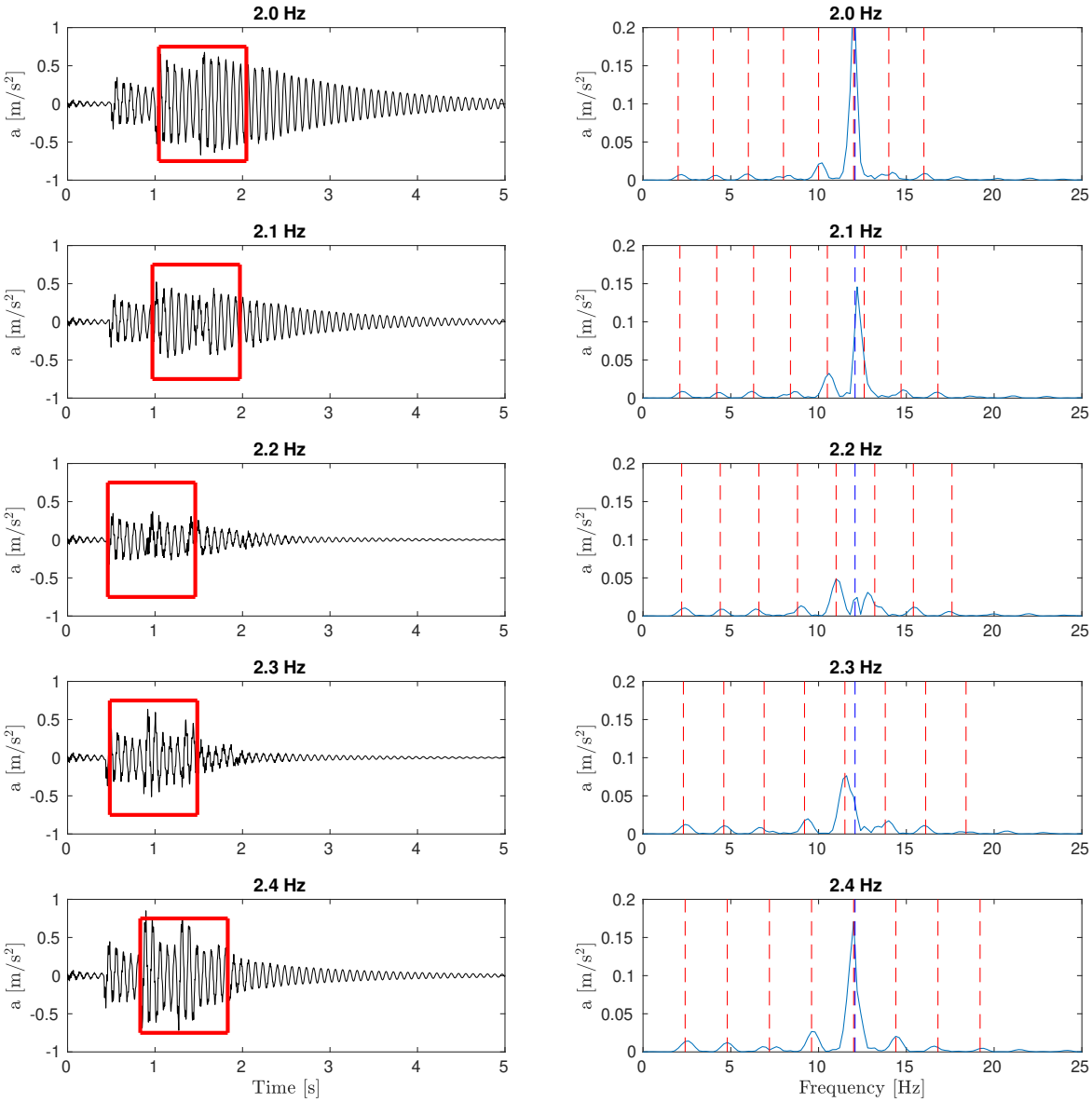

Figure B.6: Acceleration response (left column) and FFT of acceleration response (right column) walking frequencies between 2.0 to 2.4 Hz for high birch. Dashed red lines are walking harmonics, and dashed blue line the fundamental frequency.

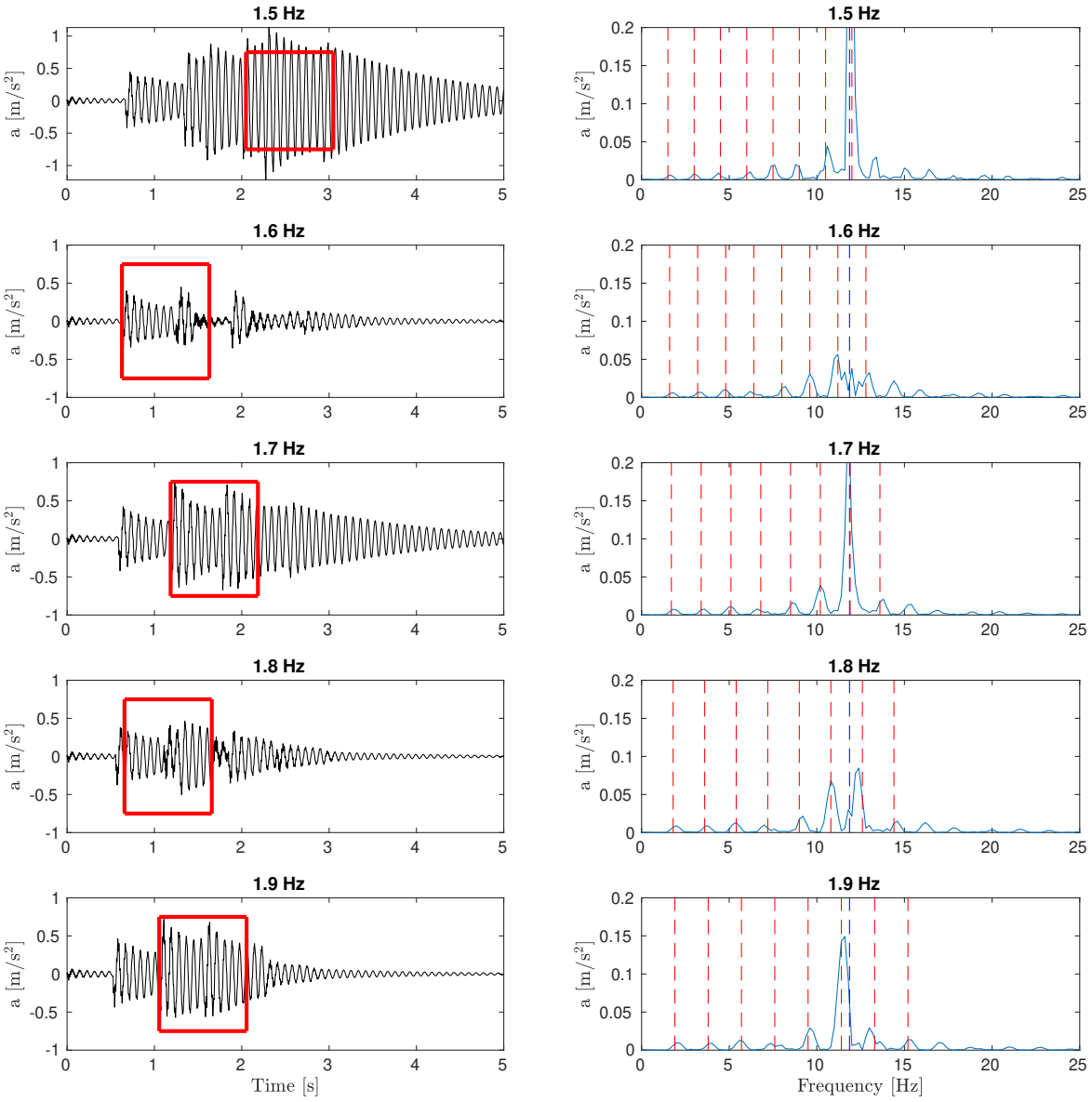

Figure B.7: Acceleration response (left column) and FFT of acceleration response (right column) walking frequencies between 1.5 to 1.9 Hz for low beech. Dashed red lines are walking harmonics, and dashed blue line the fundamental frequency.

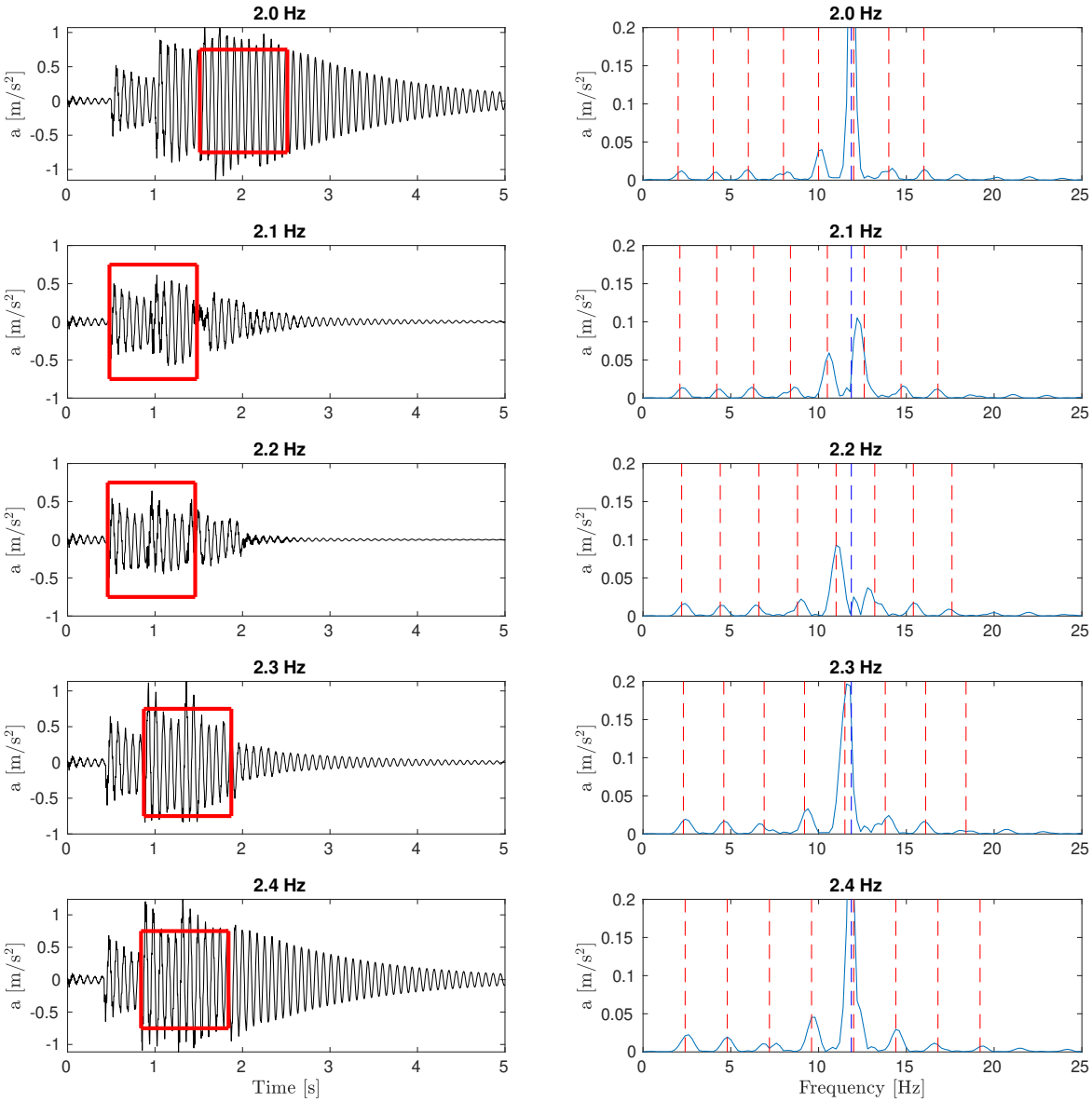

Figure B.8: Acceleration response (left column) and FFT of acceleration response (right column) walking frequencies between 2.0 to 2.4 Hz for low beech. Dashed red lines are walking harmonics, and dashed blue line the fundamental frequency.

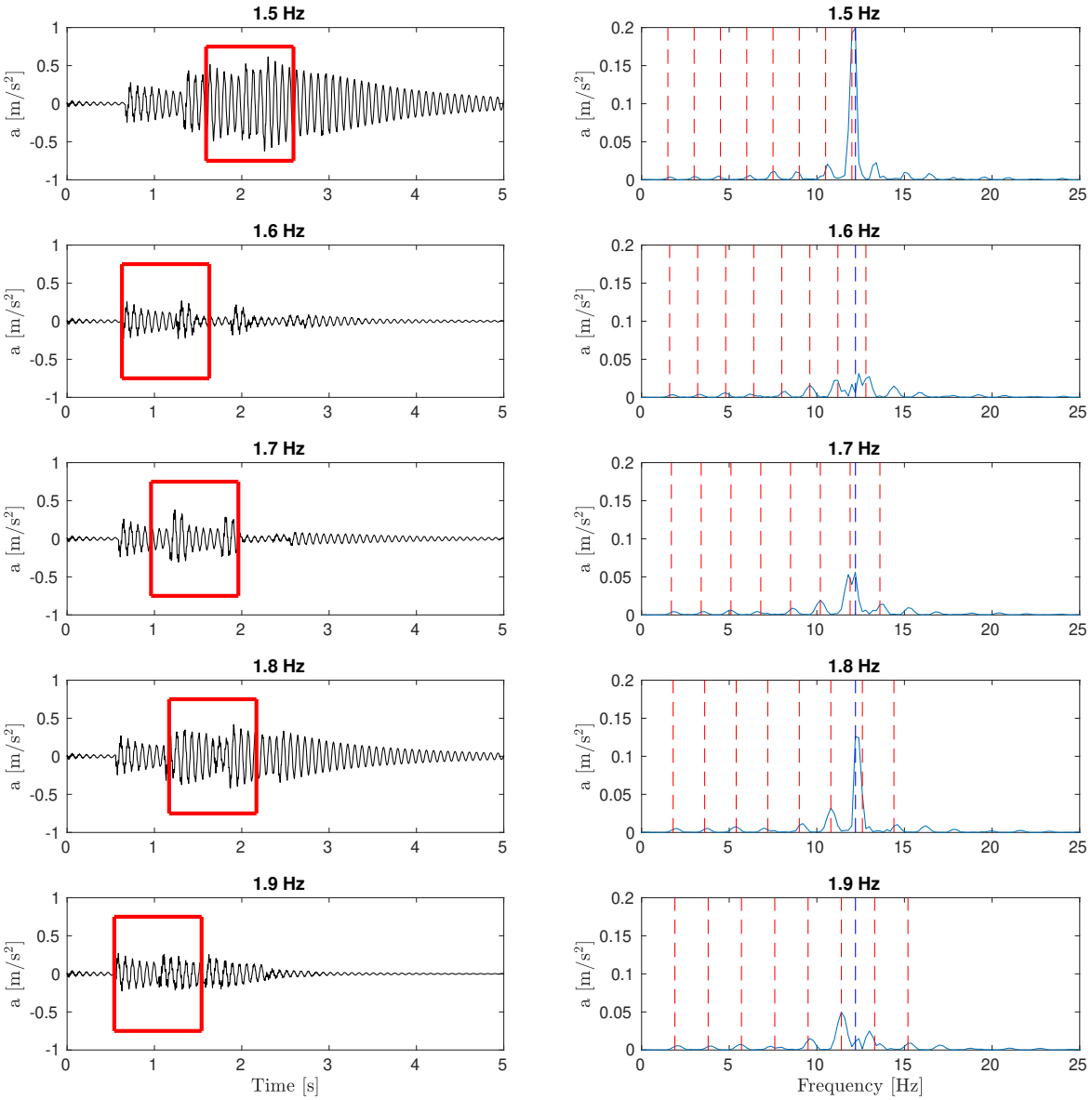

Figure B.9: Acceleration response (left column) and FFT of acceleration response (right column) walking frequencies between 1.5 to 1.9 Hz for high beech. Dashed red lines are walking harmonics, and dashed blue line the fundamental frequency.

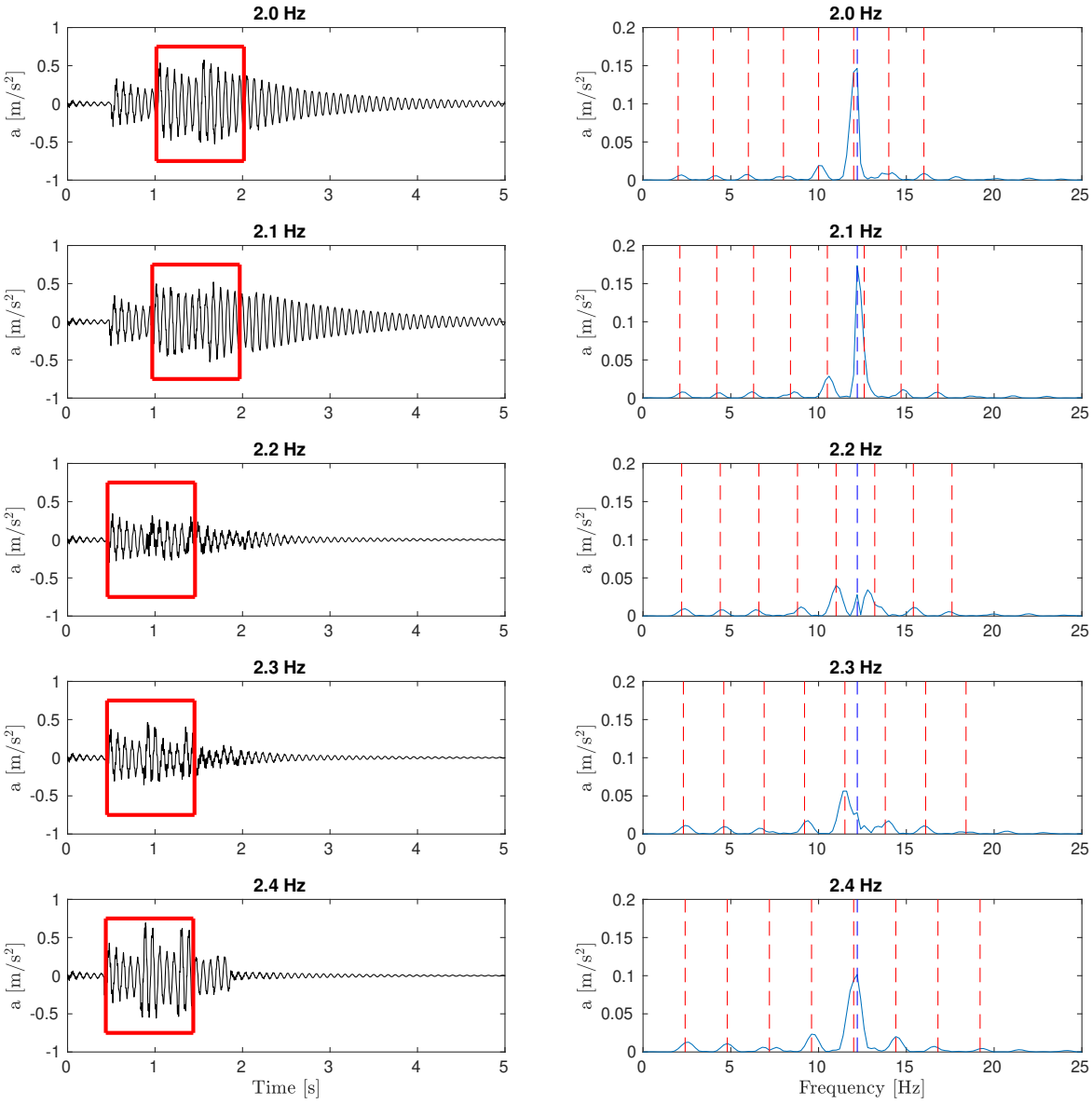

Figure B.10: Acceleration response (left column) and FFT of acceleration response (right column) walking frequencies between 2.0 to 2.4 Hz for high beech. Dashed red lines are walking harmonics, and dashed blue line the fundamental frequency.

C Acceleration response and FFTs of medium panel

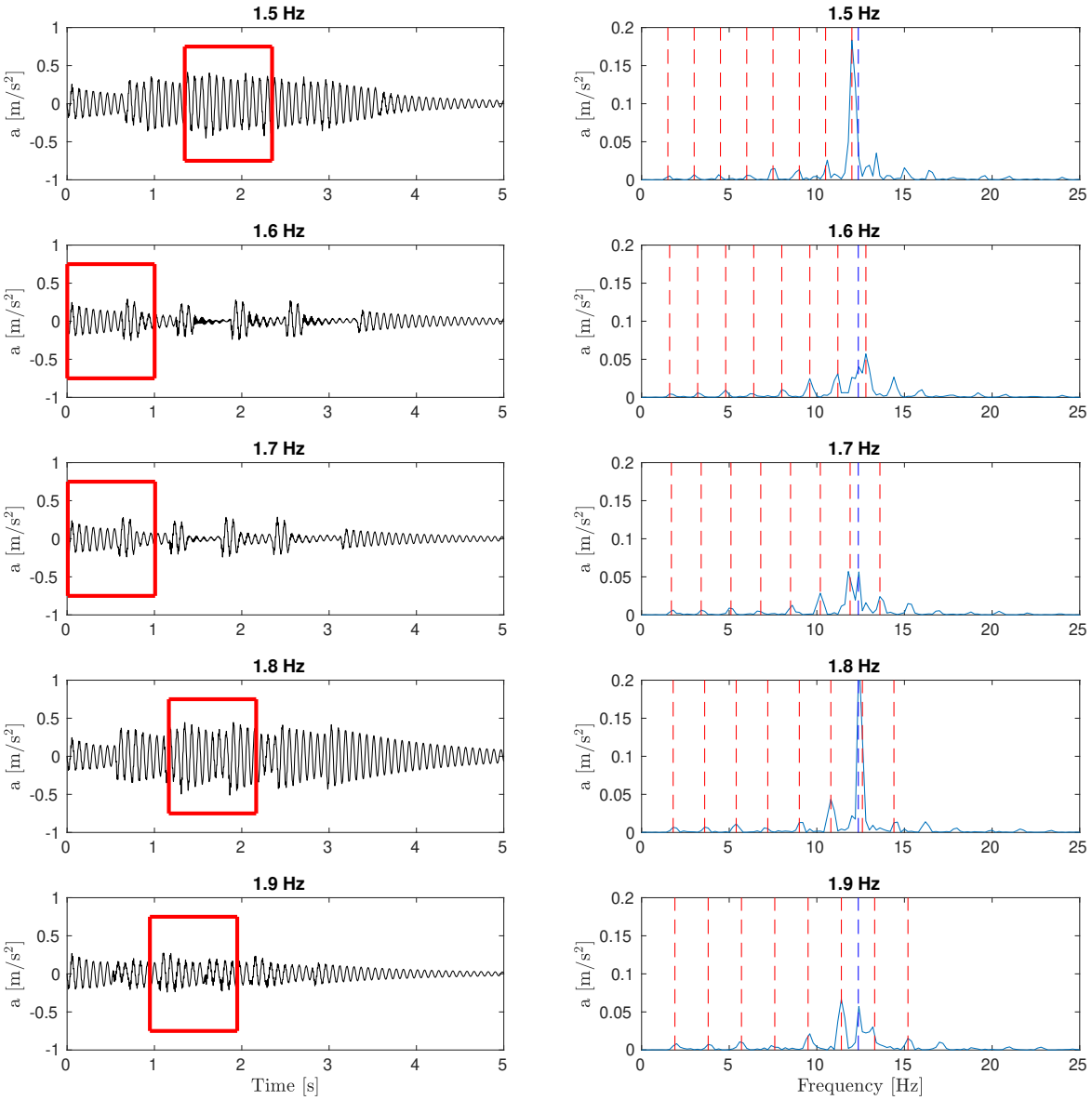

Figure C.1: Acceleration response (left column) and FFT of acceleration response (right column) walking frequencies between 1.5 to 1.9 Hz for spruce. Dashed red lines are walking harmonics, and dashed blue line the fundamental frequency.

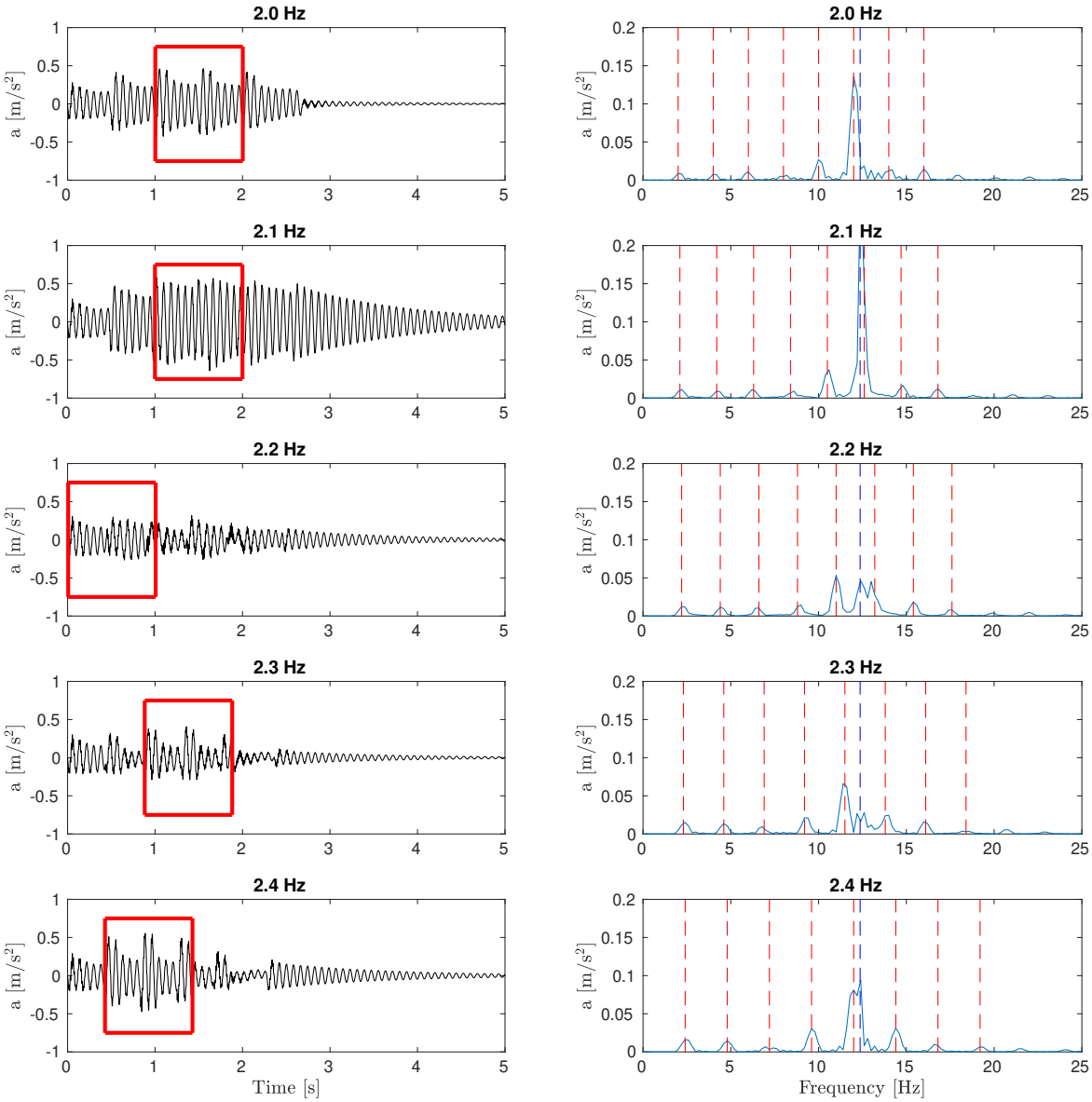

Figure C.2: Acceleration response (left column) and FFT of acceleration response (right column) walking frequencies between 2.0 to 2.4 Hz for spruce. Dashed red lines are walking harmonics, and dashed blue line the fundamental frequency.

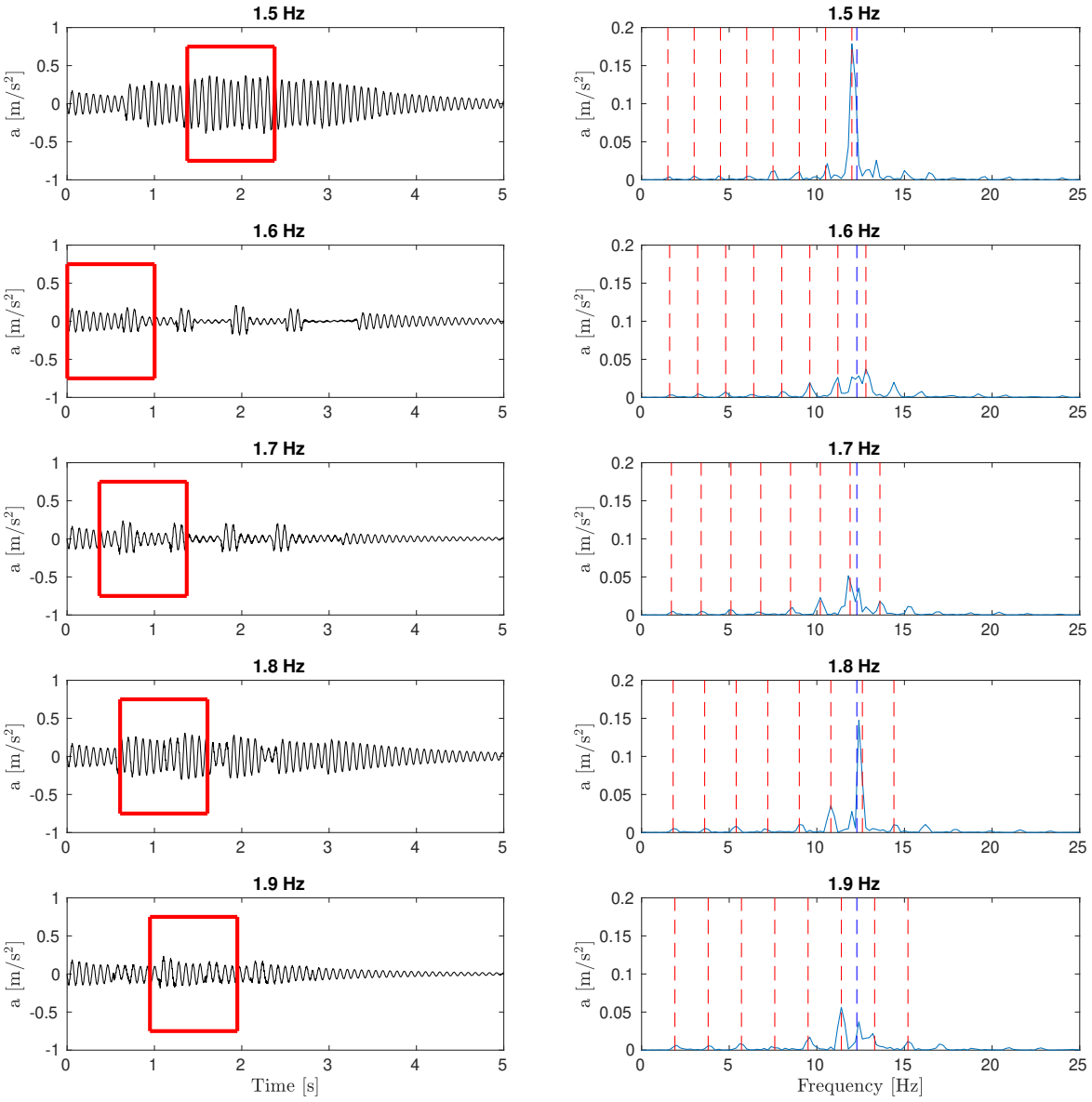

Figure C.3: Acceleration response (left column) and FFT of acceleration response (right column) walking frequencies between 1.5 to 1.9 Hz for low birch. Dashed red lines are walking harmonics, and dashed blue line the fundamental frequency.

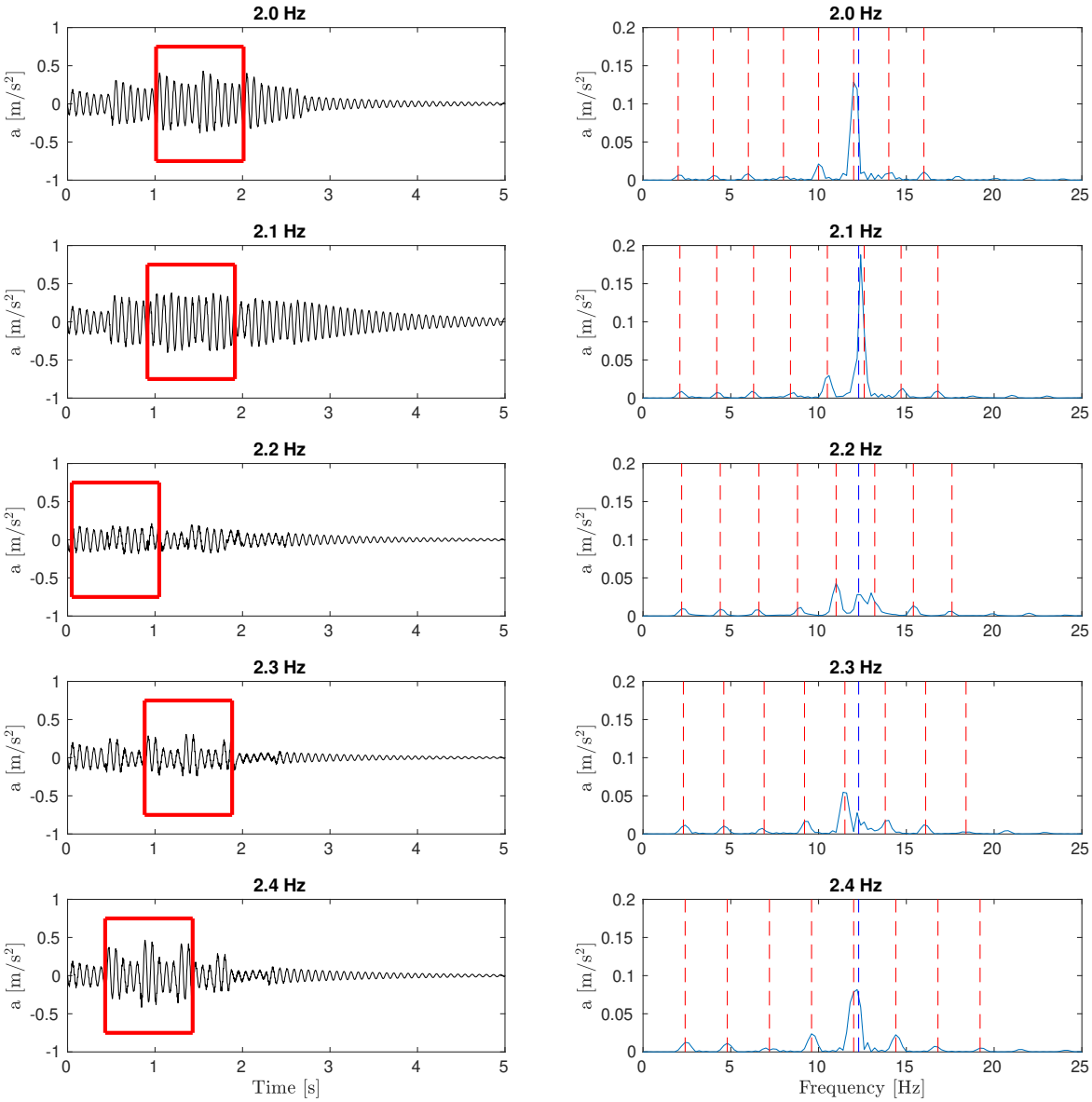

Figure C.4: Acceleration response (left column) and FFT of acceleration response (right column) walking frequencies between 2.0 to 2.4 Hz for low birch. Dashed red lines are walking harmonics, and dashed blue line the fundamental frequency.

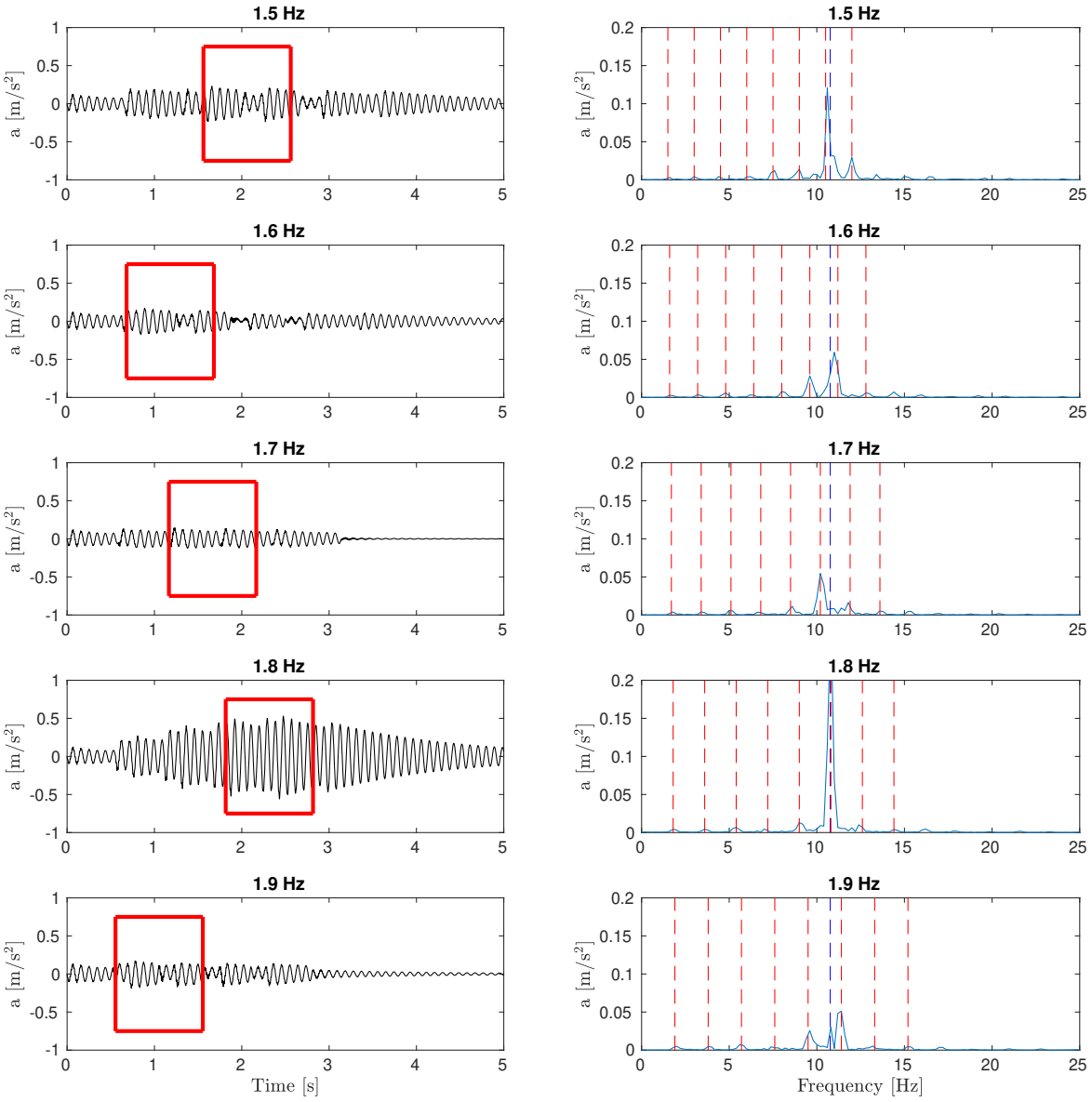

Figure C.5: Acceleration response (left column) and FFT of acceleration response (right column) walking frequencies between 1.5 to 1.9 Hz for high birch. Dashed red lines are walking harmonics, and dashed blue line the fundamental frequency.

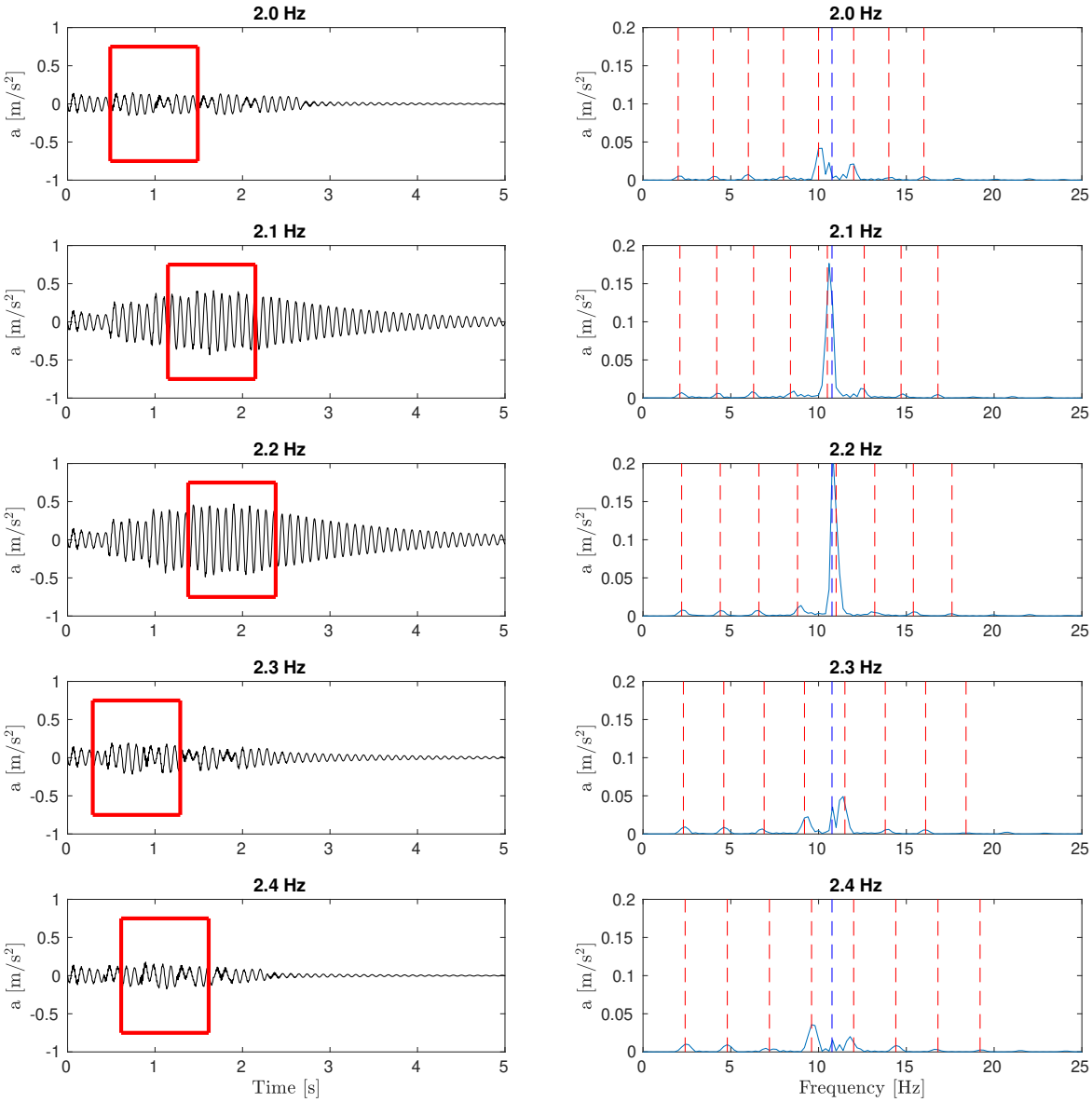

Figure C.6: Acceleration response (left column) and FFT of acceleration response (right column) walking frequencies between 2.0 to 2.4 Hz for high birch. Dashed red lines are walking harmonics, and dashed blue line the fundamental frequency.

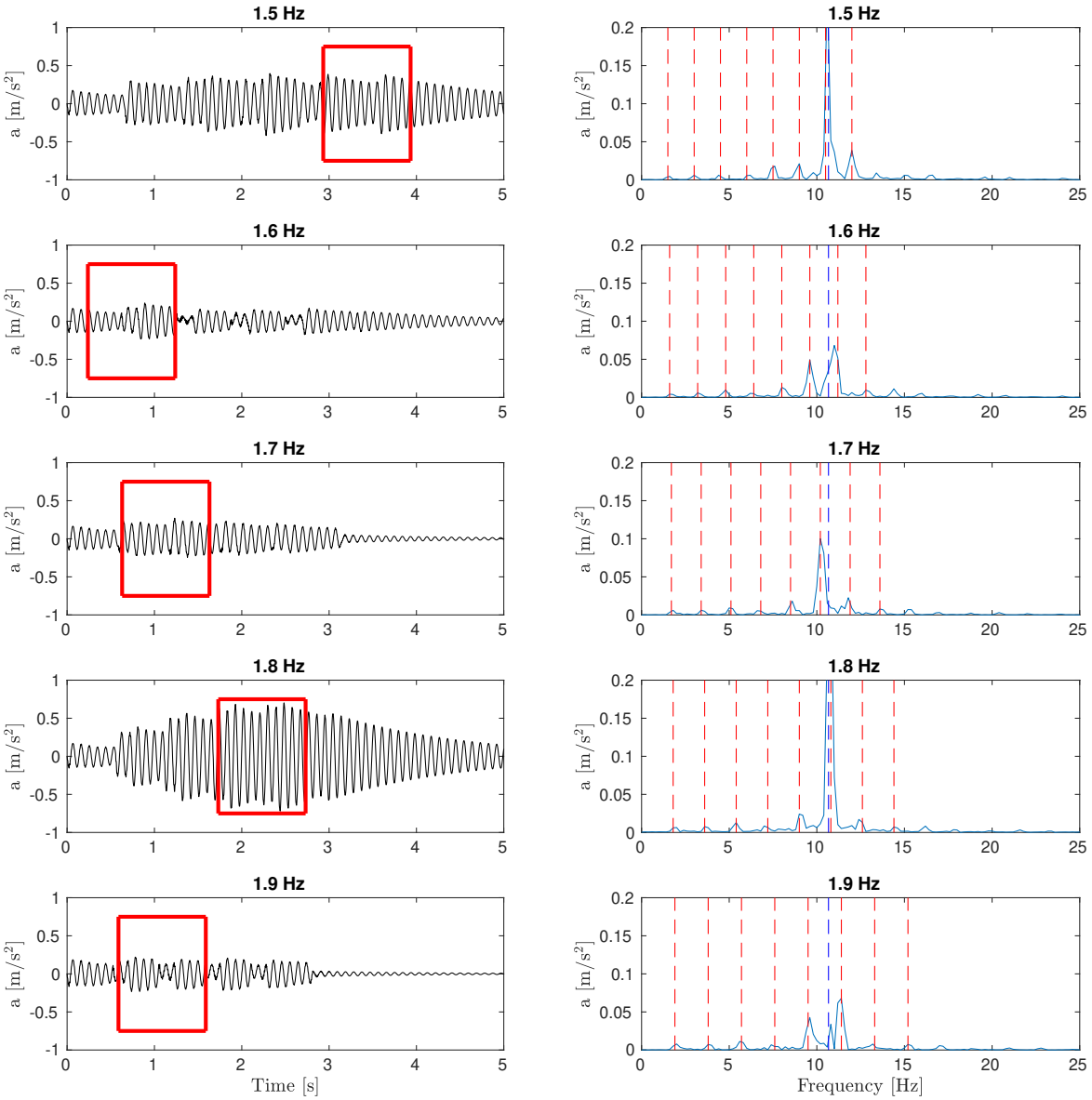

Figure C.7: Acceleration response (left column) and FFT of acceleration response (right column) walking frequencies between 1.5 to 1.9 Hz for low beech. Dashed red lines are walking harmonics, and dashed blue line the fundamental frequency.

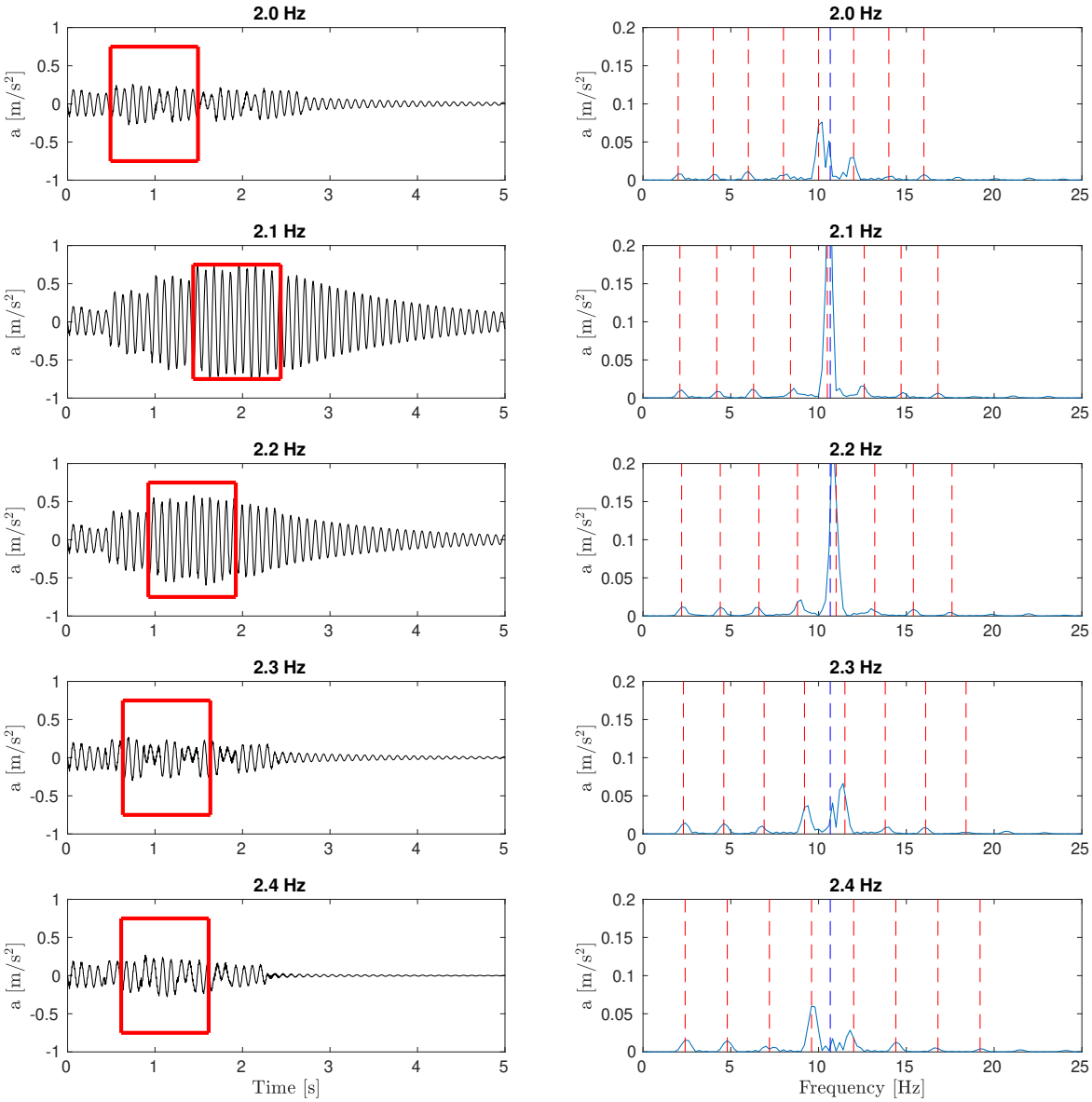

Figure C.8: Acceleration response (left column) and FFT of acceleration response (right column) walking frequencies between 2.0 to 2.4 Hz for low beech. Dashed red lines are walking harmonics, and dashed blue line the fundamental frequency.

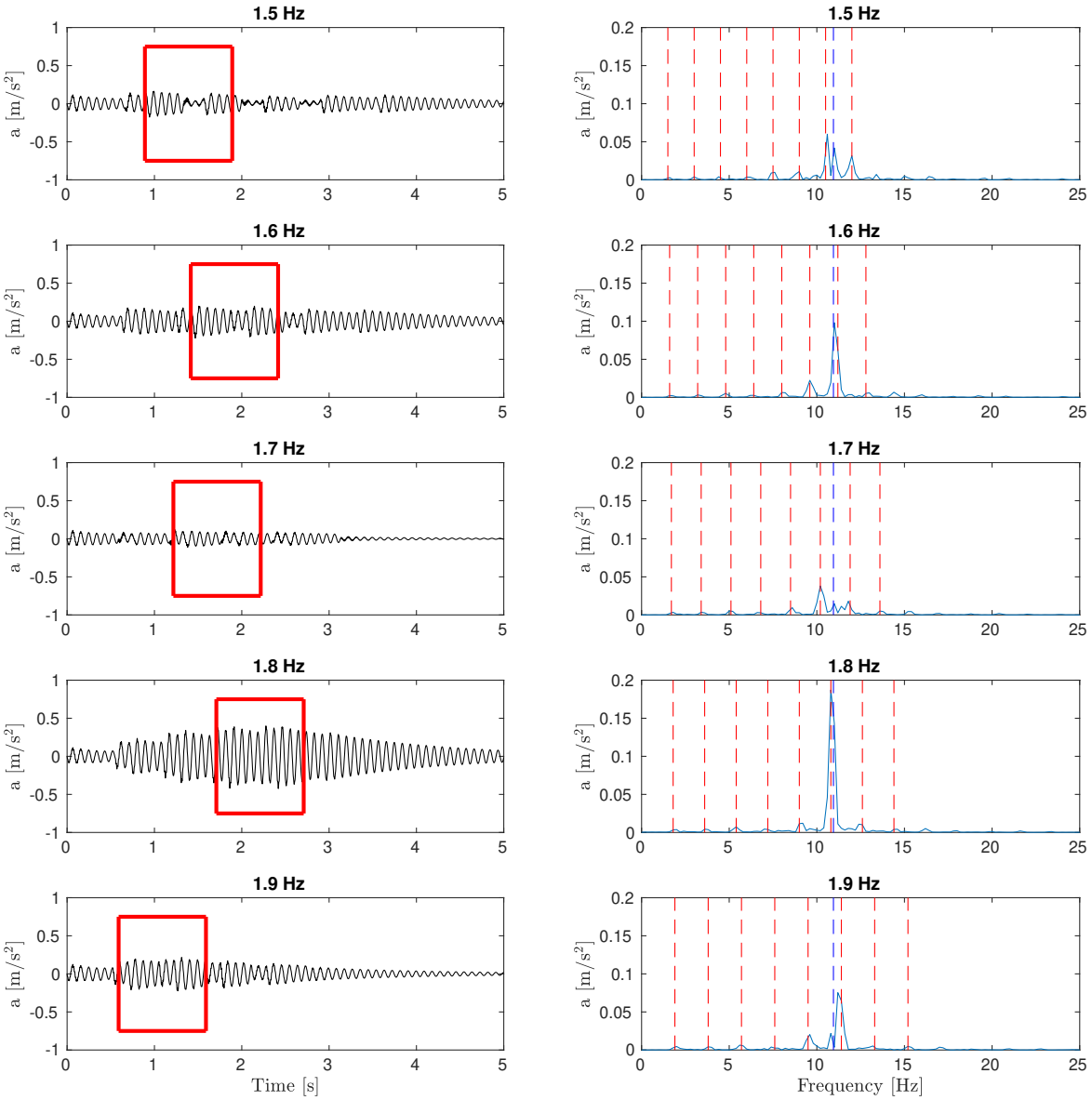

Figure C.9: Acceleration response (left column) and FFT of acceleration response (right column) walking frequencies between 1.5 to 1.9 Hz for high beech. Dashed red lines are walking harmonics, and dashed blue line the fundamental frequency.

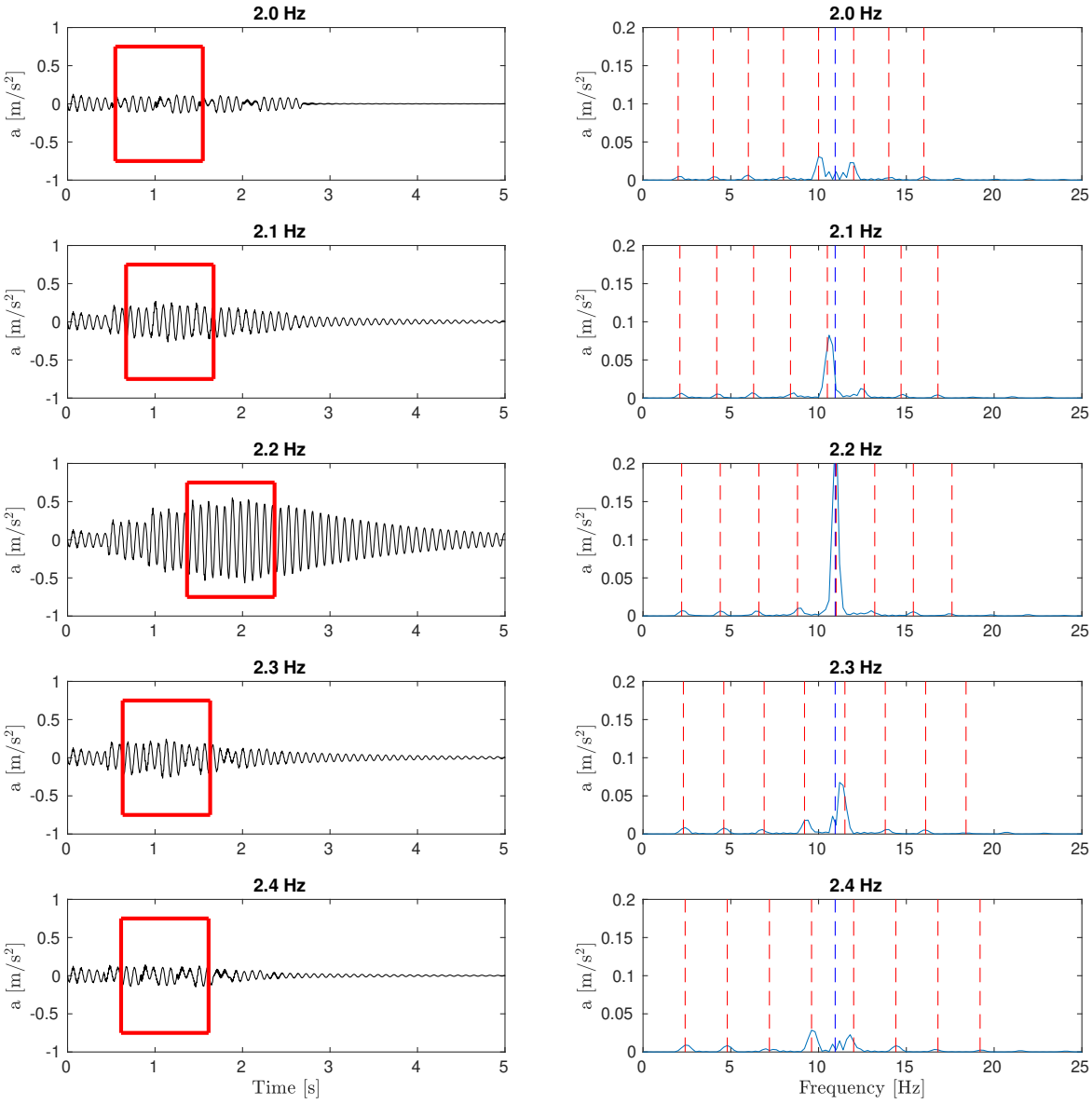

Figure C.10: Acceleration response (left column) and FFT of acceleration response (right column) walking frequencies between 2.0 to 2.4 Hz for high beech. Dashed red lines are walking harmonics, and dashed blue line the fundamental frequency.

D Acceleration response and FFTs of large panel

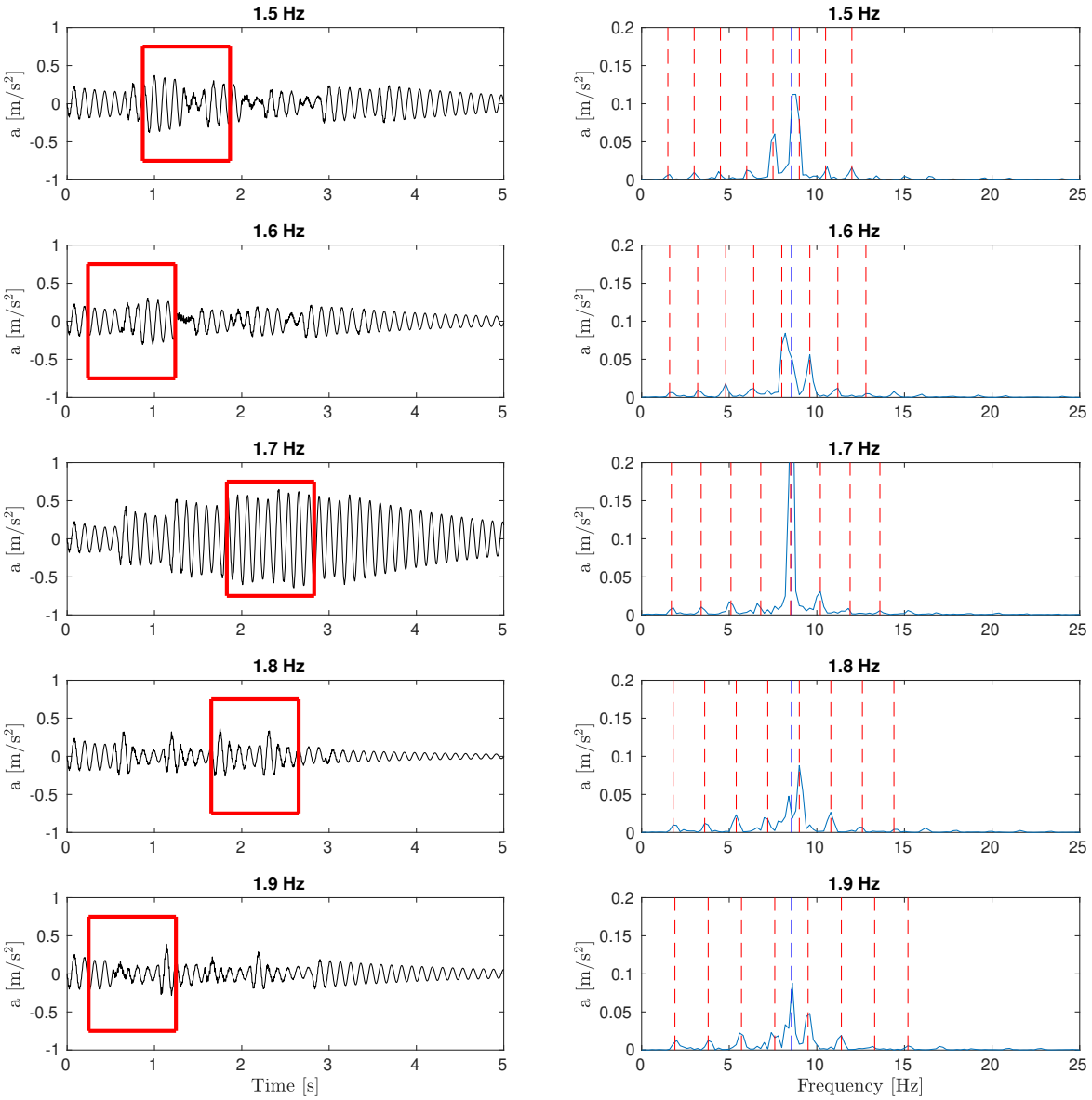

Figure D.1: Acceleration response (left column) and FFT of acceleration response (right column) walking frequencies between 1.5 to 1.9 Hz for spruce. Dashed red lines are walking harmonics, and dashed blue line the fundamental frequency.

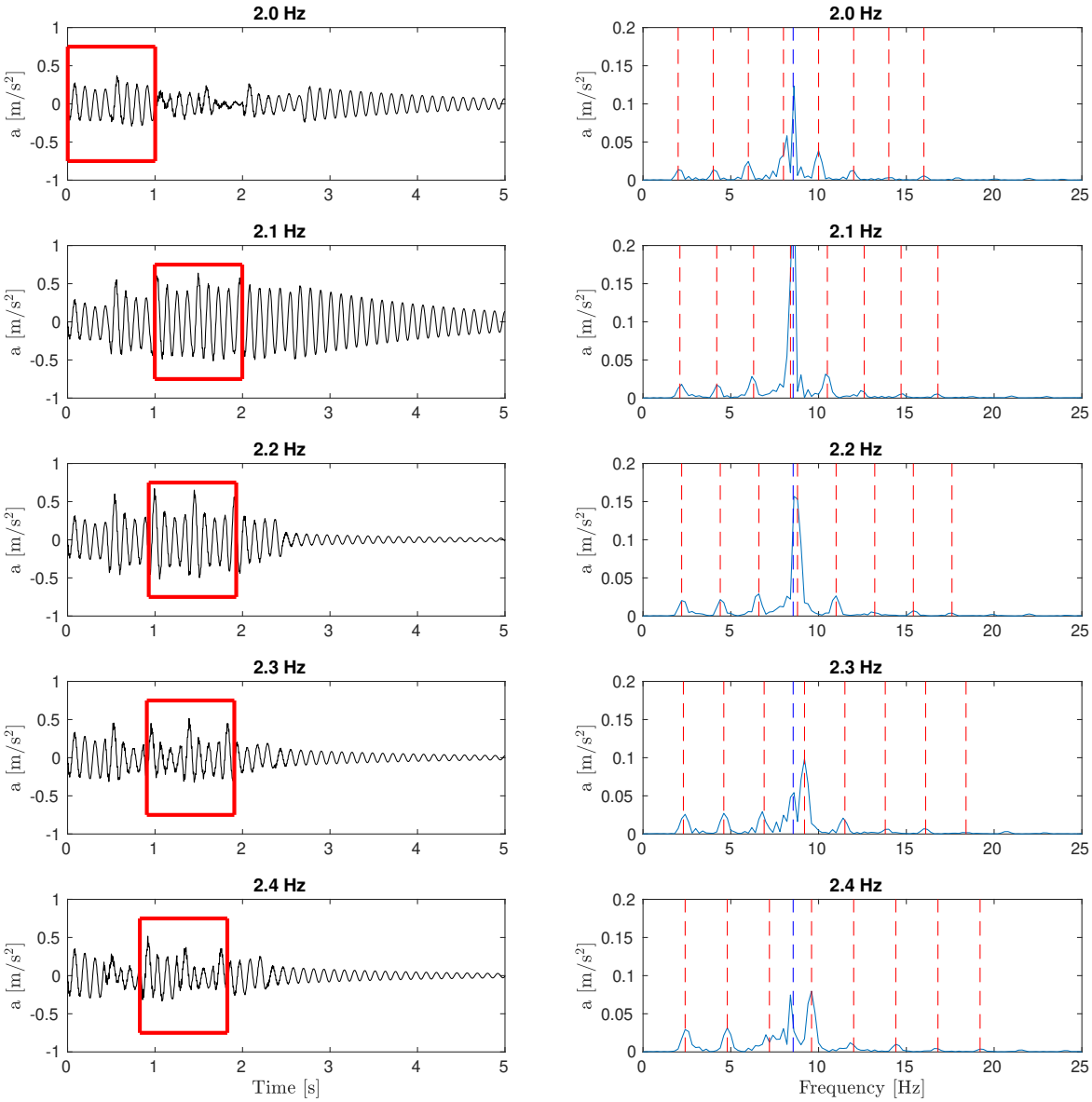

Figure D.2: Acceleration response (left column) and FFT of acceleration response (right column) walking frequencies between 2.0 to 2.4 Hz for spruce. Dashed red lines are walking harmonics, and dashed blue line the fundamental frequency.

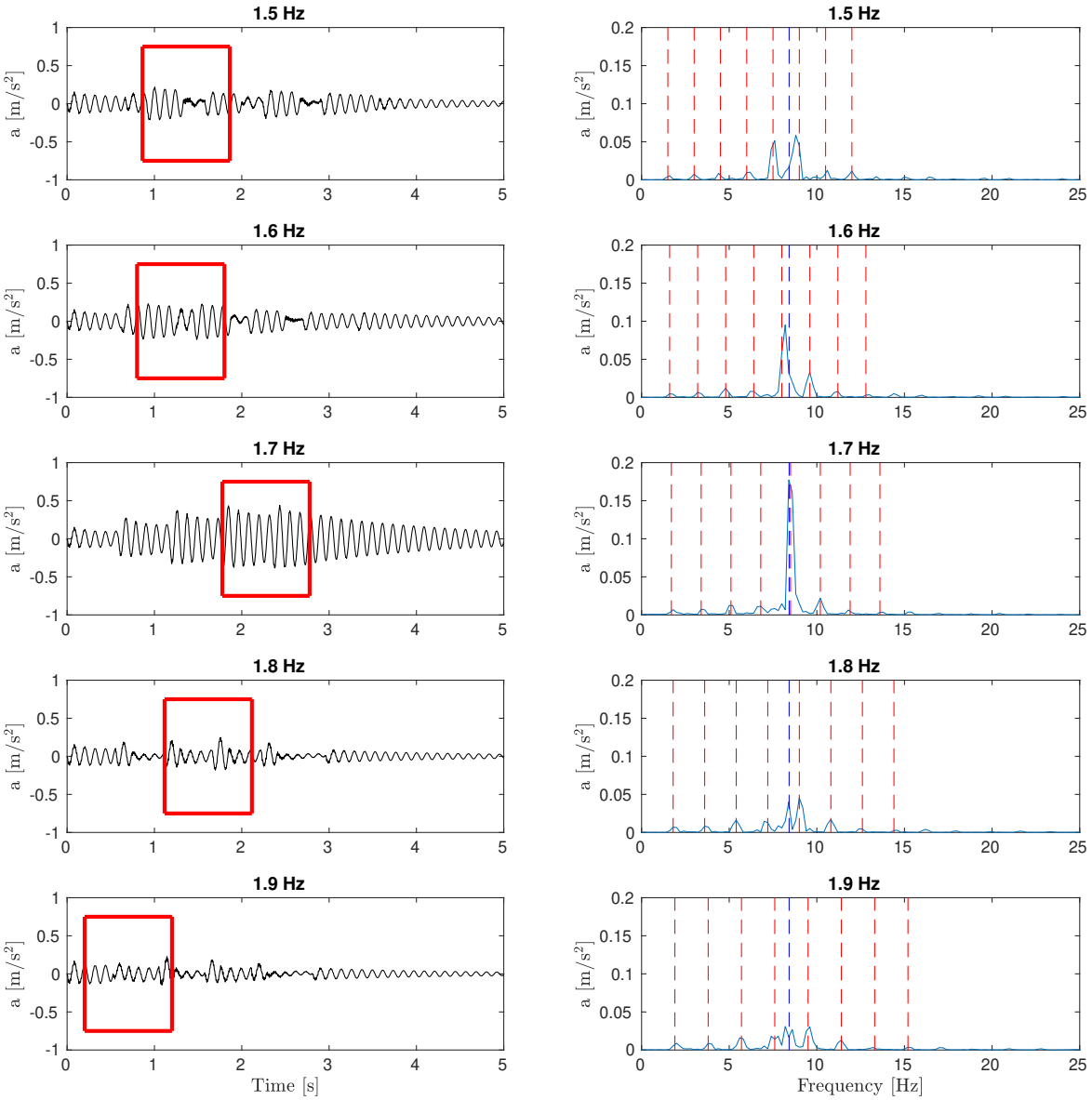

Figure D.3: Acceleration response (left column) and FFT of acceleration response (right column) walking frequencies between 1.5 to 1.9 Hz for low birch. Dashed red lines are walking harmonics, and dashed blue line the fundamental frequency.

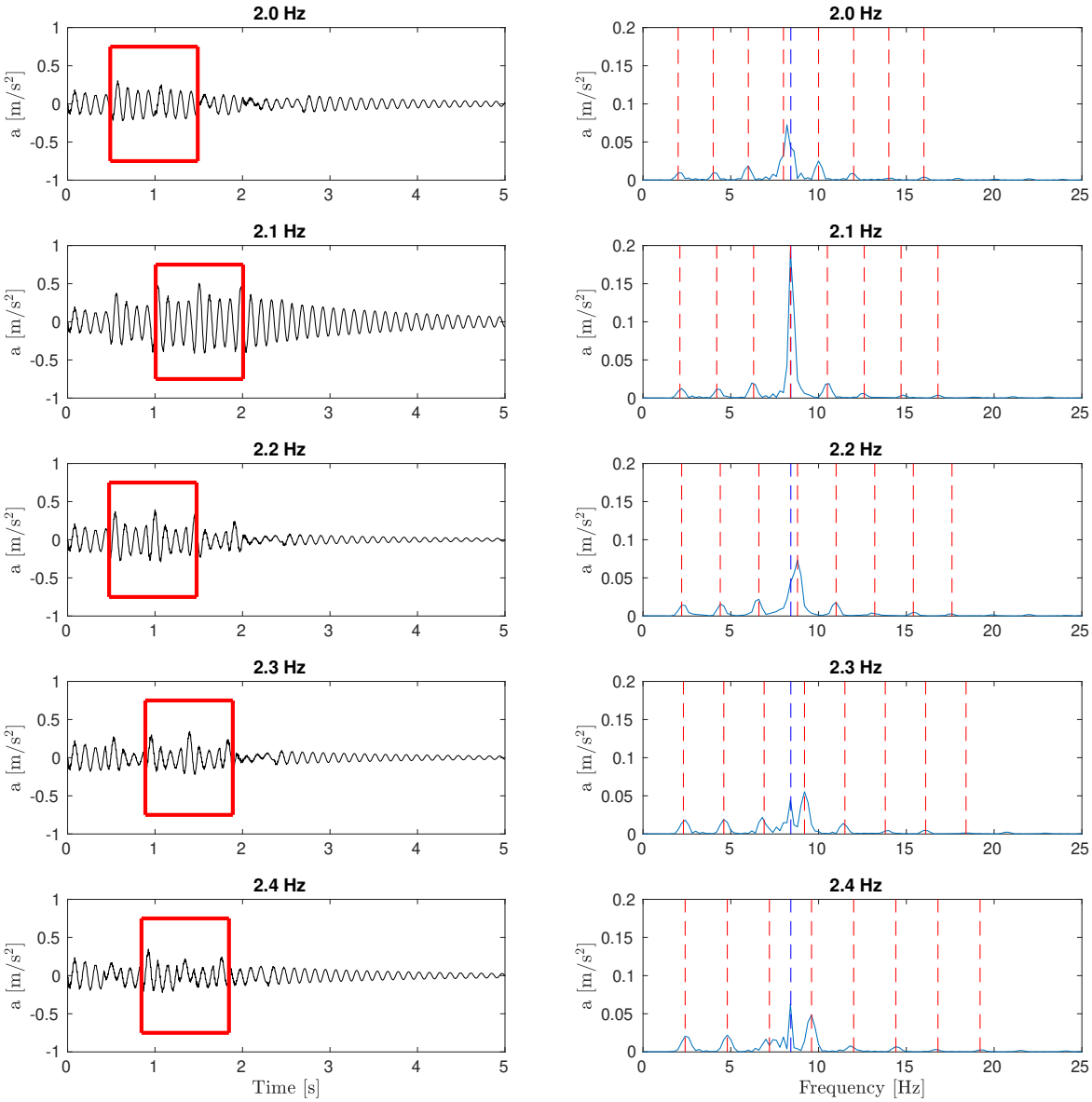

Figure D.4: Acceleration response (left column) and FFT of acceleration response (right column) walking frequencies between 2.0 to 2.4 Hz for low birch. Dashed red lines are walking harmonics, and dashed blue line the fundamental frequency.

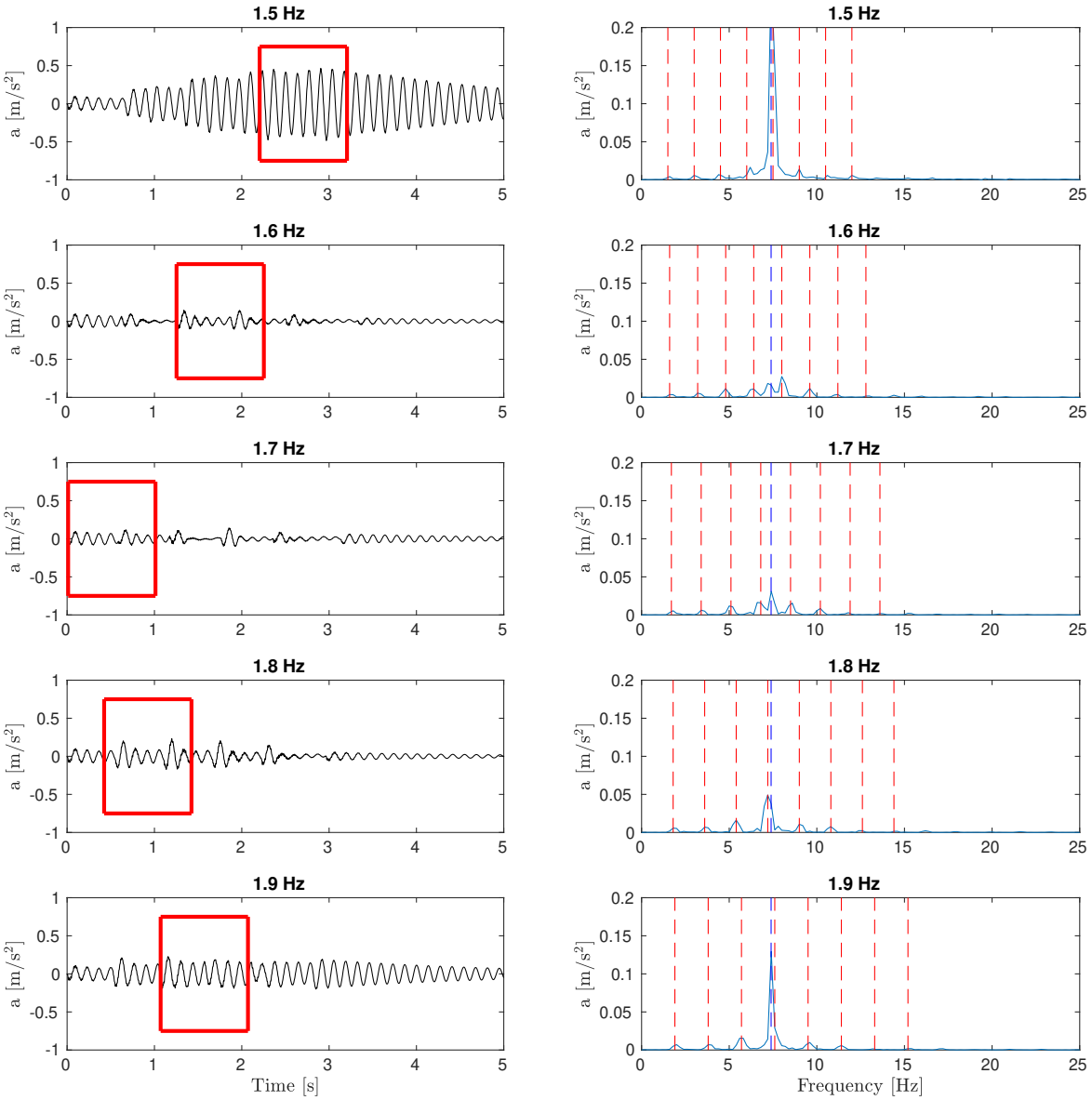

Figure D.5: Acceleration response (left column) and FFT of acceleration response (right column) walking frequencies between 1.5 to 1.9 Hz for high birch. Dashed red lines are walking harmonics, and dashed blue line the fundamental frequency.

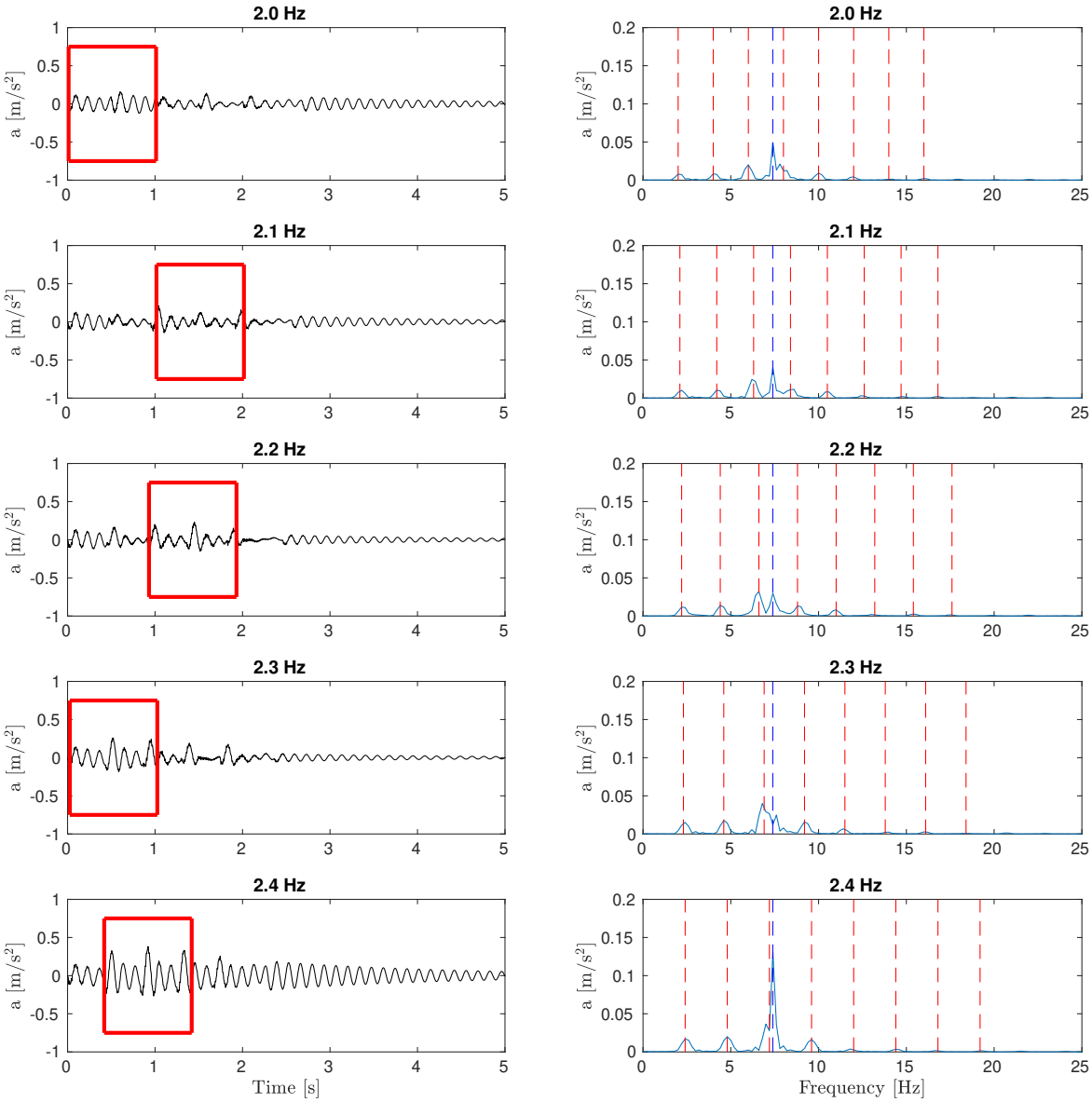

Figure D.6: Acceleration response (left column) and FFT of acceleration response (right column) walking frequencies between 2.0 to 2.4 Hz for high birch. Dashed red lines are walking harmonics, and dashed blue line the fundamental frequency.

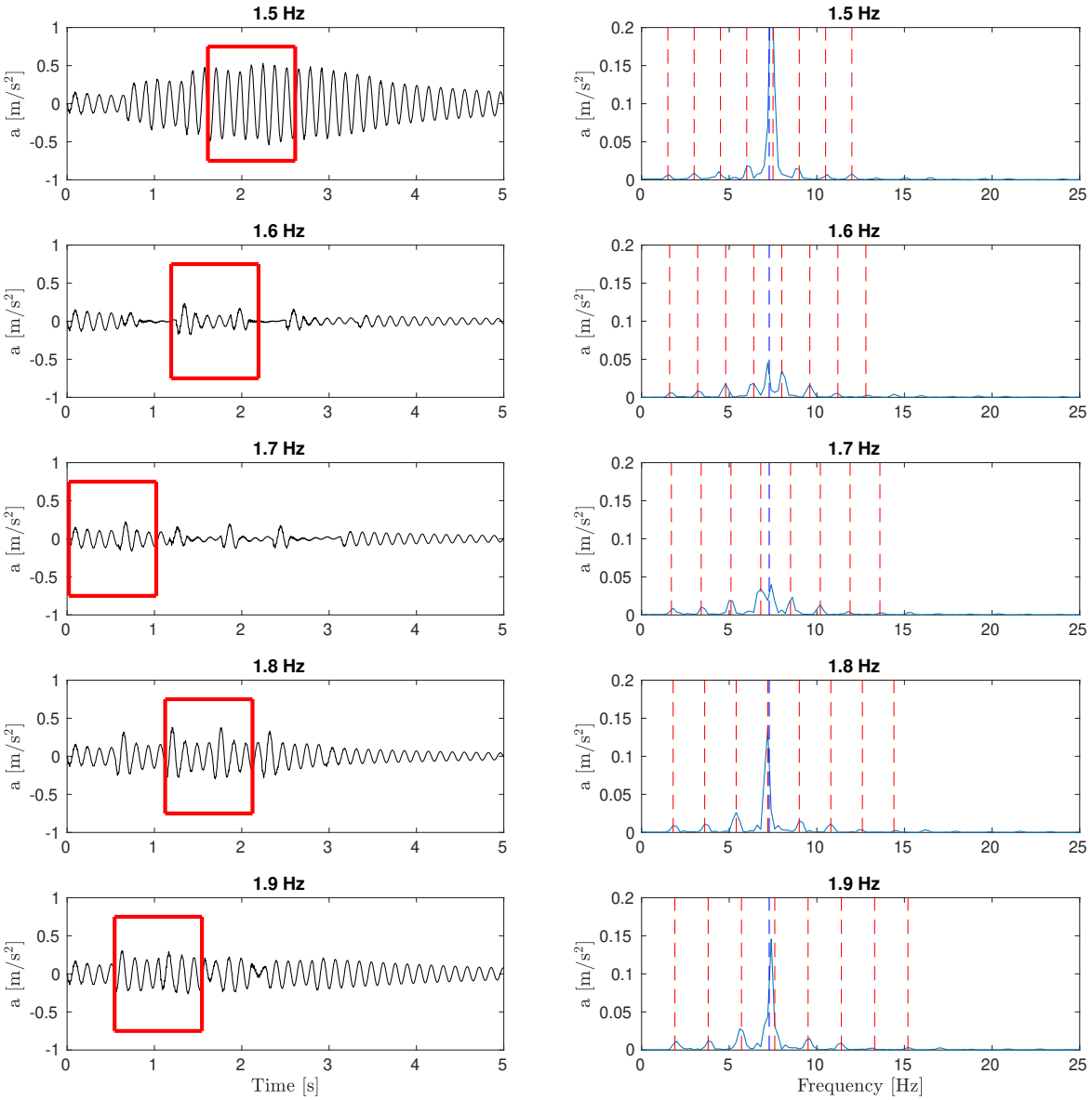

Figure D.7: Acceleration response (left column) and FFT of acceleration response (right column) walking frequencies between 1.5 to 1.9 Hz for low beech. Dashed red lines are walking harmonics, and dashed blue line the fundamental frequency.

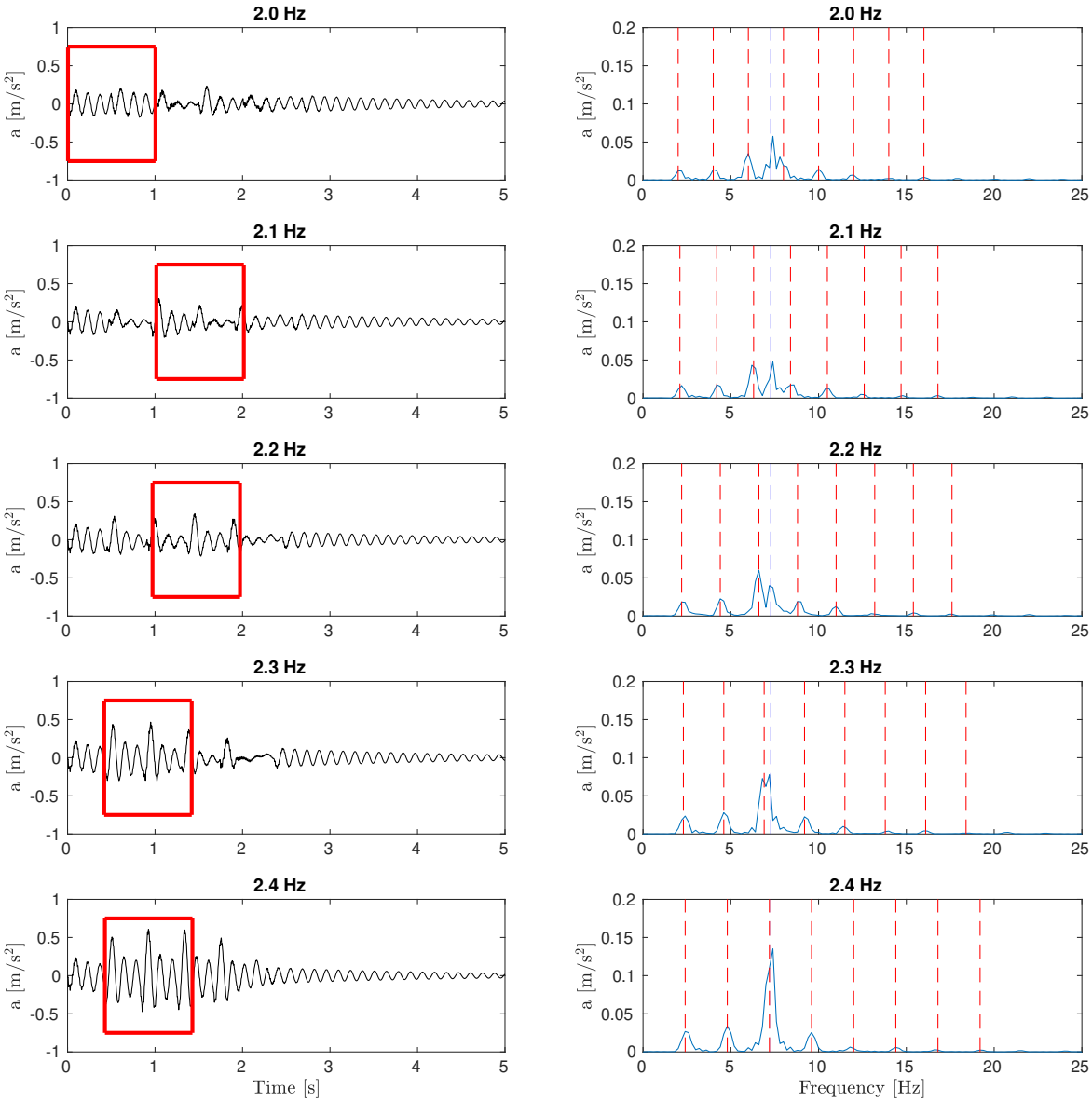

Figure D.8: Acceleration response (left column) and FFT of acceleration response (right column) walking frequencies between 2.0 to 2.4 Hz for low beech Dashed red lines are walking harmonics, and dashed blue line the fundamental frequency.

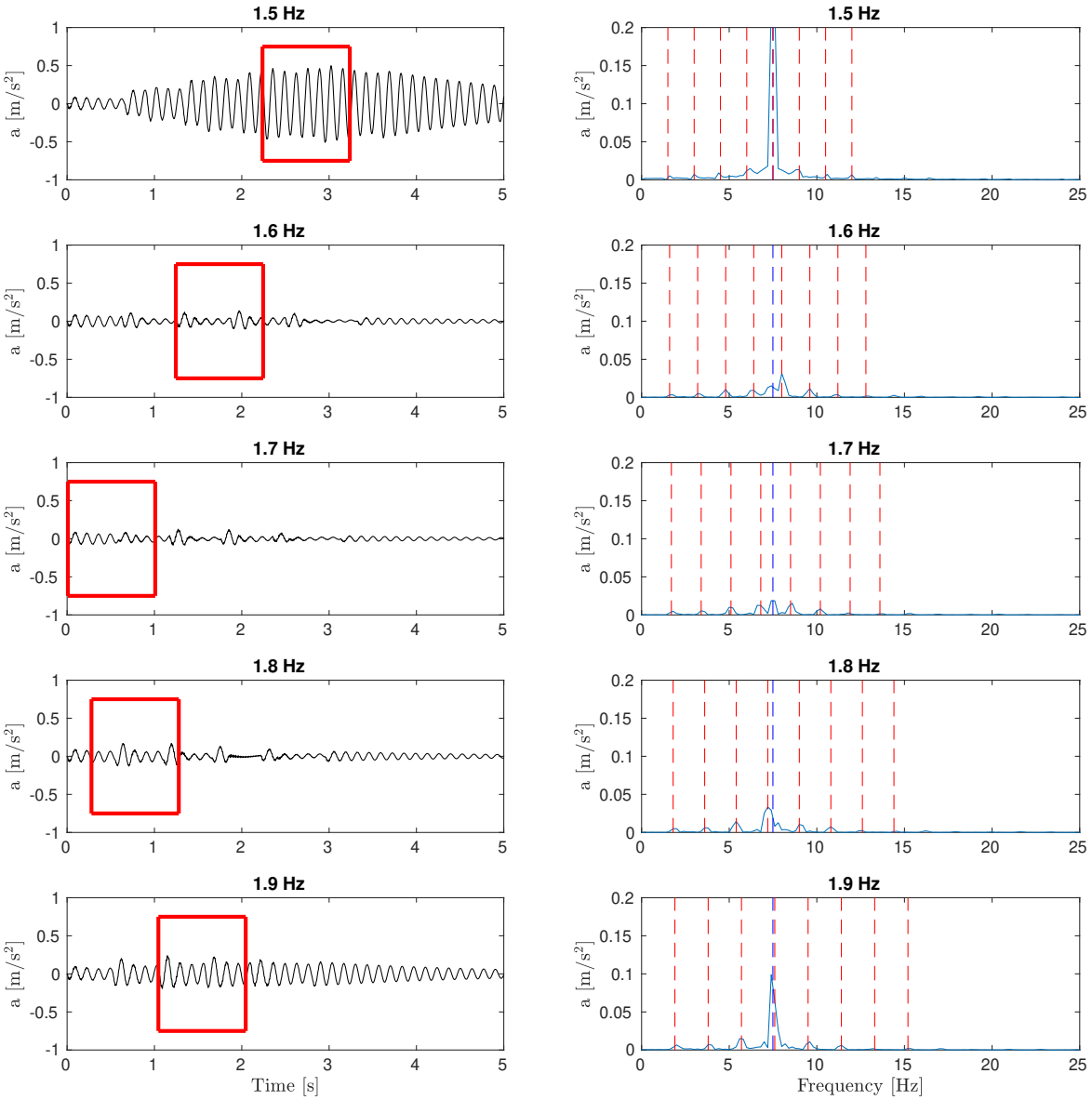

Figure D.9: Acceleration response (left column) and FFT of acceleration response (right column) walking frequencies between 1.5 to 1.9 Hz for high beech. Dashed red lines are walking harmonics, and dashed blue line the fundamental frequency.

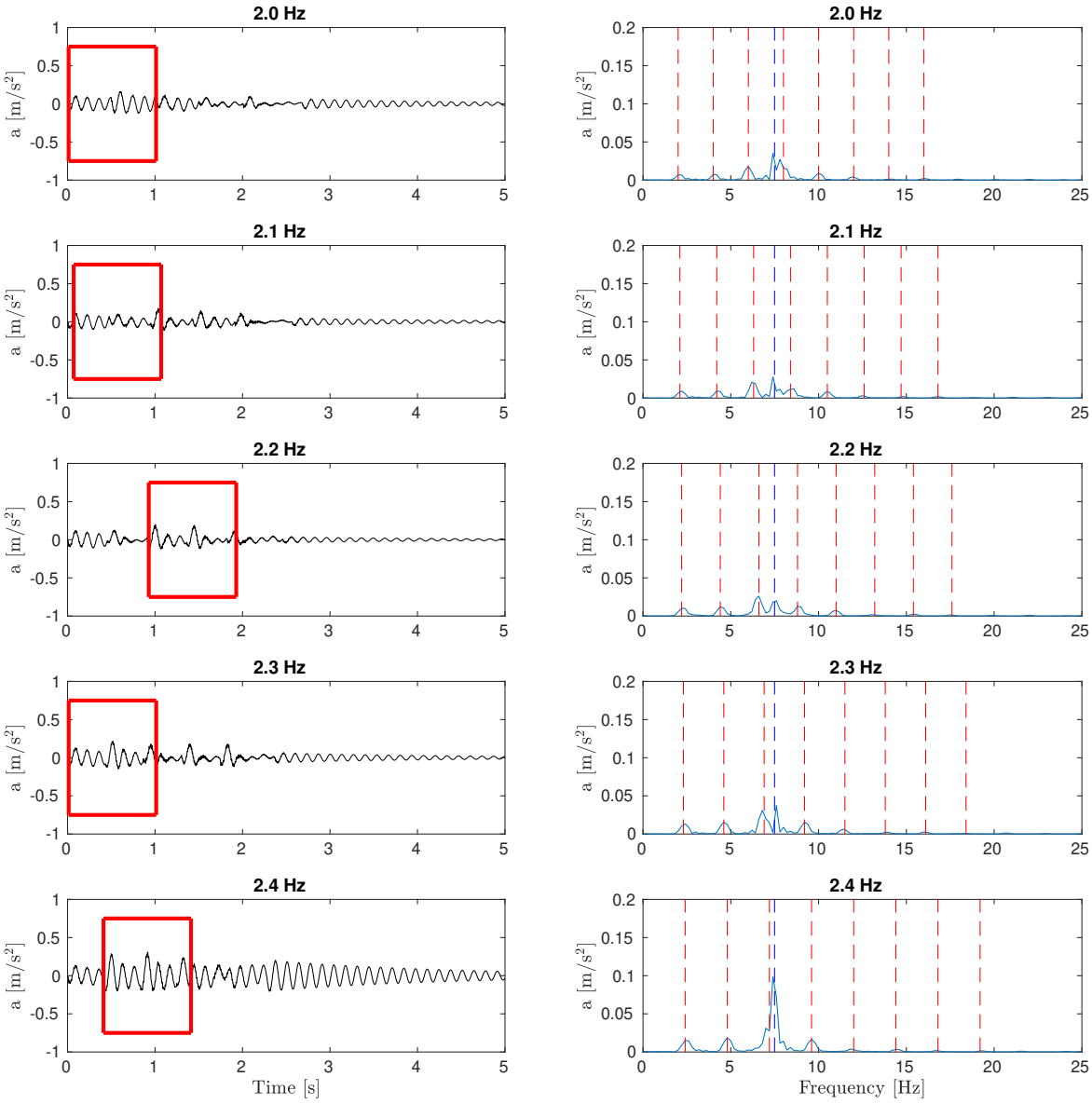

Figure D.10: Acceleration response (left column) and FFT of acceleration response (right column) walking frequencies between 2.0 to 2.4 Hz for high beech. Dashed red lines are walking harmonics, and dashed blue line the fundamental frequency.